이학박사 학위논문

Studies on Molecular Design of Vinylene and Cyano-Vinylene Containing Conjugated Polymers for High Performance Organic Solar Cells and Organic Field-Effect Transistors

고성능 유기 태양 전지 및 유기 전계 효과 트랜지스터 응용을위한 비닐 렌 및 시아 노 비닐 렌 함유 공액 고분자의 분자 설계에 관한 연구

2017 년 8 월

서울대학교 대학원

화학부

박 준 모

Studies on Molecular Design of Vinylene and Cyano-Vinylene Containing Conjugated Polymers for High Performance Organic Solar Cells and Organic Field-Effect Transistors

고성능 유기 태양 전지 및 유기 전계 효과 트랜지스터 응용을위한 비닐 렌 및 시아 노 비닐 렌 함유 공액 고분자의 분자 설계에 관한 연구

지도 교수 최 태 림

공동지도교수 박 수 영

이 논문을 이학박사 학위논문으로 제출함

2017 년 7 월

서울대학교 대학원

화학부

박 준 모

박준모의 이학박사 학위논문을 인준함

2017 년 7 월

위 원 장 홍 종 인 (인)

부위원장 최 태 림 (인)

위 원 박 수 영 (인)

위 원 김 경 택 (인)

위 원 김 봉 기 (인)

Abstract

Studies on Molecular Design of Vinylene and Cyano-Vinylene Containing Conjugated Polymers for High Performance Organic Solar Cell and Organic Field-Effect Transistor Applications

Jun-Mo Park
Department of Chemistry
The Graduate School
Seoul National University

Conjugated polymers have been extensively studied because of their conducting and semiconducting properties since their discovery in 1977. Their charge transport properties enable their use in various electronic applications, such as in organic solar cells (OSCs) and organic field-effect transistors (OFETs). These applications require semiconductors that have two characteristics: a proper energy level and high charge mobility. The key design for realizing these properties requires efficient π-π stacking of the conjugated backbone and utilization of appropriate electron-monomer and electron-accepting monomer to match the desired energy level. In this study, I have focused on vinylene-containing conjugated polymers and their deverivatives, cyanovinylene-containing conjugated polymers. While vinylene group has attractive features, such as ability to make coplanar backbones and the easy tunability of their energy levels by

substitution with cyano group, they have received little attention as semiconductors for OSCs and OFETs, because of the low device performance arising from their poor charge transport properties. This poor charge transport properies are be attributed to the structural disorders of the vinylene group, which is disadvantageous for π-π stacking. In this study, high performance conjugated polymers containing vinylene and cyanovinylene for OSC and OFET applications have been designed by controlling the structural disorders

First, vinylene containing conjugated polymer has been designed for OSC applications. Poly(phenylenevinylene) (PPV) is a representative vinylene polymer. However, PPV has a poor charge transport properties. Recently, thiophene introduced PPV type polymer (PPVTV) has showed relatively high hole mobility, and thus achieved relatively high efficiency (3.5%) for OSCs as compared to PPVs. However, I have thought that the polymer contains a possibility of further improvement of performance by using the well known good moiety. In this respect, the new vinylene polymer (PBDS) has beed designed. This polymer design was implemented by introducing a two-dimensional benzo[1,2-b:4,5-b]dithiophene (2D-BDT), which is known to be a good charge transport moiety, into the highly coplanar and trans-stereoregular PPVTV. Interestingly, it was found that 2D-BDT plays a role in not only in improving the space charge limited current (SCLC) hole mobility but also in lowering the HOMO energy via a comparative analysis with polymer without 2D-BDT. Consequently, PBDS:$PC_{71}BM$-based solar cell exhibited an enhanced open-circuit

voltage (V_{OC}) of 0.81 V and a short-circuit current (J_{SC}) of 10 mA cm^{-2} compared to that without 2D-BDT, resulting in a power conversion efficiency (PCE) of 5%. This is a large PCE considering that the polymer has a wide bandgap of 2.0 eV, and it is, thus, suitable for tandem solar cell and ternary blend solar cell applications. (Chapter 2)

Next, for further improvement of the PCE, PBDS has been modified by substitution with cyano group. While, cyanovinylene containing polymers have showed good optical properties, they have not showed high performances in OFET and OPV applications, due to their trans to cis photoisomerization reaction. In this work, cyano group was substitutied on beta site of vinylene, because beta cyanovinylene molecules are known to have coplanar structure and strong intermolecular interaction. Interestingly, the resulting polymer (PBDCS) exhibited 100% trans-stereoregularity and no trans-to-cis photoisomerization on exposure to UV light, unlike other cyanostyrylbenzene molecules. Besides, PBDCS has a much deeper FMOs and a lower band gap compared to PBDS, and shows storng aggregation properties in solution. Subsequently, an OSC based on PBDCS:$PC_{71}BM$ was found to have a high short-circuit current (J_{SC}) of 15 $mAcm^{-2}$ and a high open-circuit voltage (V_{OC}) of 0.95 V, resulting in a relatively low E_{loss} of 0.80 eV, high EQE_{max} of 82.7%, and a high PCE of 8.75%. Furthermore, OSC based on PBDCS:ITIC exhibited a high PCE of 7.81% with a remarkably high V_{OC} of 1.08 V and high J_{SC} of 15.9 $mAcm^{-2}$. In addition, the OSC has an extremely small Eloss of 0.49 eV despite the high EQE_{max} of 74.2%. This E_{loss} is the smallest value in an efficient OSC. From these results, we found that the

cyanovinylene group provides strong intermolecular interactions and strongly stabilized FMOs (Chapter 3).

Finally, we have used the cyanovinylene group to design an ambipolar semiconducting polymer. In general, the design of semiconductors with ambipolar charge transport properties is very limited due to their restrictive requirement of HOMO and LUMO energy levels, which must be close to the electrode work function. Donor-acceptor alternating polymer is the most widely used design. Howere, these polymers shows unipolar, especially p-type, because sufficiently strong accepting unit is very few, compared with donating units. In this study, ambipolar semiconducting polymer (PBDCS) has been designed by introducing the trans-cyanovinylene group into conventional donor-acceptor alternating polymers, p-type semiconductor. As a result, the polymer showed highly balanced hole and electron mobilities of $\mu_{h,max}$ ~ 0.2 $cm^2\ V^{-1}s^{-1}$ and $\mu_{e,max}$ ~ 0.2 $cm^2\ V^{-1}s^{-1}$, respectively, besides, which are virtually independent of the annealing temperature over the range of 80°C to 250°C. (chapter 4)

Keyword: vinylene polymer, poly(arylenevinylene), cyanovinlyene polymer, low band gap polymer, strong intermolecular interaction, organic field-effect transistor, organic solar cell, ambipolar transistor.

Student Number: 2010-30092

Contents

List of Tables

List of Figures

Chapter 1. Introduction

1.1. Conjugated polymers

1.1.1. Fundamentals

π-Conjugated polymers have the electrical conductivity.[1] This property was discovered in 1977 for polyacetylene by Hideki Shirakawa, Alan G. MacDiarmid, and Alan J. Heeger.[2,3] Since then, research on conjugated polymers has made rapid progress, and this discovery brought in 2000 the Nobel Prize to the three discoverers mentioned.

Such metal-like high conductivity is achieved only by doping. In the intrinsic state, the conjugated polymers are semiconductors. Therefore, the highest occupied molecular orbital (HOMO) and lowest unoccupied molecular orbital (LUMO) are formed in the bonding π orbital and antibonding π^*orbital. The potential energy difference between the HOMO and the LUMO is the band gap (E_g). The Eg is affected by degree of the bond length alternation (BLA), which was predicted by Rudolf Peierls in 1956.[4]

Electronic structures of conjugated polymers are classified into two types according to the change in the electronic structure after interchange between single and double bonds: degenerate ground state (e.g., trans-polyacetylene) and non-degenerate ground state (e.g., cis-polyacetylene and other conjugated polymers).[5] Figure 1-1

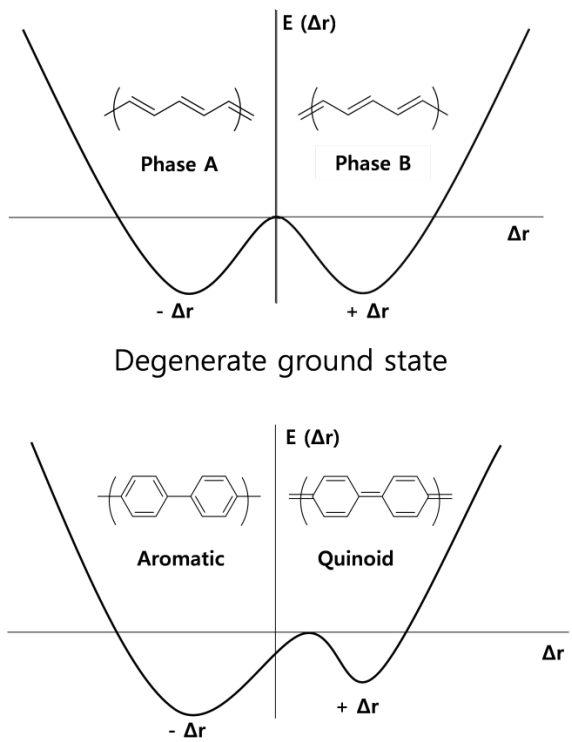

Figure 1-1. Potential energy as a function of bond length alternation for trans-poly(acetylene) (degenerate ground state) and poly(p-phenylene) (non-degenerate ground state).

shows the relationship between the potential energy and the bond length alternation (BLA) for trans-poly(acetylene) (degenerate ground state) and poly(p-phenylene) (non-degenerate ground state). The conjugated polymer with a degenerate ground state has two same minima and one maximum at $\Delta r = 0$, because interchange between single and double bonds produces identical electronic structures (phase A and phase B). On the other hand, the conjugated polymer with a non-degenerate ground state has two different minima and one maximum at $\Delta r \neq 0$, due to interchange between single and double bonds leading to two different electronic structures (aromatic and quinoid). At the maximum, the π electrons are not paired and thus the band gap takes the minimum value.

Such different electronic structures generate different charge-carrying species. Degenerate ground state conjugated polymers form solitons, such as empty (positive soliton), singly occupied (neutral soliton), and doubly occupied (negative solitons) ones (Figure 1-2). Non-degenerate ground state conjugated polymers form excitons (neutral), polarons (singly charged), and bipolarons (doubly charged) (Figure 1-3).[7]

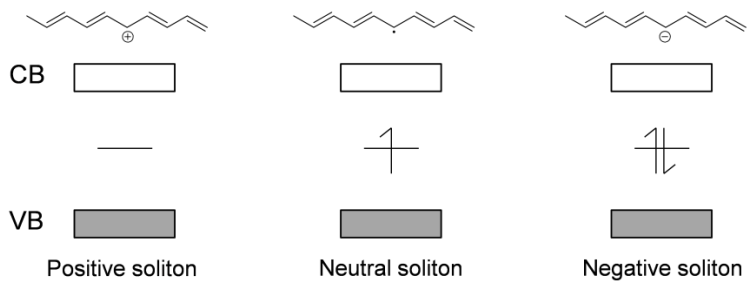

Figure 1-2. Schematic representations and energy diagram is shown for solitons in CP ´ s. One new energy state is induced in the gap. This can be either empty (positive soliton), half (neutral soliton) or double filled (negative soliton).

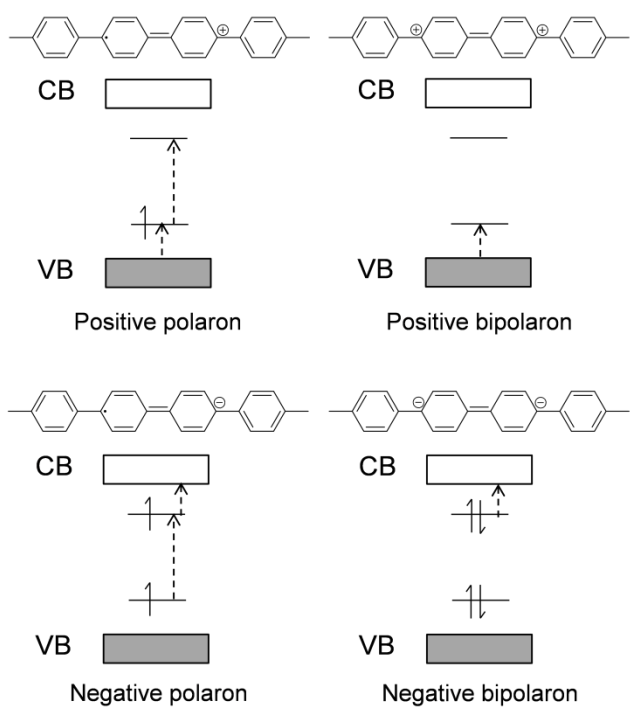

Figure 1-3. Schematic representation and band diagrams for nonlinear excitation in non-degenerate ground state. Allowed optical transitions are shown as dashed arrow

1.1.2. Charge transport in conjugated polymer

In the solid state, organic semiconducting molecules are bonded together by van der Waals forces. This intermolecular interaction is not strong enough to form an electronic band, which is created in covalently bonded inorganic semiconductor. Thus, charge transport in organic semiconductors is commonly described by a hopping mechanism. The Marcus theory of electron transfer is useful to explain charge transport in organic semiconductors.[8] According to the Marcus theory, the electron transfer rate (ket) is expressed as follows:

$$k_{et} = (\frac{4\pi^2}{h})t^2(4\pi\lambda RT)^{-0.5}e^{\frac{-\lambda}{4RT}}$$

where t is the transfer integral, λ is the reorganization energy, ħ is Planck's constant, R is the distance between molecular centers, and T is the temperature. The equation suggests that, among the several parameters, the transfer integral t is the most important factor for efficient charge transport in organic semiconducting molecules according to the hopping mechanism. The transfer integral depends on the degree of wave function overlap with adjacent molecules. Therefore, the size of π-orbitals and intermolecular π-π distance are factors of increasing charge transport properties, assuming wave function overlap between adjacent molecules is well matched.8 While small molecules have various stacking modes, conjugated polymers usually favor being stacked together with a face-to-face orientation; thus, efficient π-π stacking is the

most important factor for achieving high charge mobility. In addition, unlike small molecules, charge transport is available through intrachain spaces, which are known to show extremely high charge mobility.[9,10] Although it is difficult to determine the contribution of intrachain charge transport to bulk mobility, the general trend of increasing mobility with increasing molecular weight, even in the same structure, verifies the significant contribution of intrachain charge transport.

1.1.3. Design of conjugated polymer

As described in Figure 1-1, most of conjugated polymers have a non-degenerate ground state electronic structure, which has two different minima electronic structure (aromatic and quinoid form) and one maximum (minimum bandgap point) between two minima point. Figure 1-4 shows the potential energy as a function of the BLA. In general, conjugated polymers have aromatic units as monomers, where the aromaticity is preserved in the polymer structure. Therefore, aromatic form is generally more stable than the quinoid form, and thus maximum point is shifted to the quinoid form. For this reason, to lower the bandgap, the BLA must be shifted to the quinoid form. On the contrary, to enlarge the bandgap, the BLA should be shifted into aromatic form. The individual strategies for controlling the bandgap will be discussed in the following:.

i) Stabilization of the quinoid form

As shown in Figure 1-5, the quinoid form can be stabilized by substituents, which have resonance structure, for example, isothianaphtenes (ITNs)[6], thieno[3,4-b]thiophenes (TTs)[11], cyanostyrylbenezenes, amine and nitro substituted aromatic rings.[12]

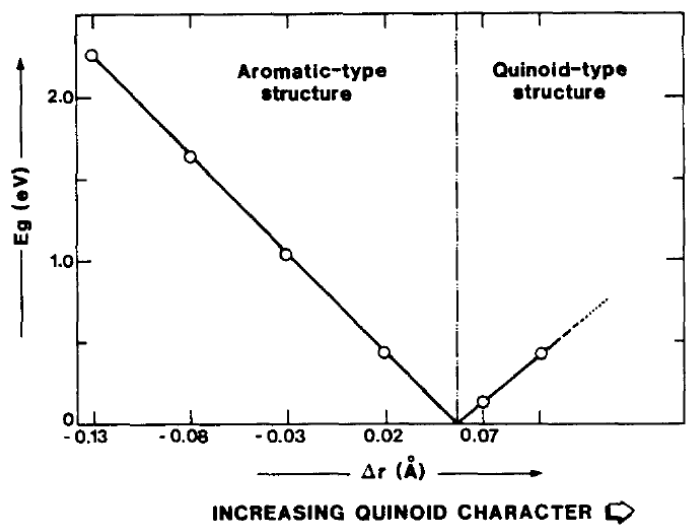

Figure 1-4. Evolution of the band gap as a function of increasing quinoid character of the backbone for polythiophene. ⊿r is the degree of bond-length alternation along the chain and corresponds to the difference between a carbon-carbon bond parallel to the chain axis and a carbon-carbon bond inclined with respect to that axis.[6]

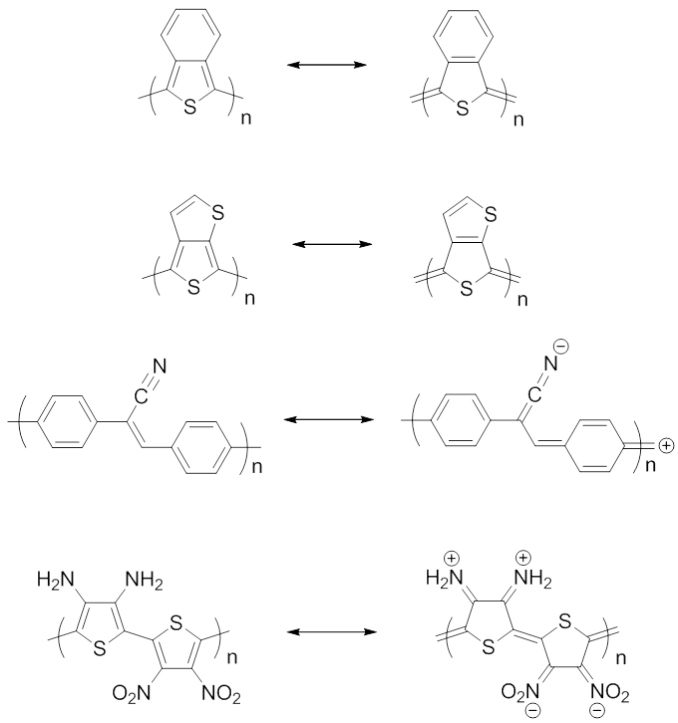

Figure 1-5. Stabilization of quinoid form (right side) by substituents.

ii) Aromaticity

Aromaticity leads to a confinement of the π-electron on the ring and competes with the delocalization. Therefore, the HOMO-LUMO gap is increased. For example, although 2,5-dialkylpyrrolo[3,4-c]pyrrole-1,4-dione (DPP) and 1,5-naphthyridine-2,6-dione (NDT) is very similar structure, NTD molecule and polymer have larger bandgap than that of DPP molecule and polymer, due to aromaticity of NTD molecule (Figure 1-6).[13]

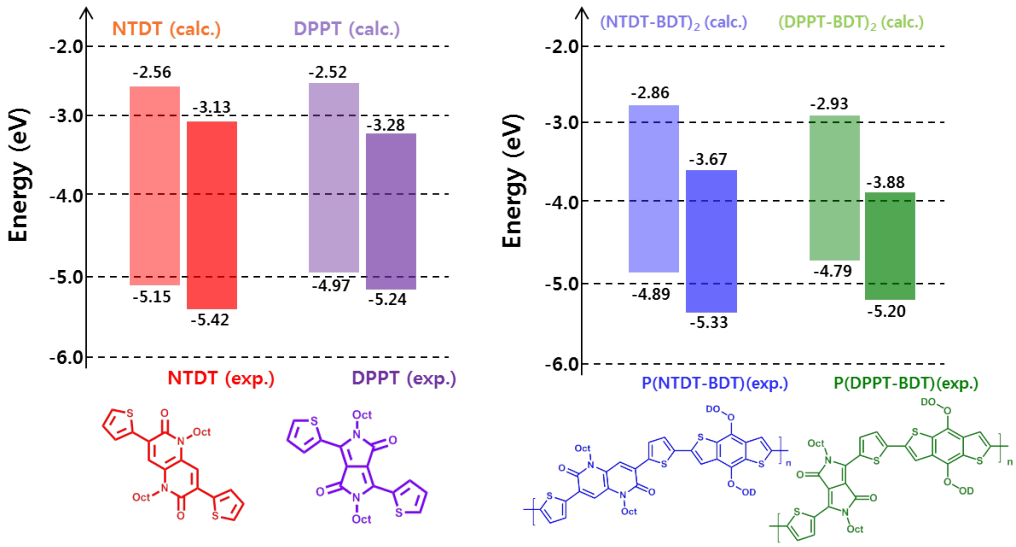

Figure 1-6. Energy levels of NTDT, DPP, and their polymers

iii) Donor-Acceptor alternating copolymer

An electron-rich donor unit and an electron-deficient acceptor alternating copolymer (D-A polymer) is a general design of low band gap polymer. This structure facilitates electron delocalization and the stabilization of quinoid form by resonance effect (D—A ↔ D^{+}=A^{-}) which lead to reduce the BLA. The low bandgap of D-A polymer can be explained by hybridization of the molecular orbital between the donor and acceptor in the D-A polymer. As shown in Figure 1-7, the HOMO of the donor interacts with that of the acceptor to yield two new HOMOs, and the LUMO of the donor will interact with that of the acceptor to yield two new LUMOs. As a result, a higher lying HOMO

and a lower lying LUMO are formed. In addition, HOMO and LUMO levels can be controlled by manipulating the intensity of donating and accepting abilities.[14]

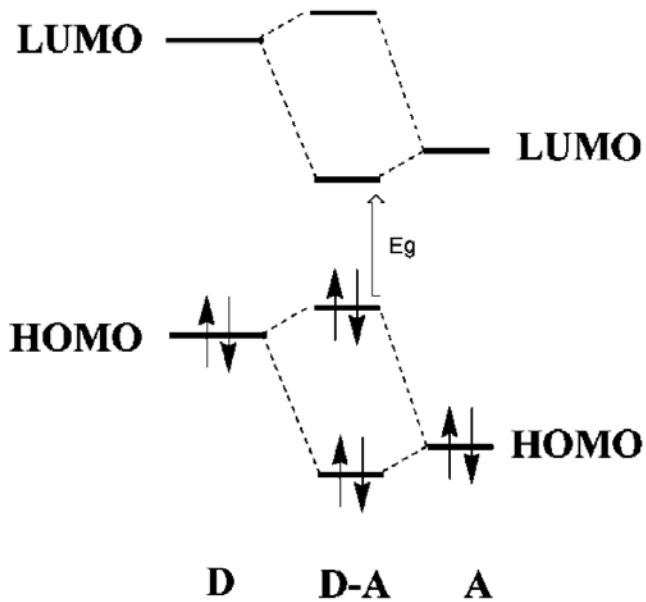

Figure 1-7. Orbital interactions of donor and acceptor units leading to a smaller band gap in a D-A conjugated polymer.[14]

As referred to earlier, for conjugated polymer efficient π-π stacking is the most important factor to achieve the high charge mobility. There are three strategies for efficient π-π stacking as follows:

a. Coplanarity

Planarity of conjugated backbone affects π-π stacking structure and molecular orientation. For conjugated polymer, coplanar structure in particular is essential for obtaining efficient π-π stacking. To achieve coplanarity, steric hindrance between

adjacent molecules should be reduced.[14,15] Therefore, less hindered five membered aromatic rings are most widely used as monomer. Another way to achieve high coplanarity is to use the intramolecular non-bonding interaction (Figure 1-8),[18] such as sulfur-fluorine interaction, carbonyl oxygen-sulfur interaction, and alkoxy oxygen-sulfur interaction.[16–18] In addition, the quinoid structure also enhances the planarity by increasing the double bonding characteristic of single bond between monomers.[14,]

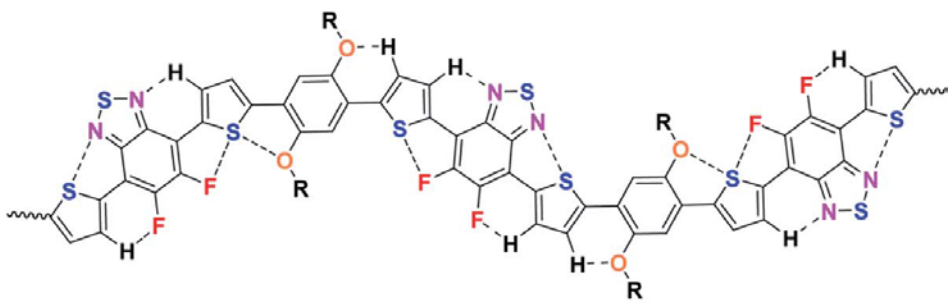

Figure 1-8. Noncovalent attractive interactions within the polymer chain.[18]

b. Tight packing

According to the Marcus theory, intermolecular π-π stacking distance affects efficient charge transport. To achieve the tight packing structure, coplanar structure is basically required. In addition, strong intermolecular interactions, such as dipole-dipole interaction, must be introduced in the molecular structure. The intermolecular interactions can be usually achieved by using the molecule consisting of sp2- or sp-hybridized nitrogen, sp2-hybridized oxygen, and fluorine.[15–18]

c. Large fused ring

According to the Marcus theory, transfer integral value is considered as most important factor for efficient charge transport in organic semiconducting molecules by hopping mechanism. Large π-orbitals increase the opportunities of wavefunction overlap between adjacent molecules.[19,20]

1.2. Organic solar cell

Organic solar cells (OSCs) have been extensively researched, because of their solution processability, light weight, and mechanical flexibility.[21] Typically, OSC devices consist of anode, anode interlayer, active layer, cathode interlayer, and cathode (Figure 1-9). For OSCs, most of active layers are a bulk heterojunction type, which can overcome the exciton diffusion length of organic semconductors (Figure 1-9).[22]

Figure 1-9. Device architecture of the bulk heterojunction solar cell.[22]

The operation of OSCs proceeds in the order of photoexcitation of donor and/or acceptor, charge-transfer (CT) exciton generation in the donor-acceptor interface by photoexcited electron transfer (PET), and then free charge carrier generation by CT exciton dissociation. The free charge carriers transport to each electrodes (Figure 1-10).[14] In general, free carriers are generated though two pathways, channel I and channel II (Figure 1-11).[23] For channel I case, because of photoinduced electron transfer mechanism, charge separation process requires EA_A-EA_D > $E_D^{binding}$ (EA often equated to the LUMO energy). For channel II case, because of photoinduced hole transfer mechanism, charge separation process requires IP_A-IP_D > $E_A^{binding}$ (IP often equated to the HOMO energy).

The power conversion efficiency (PCE) is determined by the percentage ratio of output maximum electrical power (P_{max}) over the incident light power density (P_{in}). The Pmax is determined by open-circuit voltage (V_{OC}), short-circuit current density (J_{SC}), and fill factor (FF). Thus, PCE is determined by the following formula:

$$\eta_e = \frac{V_{oc} * I_{sc} * FF}{P_{in}}$$

These parameters evaluated from the current density-voltage (*J*-*V*) curve (Figure 1-12). The V_{OC} is the maximum voltage delivered when the current is zero. The V_{OC} is known to be proportional to the energy difference between HOMO of the donor and LUMO of the acceptor. The OSC device shows the V_{OC} that is always less than the absorbed minimum photon energy, because of energy loss (E_{loss}) during the OSC operation. E_{loss}

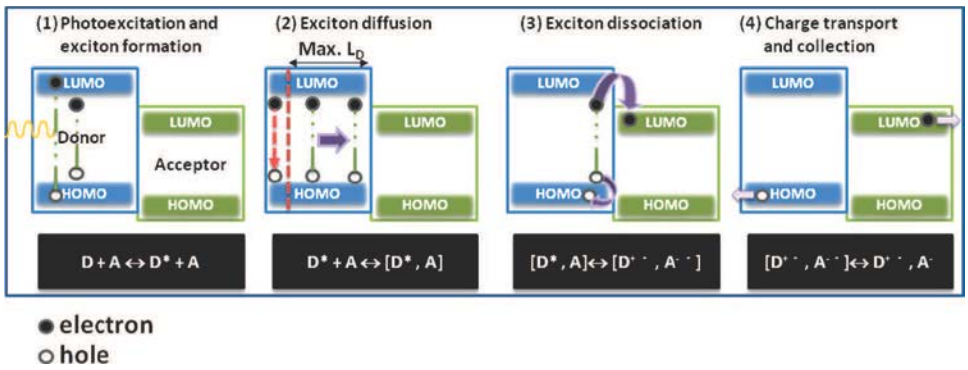

Figure 1-10. Working mechanism for donor-acceptor heterojunction solar cells.[14]

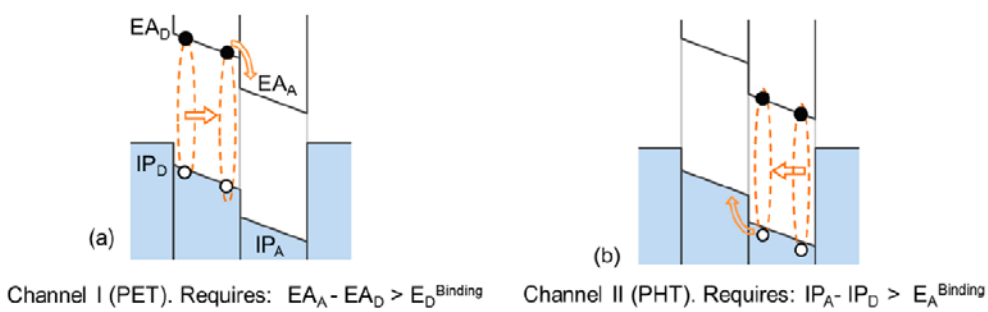

Figure 1-11. Charge generation pathways.[13]

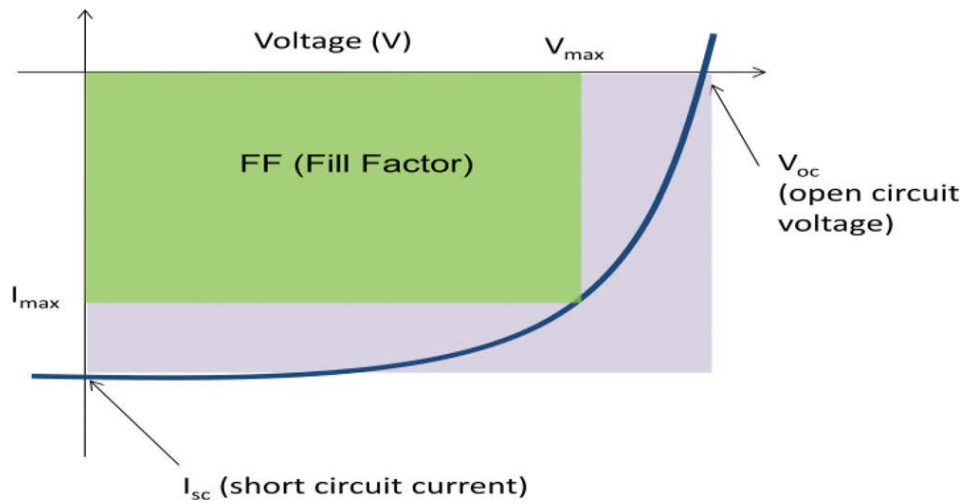

Figure 1-12. Current density vs. voltage (j vs. V) of a solar cell.[22]

is known to be sum of the three energy loss terms (Figure 1-13): energy loss from charge transfer exciton formation (ΔE2), energy loss induced by radiative recombination (ΔE1), and energy loss induced by non-radiative recombination (ΔE3). For OSC device, ΔE2 is known to be over 0.3 eV, which is exciton binding energy, and thus E_{loss} in OSCs (usually 0.7~1.0 eV) is much larger than those of inorganic and perovskite devices (0.4 ~ 0.55 eV).[24–26]

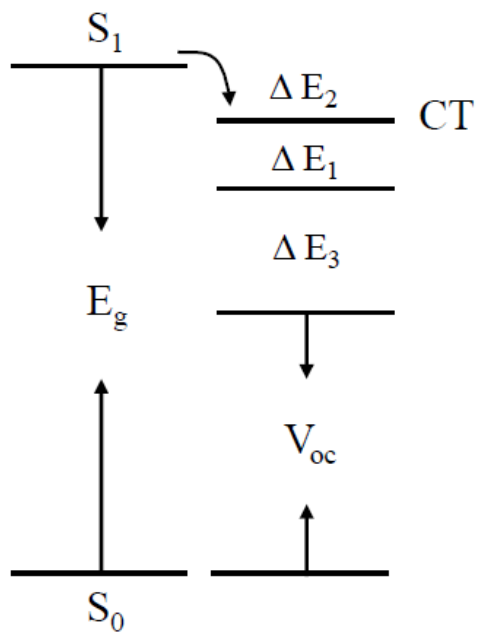

Figure 1-13. Energy diagrams of organic solar cells. Energy diagram showing the relationship of optical bandgap (E_{gap}), lowest singlet state (S^1), chargetransfer (CT) state, V_{OC} and the three terms of energy losses.[26]

The FF means the efficiency of the generated free electrons and holes reaching the electrode. Therefore, the FF is affected by carrier extraction and recombination. For this reason, hole and electron mobilities and their balance of the device is important factor to achieve high FF.[27]

The J_{SC} is the maximum current delivered when the voltage is zero. The J_{SC} is affected by various factors, such as active morphology, light absorption, mobility, FF, and energy offset of donor and acceptor.[28]

1.3. Organic Field-Effect Transistor

Organic Field-Effect Transistor (OFET) devices consist of gate electrode, insulating gate dielectric layer, organic semiconductor, source electrode, and drain electrode. OFET devices are classified according to the electrode and semiconductor positions as follows: i) bottom-gate top-contact, ii) bottom-gate bottom-contact, iii) top-gate bottom-contact, iv) top-gate top-contact (Figure 1-14). OFETs are also classified according to carrier charge type as follows: i) p-type (hole), ii) n- type (electron), iii) ambipolar (hole and electron).[29]

OFET device works by manipulating the gate voltage (V_g) and the source/drain voltage (V_{ds}) (Figure 1-15).[29] When $V_g = 0$, only a small amount of currents can flow between the source and drain electrodes, which is called off-state. For p-type OFET, a negative voltage is applied in gated electrode, and then hole carriers in the organic

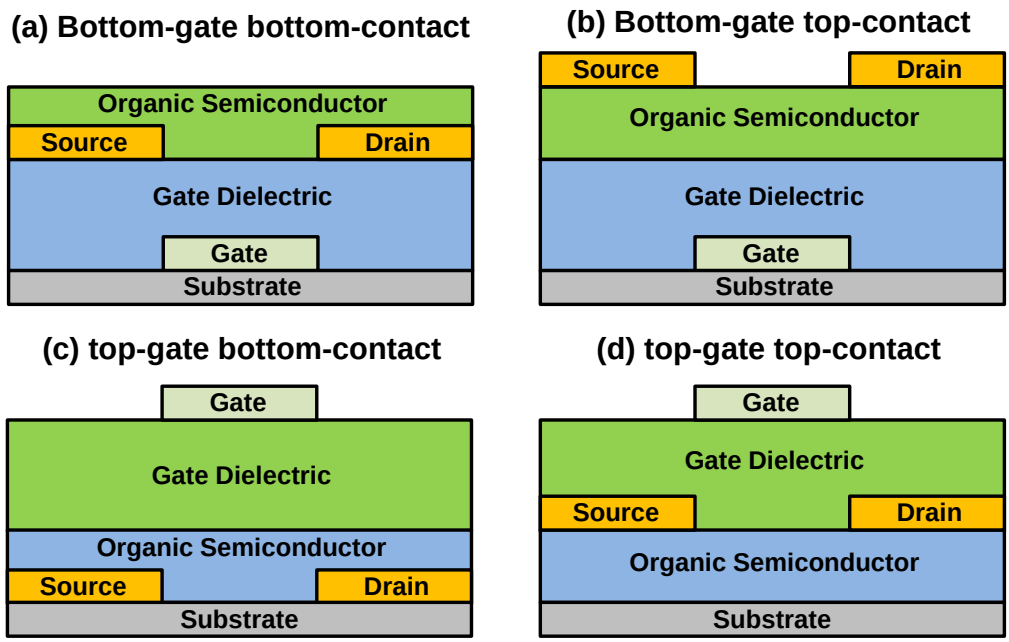

Figure 1-14. OFET device types: (a) Bottom-gate bottom-contact, (b) bottom-gate top-contact, (c) top-gate bottom-contact, (d) top-gate top-contact

semiconductor layer are accumulated at the interface with the gate dielectric. The charge carriers in semiconductors are usually supplied by injection from the source electrode into the semiconductor. If a negative voltage is applied in drain electrode, the Fermi level of drain electrode become close to the HOMO level of semiconductor, and then hole carrier transport from source to drain occurs, which is called on-state. When $V_{ds} \ll V_g$, current flowing through the channel is directly proportional to V_{ds}, which is called the linear regime. When the V_{ds} is further increased, a point $V_{ds} = V_g$ - threshold voltage (V_{Th}) is reached, where the channel is "pinched off". If Vds is further increased, the V_{ds} gradually becomes saturated, which is called the saturation regime. In case of n-type OFET, working principle is the same, but the voltages (V_g and V_{ds}) are opposite.[29] The field-effect mobility can be calculated by the following equation.

<linear regime>

$$\mu_{lin.} = \frac{\partial I_{ds}}{\partial V_g} \cdot \frac{L}{W C_i V_{ds}}$$

<saturation regime>

$$\mu_{sat.}(V_g) = \frac{\partial I_{ds,sat}}{\partial V_g} \cdot \frac{L}{W C_i} \cdot \frac{1}{V_g - V_{thi}}$$

Where, Ci is the capacitance per unit area of the gate dielectric, W is th channel width.

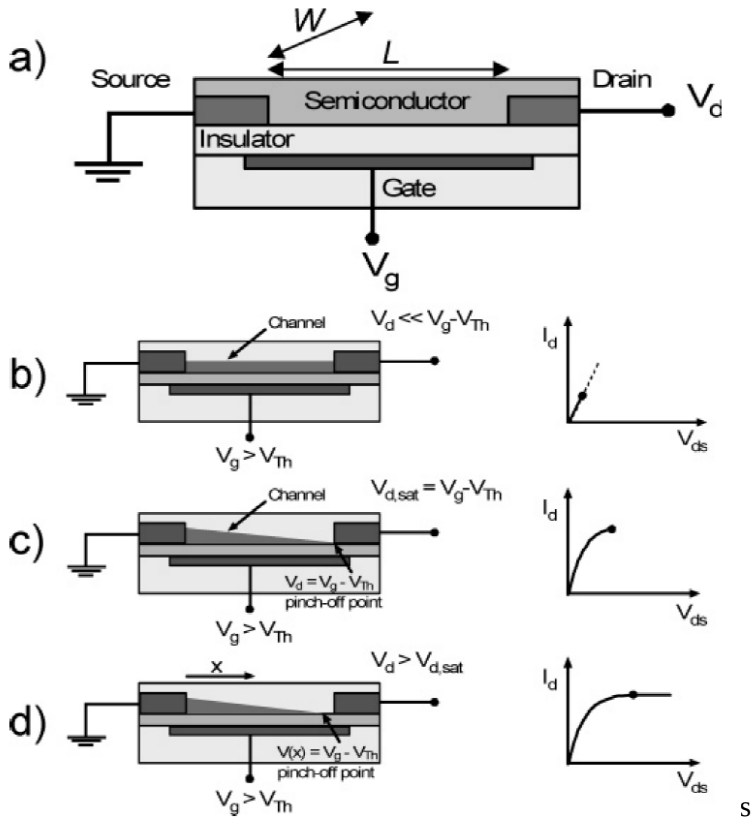

Figure 1-15. Schematic structure o of operating regimes of field-effect transistors: (b) linear regime; (c) start of saturation regime at pinchoff; (d) saturation regime and corresponding current-voltage characteristics.f a field-effect transistor and applied voltages: (b-d) Illustrations.[29]

1.4. Research Objective

The numerous conjugated polymer designs have been developed for high charge transporting properties. Among them, although the vinylene group has fascinating features for designing the conjugated polymer with good charge transport properties, it has received little attention as a semiconductor for OFET and OPV applications, due to their low device performance arising from the poor charge transport properties. The reason of this poor charge transport based on the structural disorders of the vinylene group, which is disadvantageous to π-π stacking. In this respect, vinylene containing polymers have the potential to enhance the charge transport properties by improving this problem. In this study, I will provide new vinylene conjugated polymers for high performance OSC and OFET applications, and also propose design strategies to realize the high performances.

In Chapter 2, design of a stereoregular vinylene containing conjugated polymer will be presented for high-performance OSC applications.

In Chapter 3, development of a stereoregular cyano-vinylene containing conjugated polymer will be presented for high-performance and small energy loss OSC applications.

In Chapter 4, design of highly balanced and thermally stable ambipolar semiconducting polymer using cyanovinylene linker will be presented for high-performance OFET applications.

1.5. References

[1] A. J. Heeger, Journal of Physical Chemistry B 2001, 105, 8475

[2] H. Shirakawa, E. J. Louis, A. G. MacDiarmid, C. K. Chiang, A. J. Heeger, Journal of The Chemical Society: Chemical Communication 1977, 578

[3] C. K. Chiang, C. R. Jr. Fincher, Y. W. Park, A. J. Heeger, H. Shirakawa, E. J. Louis, S.C. Gau, A. G. MacDiarmid, Physical Review Letters 1977, 39, 1098

[4] R. E. Peierls, “Quantum Theory of Solids”, Oxford, Clarendon Press, London 1956

[5] Y. Lu. “Solitons & polarons in conducting polymers”, World Scientific Publishing, 1988

[6] Bredas, J.-L., A. J. Heeger, F. Wudl, 1986, J. Chem. Phys.85, 4673

[7] A. J. Heeger, S. Kivelson, J. R. Schrieffer, and W.-P. Su, Rev. Mod. Phys 1988, 60, 781

[8] Bredas, J.-L. et al. Chem. Rev. 2007, 107, 926–952

[9] Prins, P.; Grozema, F. C.; Schins, J. M.; Patil, S.; Scherf, U.; Siebbeles, L. D. A. Phys. Rev. Lett. 2006, 96, 146601

[10] F. C. Grozema et al., Adv. Mater. 2002, 14, 228.

[11] Pomerantz, M.; Gu, X. Synth. Mater. 1997, 84, 243

[12] Zhang, Q. T.; Tour, J. M. J. Am. Chem. Soc. 1998, 120, 5355.

[13] W. S. Yoon, D. W. Kim, J.-M. Park, I. Cho, O. K. Kwon, D. R. Whang, J. H. Kim, J.-H. Park and S. Y. Park, Macromolecules, 2016, 49, 8489-8497.

[14] Cheng, Y. J., Yang, S. H., Hsu, C. S. Chem. Rev. 2009, 109, 5868–5923.

[15] J. M. Jiang, M. C. Yuan, K. Dinakaran, A. Hariharan and K. H. Wei, J. Mater. Chem. A, 2013, 1, 4415–4422

[16] J. W. Jo, J. W. Jung, H.-W. Wang, P. Kim, T. P. Russell and W. H. Jo, Chemistry of Materials, 2014, 26, 4214-4220.

[17] N. Leclerc, P. Chávez, O. Ibraikulov, T. Heiser and P. Lévêque, Polymers, 2016, 8, 11.

[18] T. L. Nguyen, H. Choi, S.-J. Ko, M. A. Uddin, B. Walker, S. Yum, J.-E. Jeong, M. H. Yun, T. J. Shin, S. Hwang, J. Y. Kim, H. Y. Woo, Energy Environ. Sci. 2014 , 7 , 3040 .

[19] H. Yao, L. Ye, H. Zhang, S. Li, S. Zhang and J. Hou, Chemical reviews, 2016, 116, 7397-7457.

[20] S. Zhang, L. Ye and J. Hou, Advanced Energy Materials, 2016, 6, 1502529.

[21] L. Lu, T. Zheng, Q. Wu, A. M. Schneider, D. Zhao and L. Yu, Chemical reviews, 2015, 115, 12666-12731.

[22] Heeger, A. J. Adv. Mater. 2014, 26, 10-28.

[23] D. M. Stoltzfus, J. E. Donaghey, A. Armin, P. E. Shaw, P. L. Burn and P. Meredith, Chem. Rev., 2016, 116, 12920-12955

[24] D. Veldman, S. C. J. Meskers and R. A. J. Janssen, Advanced Functional Materials, 2009, 19, 1939-1948.

[25] W. Li, K. H. Hendriks, A. Furlan, M. M. Wienk and R. A. Janssen, Journal of the American Chemical Society, 2015, 137, 2231-2234.

[26] J. Liu, S. Chen, D. Qian, B. Gautam, G. Yang, J. Zhao, J. Bergqvist, F. Zhang, W.

Ma, H. Ade, O. Inganäs, K. Gundogdu, F. Gao and H. Yan, Nature Energy, 2016, 1, 16089.

[27] Guo, X. et al. Nature Photon. 2013, 7,825-833

[28] Li, G., Zhu, R., Yang, Y. Nature Photon. 2012, 6, 153–161.

[29] J. Zaumseil, H. Sirringhaus, Chem. Rev. 2007, 107, 1296

Chapter 2.

Application of a Two-Dimensional Benzo[1,2-b:4,5-b □]dithiophene Poly(arylene vinylene) Copolymer for High-Performance Polymer Solar Cells

2.1. Introduction

Over the past decades, bulk-heterojunction (BHJ) polymer solar cells (PSCs) have been extensively researched because of their advantages such as solution processability, mechanical flexibility, and light weight.[1] The progress of research into PSCs has increased mainly because of the development of donor polymers.[2–5] To achieve high power conversion efficiencies (PCE), the donor material should meet several requirements: it should have a narrow bandgap, good charge transport properties, a deep HOMO level, and a proper domain size.[6] In addition, recently, high-performance donor polymers with wide band gap for tandem solar cells and non-fullerene solar cells have been actively studied.[1,7–9]

In principle, the charge transport properties, which are the most important property of donor polymers, are proportional to the degree of intermolecular π-orbital overlap, which can be increased by using a fused aromatic ring or by improving the coplanarity of the conjugated backbone.[10] In particular, coplanarity is known to play an important role in the molecular stacking of conjugated polymers. Indeed, state-of-the-art donor

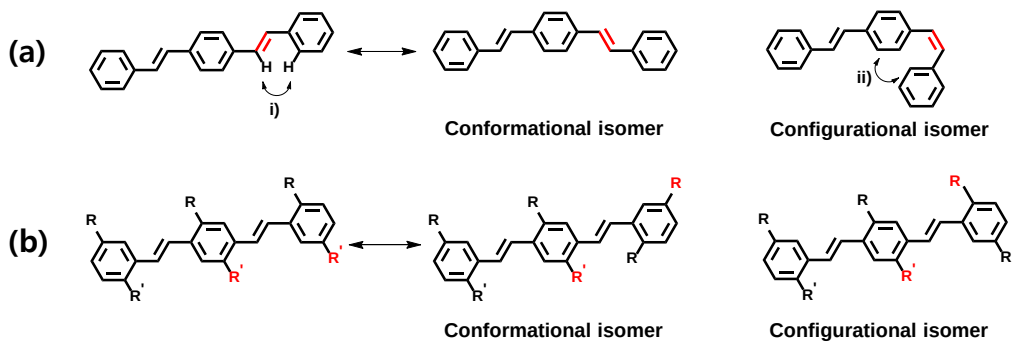

Figure 2-1. Structural disorder of the (a) vinylene group, (b) asymmetric side chain of the poly(phenylene vinylene) backbone, and possible steric repulsion between i) vinyl and phenyl protons ii) cis-phenyl protons.

polymers, for example, PTB7-Th[5,11] and PffBT4T,[12,13] are predominantly composed of five-membered aromatic rings and aromatic rings substituted with fluorine atoms, which relieve the angular strain in a coplanar conformation and induce nonbonding interactions between adjacent molecules that force a coplanar backbone.[14,15] On the other hand, although the introduction of vinylene is another efficient way to increase the coplanarity of backbone, poly(arylene vinylene)s have received little attention as semiconductors for PSCs and organic field-effect transistors (OFETs) because of the low performance arising from the poor charge transport properties. For example, poly(phenylene vinylene) (PPV) exhibits a low hole mobility ($\mu_{h,FET}$ ~ 10^{-4} cm^2 $V^{-1}s^{-1}$, $\mu_{h,SCLC}$ ~$10^{-7}cm^2$ $V^{-1}s^{-1}$)[16,17] compared to other conjugated polymers without vinylene, such as poly(3-hexylthiophene) (P3HT) ($\mu_{h,FET}$ ~ 10^{-2} cm^2 $V^{-1}s^{-1}$, $\mu_{h,SCLC}$ ~ ~10^{-4} cm^2 $V^{-1}s^{-1}$).[18,19] This poor charge transport arises from structural disorder in the vinylene group and the asymmetric side chain and from insufficient coplanarity arising from steric repulsion between the vinylene and phenyl ring protons, as shown in Figure 2-1. This structural disorder and lack of coplanarity interfere with efficient π-π stacking.[20] There are several synthetic approaches to reduce these structural disadvantages, such as the synthesis of trans-stereoregular PPV by the Horner–Wadsworth–Emmons reaction (HWE)[21,22] and side chain regioregular PPV by homopolymerization using the HWE reaction.[23,24] In addition, PPV without side chain configurational disorder can be prepared using symmetric side chains.[25] Recently, Jian Pei et al. developed a PPV with high coplanarity and a regular backbone structure by bridging vinylene and phenyl

rings using electron deficient lactone and lactam bridges, resulting in high FET electron mobility of up to 1 $cm^2 V^{-1}S^{-1}$.[20] While this approach effectively reduces the structural disadvantages of arylene vinylene, there is little synthetic versatility.

Recently, we have reported PPV-type copolymer (PPVTV) with significantly improved charge transport properties.[22,26] This PPVTV contains phenyl ring with symmetric side chains and thiophene unit connected by trans-isomeric vinylene, inducing a regular structure and remarkably high coplanarity in the backbone (Figure S1) and resulting in excellent π-π stacking. This polymer results in an OFET hole mobility of up to 0.06 $cm^2 V^{-1}S^{-1}$ and a relatively high PCE of 3.5% in PSCs with $PC_{61}BM$ as an acceptor[22,26] compared with poly[2-methoxy-5-(3′,7′-dimethyloctyloxy)-1,4-phenylenevinylene] (MDMO)-PPVs, which have a maximum FET hole mobility of ~10^{-7} $cm^2 V^{-1}S^{-1}$ [17] and a PCE of 2.5% in PSCs with $PC_{61}BM$ as an acceptor.[27] These results demonstrate the feasibility of using poly(arylene vinylene)s as high-performance donor materials and will hopefully motivate materials chemists to explore the structural modification of poly(arylene vinylene)s to improve PSC performance.

We have focused on developing new poly(arylene vinylene) donor with good charge transport properties. A specific design for improving the charge transport properties was implemented by introducing a two-dimensional benzodithiophene (2D-BDT), which is a good charge transport moiety because of its π-extended planar molecular structure,[4] into the backbone of our previously reported trans-stereoregular and highly coplanar poly(arylene vinylene), PPVTV.[26] Finally, we designed and synthesized a

new poly(arylene vinylene), **PBDS**, that exhibits not only an improved SCLC hole mobility but also a deeper HOMO, which are beneficial characteristics for obtaining high open-circuit voltages (V_{OC}) and short-circuit currents (J_{SC}). We have analyzed the photovoltaic properties of **PBDS** using PSC devices with $PC_{71}BM$ as an acceptor. In addition, we discuss the detailed characteristics of **PBDS** and its blend film using optical, electrochemical, and morphological analysis.

2.2. Results and Discussion

Scheme 1 shows the synthetic route to **PBDS**. To obtain a trans-stereoregular polymer with a high molecular weight, we used the Stille coupling reaction using a trans-isomeric monomer (M2) instead of the HWE reaction because the HWE reaction uses a THF as a solvent, which is a poor solvent for high-molecular-weight conjugated polymers. Thus, by using the Stille coupling reaction, we successfully synthesized high-molecular-weight **PBDS** (M_n = 88 kDa, M_w = 184 kDa). To determine the molecular structure, ^{1}H-NMR spectra were measured. As shown in Figure 2-3, the NMR results show that **PBDS** has only a proton of the alkoxy side chain of the *trans*-vinylene structure.[28]

Density functional theory (DFT) calculations at the B3LYP/6–31G(d,p) level of theory were performed to analyze the optimized molecular geometry and its frontier

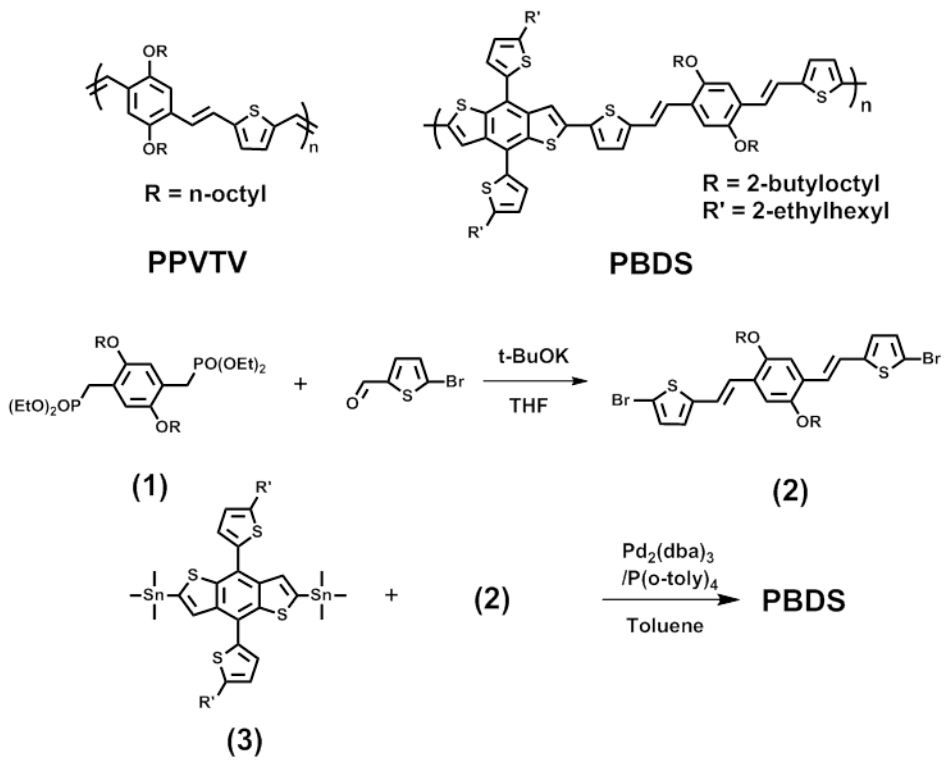

Figure 2-2. Chemical structures of PPVTV and **PBDS**, and the synthetic route to **PBDS**.

molecular orbitals. As illustrated in Figure 2-4, both the highest occupied molecular orbital (HOMO) and the lowest unoccupied molecular orbital (LUMO) of **PBDS** are delocalized over the whole conjugated backbone, which is a common feature of conjugated polymer consisting solely of donating moieties. The calculations show that the HOMO of **PBDS** is deeper than that of PPVTV, despite the similar backbones. This can be explained by the fact that the phenyl group of BDT has its HOMO delocalized over three carbons (as shown by a dashed red rectangle in Figure 2-4), unlike dialkoxy phenyl and thiophene, which have their HOMOs delocalized over only two atoms. A delocalized HOMO induces a larger aromatic stabilization energy, resulting in a deeper HOMO level, which is beneficial for obtaining high V_{OC} values. Furthermore, the BDT homopolymer has been reported to have high a V_{OC}. In the meantime, **PBDS** contains a coplanar PPVTV backbone structure (as shown by a dashed green rectangle in Figure 2) and exhibits a curved conformation, which are beneficial for OSC applications, because this curved backbone geometry provides a small crystalline size and good miscibility with PCBM.[29,30]

To investigate the effect of the structural modifications on the optical and electronic properties of the polymer, we measured UV-Vis absorption spectrum and cyclic voltammetry (CV) curves of **PBDS**, PPVTV, and MDMO-PPV films (Figure 2-5). Figure 3a shows the absorption spectra of the **PBDS**, PPVTV, and MDMO-PPV films. The optical band gap of **PBDS** is same as that of PPVTV (2.0 eV) but smaller than that of MDMO-PPV (2.15 eV). Like the spectrum of PPVTV, that of the PBD film also

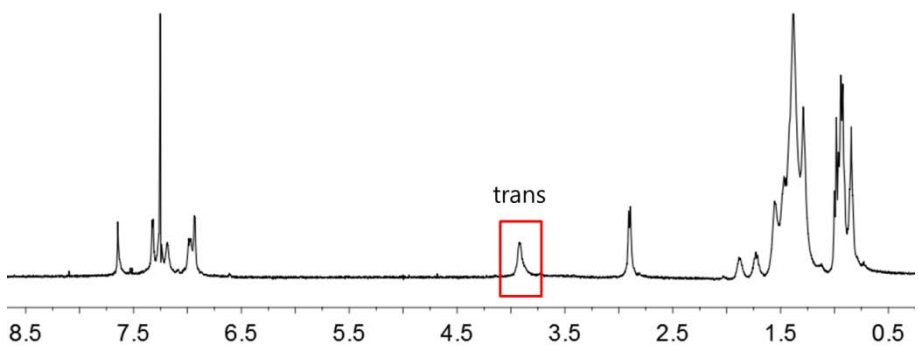

Figure 2-3. ^{1}H-NMR data of **PBDS.**

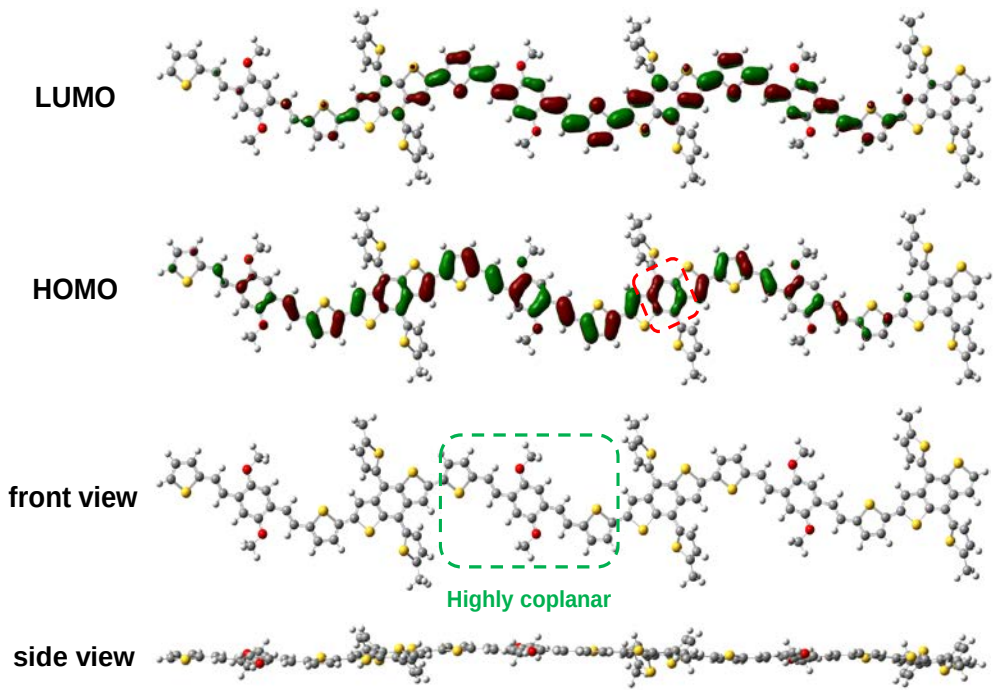

Figure 2-4. Geometries of HOMO, LUMO, and map of electrostatic potential (ESP) surfaces of optimized molecular structure for the trimer model compounds of the polymers. Calculation were performed by the DFT method at B3LYP/6-31G(d,p) level. To simplify the calculation, alkyl chains were replaced with methyl group.

exhibits a distinct 0-0 vibronic peak, corresponding to a coplanar and π-π stacking structure. The HOMO levels of the polymers were evaluated from the onset reduction potentials in the CV curves. As shown in Figure 2-5b, the HOMO level of **PBDS** (−5.20 eV) is deeper than that of PPVTV (−5.08 eV) and even that of MDMO-PPV (−5.13 eV), which is good agreement with the results of the DFT calculations. These results indicate that the introduction of 2D-BDT provides a deep HOMO level while maintaining a good stacking structure.

For a quantitative analysis of the charge transport properties, we measured the SCLC mobilities of the polymers. Because the SCLC mobility is influenced by the thickness of the semiconductors and by the morphology of the blend with the acceptor, three pure polymer films having similar thicknesses were measured. As shown in Figure 2-6, the results show that **PBDS** has a hole mobility of 6.1×10^{-4} cm $V^{-1}S^{-1}$, values increased by ~ 50 % compared to those of PPVTV (4.1×10^{-4} cm^2 $V^{-1}S^{-1}$), respectively. This increased mobility is consistent with the design objective for **PBDS** mentioned in the Introduction.

The photovoltaic performance of **PBDS** was assessed using BHJ PSC devices containing a $PC_{71}BM$ acceptor. To optimize the morphology of the active layer, two additional devices with active layers treated either by thermal annealing or the addition

of the 1,8-diiodooctane (DIO) as a solvent additive were fabricated. Details of the device fabrication procedures are described in the Experimental section. Figure 2-7

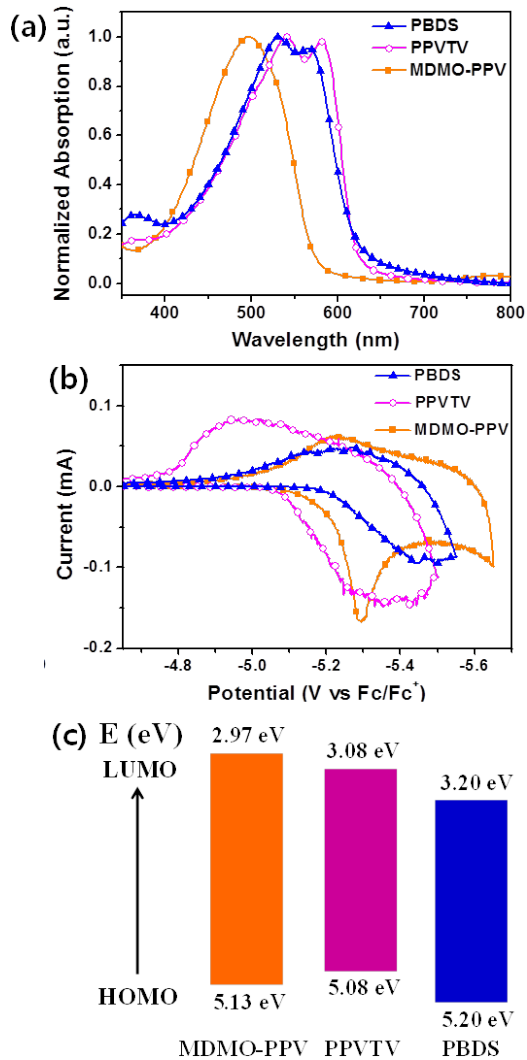

Figure 2-5. (a) UV-Vis absorption spectra, (b) cyclic voltammograms, and (c) HOMO and LUMO energy levels of PBDS, PPVTV, and MDMO-PPV.

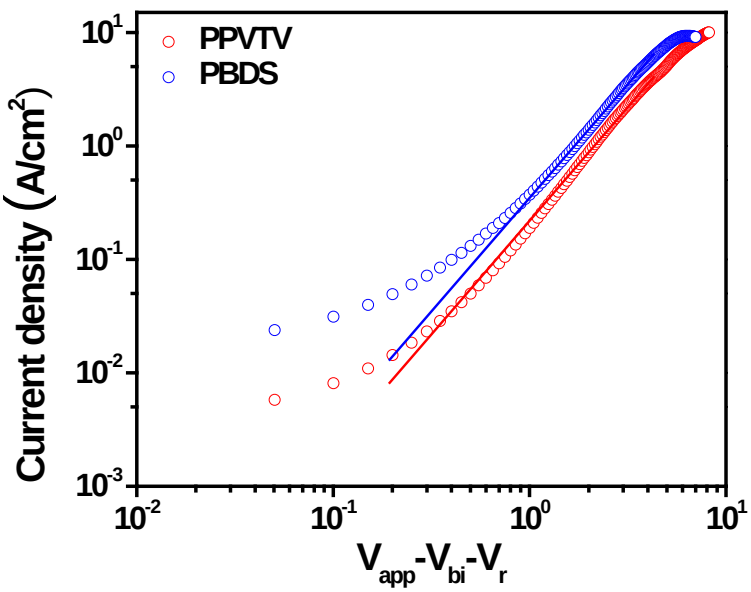

Figure 2-6. *J-V* curves of the hole-only devices of PBDS and PPVTV polymers.

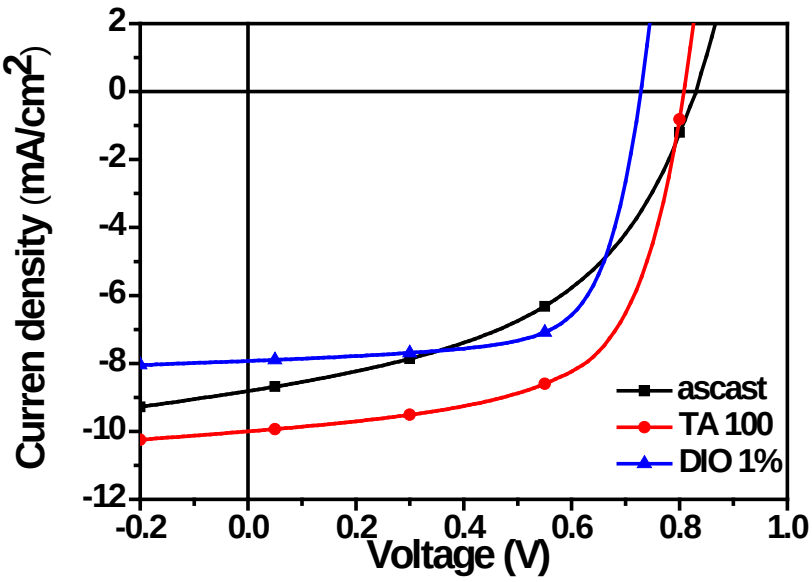

Figure 2-7. J-V curves of PBDS:$PC_{71}BM$ BHJ devices prepared under different conditions.(as cast, thermal annealing 100 C 10min, 1,8-diiodooctane 1vol %)

Polymer : Acceptor	V_{oc} [V]	J_{sc} [mA cm^{-2}]	FF	PCE [%]	
PBDS:$PC_{71}BM$[a)]	0.83	8.81	0.47	3.5	This work
PBDS:$PC_{71}BM$[b)]	0.81	10.0	0.62	5.0	This work
PBDS:$PC_{71}BM$[c)]	0.73	7.93	0.68	4.0	This work
PPVTV:$PC_{61}BM$	0.68	8.0	0.63	3.5	ref 27
MDMO-PPV:$PC_{71}BM$	0.77	7.6	0.51	3.0	ref 32

Table 2-1. Photovoltaic parameters of PBDS:$PC_{71}BM$ BHJ devices prepared under different conditions.

shows the current density–voltage (*J*–*V*) curves, and detailed photovoltaic results are listed in Table 2-1. The **PBDS**:$PC_{71}BM$ device with an as cast active layer had a PCE of 3.48%, V_{OC} of 0.83 V, J_{SC} of 8.81 $mAcm^2$, and FF of 47.6%, in which the V_{OC} value is 0.15 V higher than that of PPVTV. This high V_{oc} is due to the deep HOMO, which arises from the aromatic stabilization of 2D-BDT. After thermal annealing treatment, the J_{SC} and FF increased to 10.0 $mAcm^2$ and 61.8%, respectively, resulting in a PCE of 5%, which is the highest value among the poly(arylene vinylene):PCBM-based PSCs. On the other hand, when using the DIO solvent additive, the **PBDS**:$PC_{71}BM$ device showed a high FF of 68.4%, whereas the V_{OC} and J_{SC} decreased to 0.73 V and 7.93 $mAcm^2$, respectively, resulting in a PCE of 3.96%.

To understand the performance differences of films prepared under different conditions, we measured grazing incidence wide angle X-ray scattering (GIWAXS) patterns and used atomic force microscopy (AFM). These techniques provide information on the morphologies and packing structures of the pure polymers and blend films. As shown in Figure 2-8, the as-cast and thermally annealed **PBDS**:$PC_{71}BM$ films have smooth surfaces with small root-mean-square roughness (RMS) values of about 0.5 nm. Such smooth surfaces and well-mixed films without additives may be due to the small size of polymer crystallites and the amorphous nature of **PBDS**, induced by the curved backbone.[29,30] In contrast, the DIO added film had a rough surface (RMS = 1.40 nm) and a large domain size (~50 nm) (Figure 2-8.d).

The domains are much larger than the exciton diffusion length of conventional conjugated

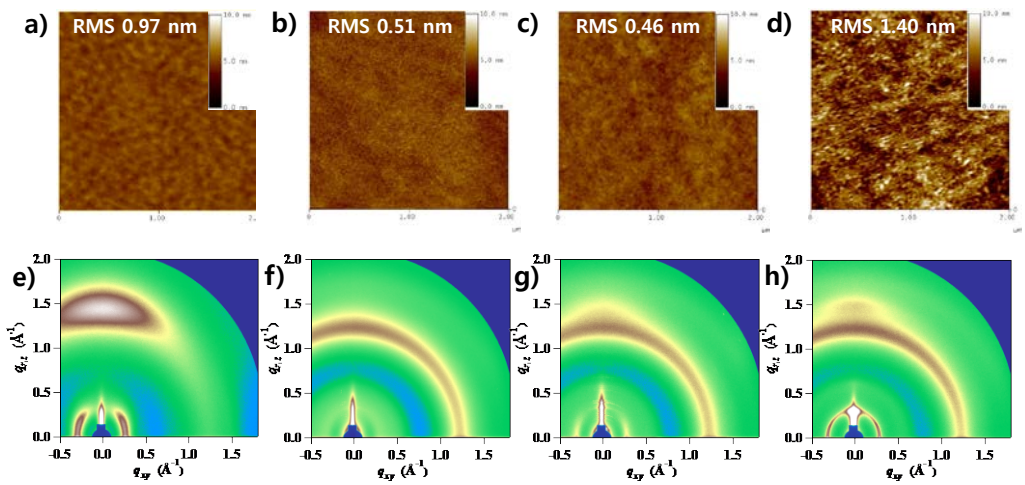

Figure 2-8. AFM height images (2 μm × 2 μm) and 2D-GIWAXS images of PBDS film (a,e) and PBDS:$PC_{71}BM$ blend films under different conditions: as a cast film (b,f), thermally annealed film (c,g), and DIO-added film (d,h).

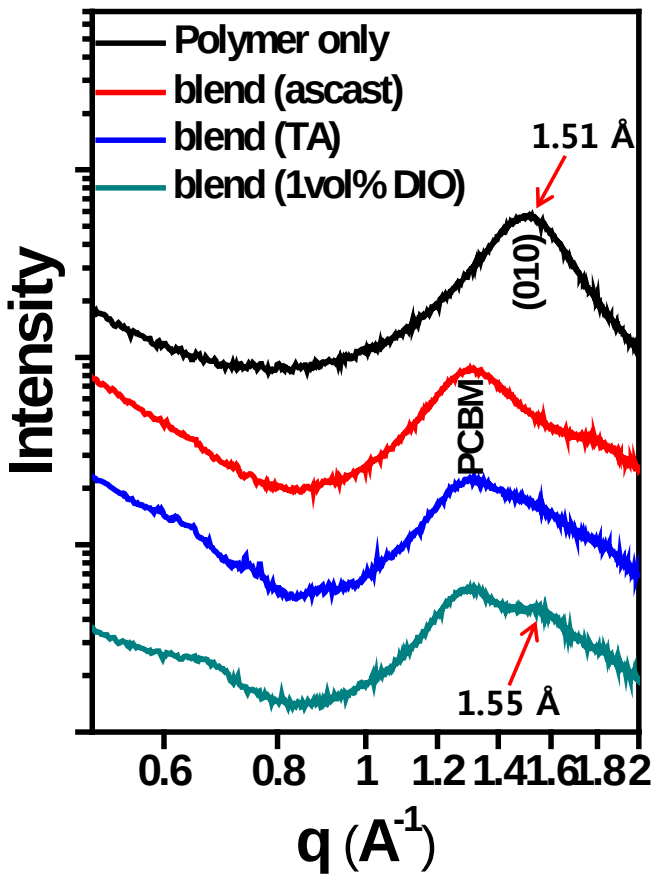

Figure 2-9. Out-of-plane (q_{xy} = 0) X-ray diffraction patterns of the PBDS film and PBDS:$PC_{71}BM$ blend films prepared under different conditions.

polymers (10–15 nm),[32] which contributes to the low J_{SC} of 7.93 mAcm^2. Figure 2-8. show the 2D-GIWAXS images of the pure polymer and blend films under different conditions. The (010) diffraction peak for the **PBDS** film was observed at $q_z \approx 1.51$ Å^{-1}, which indicates a polymer face-on orientation with a π-π stacking distance of 4.16 Å. The coherence length of the π–π stacked structures was determined by calculation using the Scherer equation and the full width at half-maximum (FWHM) of the (010) diffraction peak.[33] The FWHM of the (010) peak of the **PBDS** film is 0.34 Å^{-1} with a correspondingly small coherence length of 1.8 nm, which is similar to that of the PTB7:$PC_{71}BM$ blend film.[34] The as-cast blend film exhibits only a ring-shaped diffraction pattern arising from PCBM, which implies that **PBDS** and $PC_{71}BM$ are mixed on the molecular scale, resulting in the poor π–π stacking of **PBDS**. It is most likely that the poor stacking of **PBDS** results in a reduction in the charge transport properties, thereby resulting in poor J_{SC} and FF values. As shown in Figure 2-8g, the thermal annealing treatment recovers the π–π stacking of **PBDS**, resulting in an increase in both J_{SC} and FF. When using a solvent additive, the π–π stacking diffraction of **PBDS** is recovered, and the polymer diffraction peak separates from the diffraction peak of $PC_{71}BM$; moreover, the π–π stacking distance becomes smaller, from 4.16 Å (q = 1.51 Å^{-1}) to 4.05 Å (q = 1.55 Å^{-1}). While such tight π–π stacking results in a high FF of 68.4%, it induces large domains (Figure 2-8d), leading to a reduction in J_{SC} (Table 2-1). From the morphological analyses, we have found that the

thermal annealing treatment results in a blend film with the optimum morphology, which is consistent with the photovoltaic results.

2.3. Experimental

2.3.1. Materials

Materials obtained from commercial suppliers were used without further purification. tetraethyl ((2,5-bis((2-hexyldecyl)oxy)-1,4-phenylene)bis(methylene))bis(phosphonate) (1)[35] (4,8-bis(5-(2-ethylhexyl)thiophen-2-yl)benzo[1,2-b:4,5-b']dithiophene-2,6-diyl)bis(trimethylstannane) (3)[36] were synthesized using the procedure reported elsewhere. 1H and 13C NMR spectra were recorded on Bruker Avance 500 spectrometers. Mass spectra wre measured using a Voyager-DETM STR Biospectrometry Workstation, and elemental analyses were performed on a CE Instrument EA1110 instrument.

2.3.2. Synthesis

5,5'-((1E,1'E)-(2,5-bis((2-hexyldecyl)oxy)-1,4-phenylene)bis(ethene-2,1-diyl))bis(2-bromothiophene) (2)

Compound (1) (397 mg, 0.53 mmol), 5-bromothiophene-2-carbaldehyde (223 mg, 1.17 mmol), potassium-tert-butoxide (128 mg, 1.17 mmol), and THF (10ml) were added in 25ml flask. The mixture was heated at 70 °C for 3h. After aqueous work-up, the mixture was dried over anhydrous $MgSO_4$, and then the solvent was removed in vacuo.

Finally, the crude product was purified by column chromatography (methylene chloride/n-hexane(1:1)) to afford yellow solid (479mg, 76%)., ^{1}H NMR (500 MHz, CDCl3, δ): 7.17 (d, 2H, vinyl-H), 6.99 (s, 2H, Ar-H), 6.96 (d, 2H, Ar-H), 6.79 (d, 2H, Ar-H), 3.91 (d, 4H, -CH2-), 1.94 (m, 2H, -CH-), 1.55-1.30(m, 32H, -CH2-), 0.86(m, 12H, -CH3); ^{13}C NMR(126 MHz, CDCl3, δ): 151.11, 145.53, 130.44, 126.15, 125.81,123.74, 121.53, 110.91, 110.10, 77.00, 72.11, 38.27, 31.89, 31.77, 31.43, 29.77, 29.26, 27.01, 23.12, 22.71, 14.12 ; MS (MALDI-TOF, m/z) Calcd for $C_{50}H_{76}Br_2O_2S_2$: 930.37, found, 931.0.

PBDS

Compound (3) (90.4 mg, 0.1 mmol), compound (2) (82.1 mg, 0.1 mmol), $Pd_2(dba)_3$ (2.0 mg, 0.0022 mmol), P(o-toly) (2.7 mg, 0.0088 mmol), and dried toluene (4ml) were added in an argon charged 20ml schlenk tube. The schlenk tube was heated at 100 ℃ for 24h. After cooling to room temperature, the reaction mixture was poured into excess methanol, and then the precipitate was filtered and purified by soxhlet extraction with methanol, acetone, hexane, and chloroform. The chloroform solution was poured into excess methanol. The precipitate was filtered and dried in vacuo, yielding PBDS (112 mg, 91 %). GPC (chloroform, 35 °C): Mn = 88 kDa, Mw = 184 kDa, ^{1}H-NMR (500 MHz, CDCl3, 25 °C): δ 7.66 (s, 2H, Ar−H), 7.33-7.25 (m, 8H, Ar−H, vinyl−H), 6.98-6.94 (m, 6H, Ar−H), 3.93 (s, 4H, −O−CH2−), 2.92 (m, 4H, −Ar−CH2−), 1.90 (m, 2H, −CH−), 1.74 (m, 2H, −CH−), 1.30−1.58 (m, 48H,

−CH2−), 0.86−1.00 (m, 24H, −CH3). Anal. Calcd for $C_{76}H_{100}O_2S_6$: C, 73.73; H, 8.14; O, 2.58; S, 15.54. Found: C, 73.71; H, 8.18; O, 2.60; S, 15.51.

2.3.3. Characterizations

Gel permeation chromatography (GPC) was performed by using a Waters system and Waters styragel HR4 column eluted with Chloroform. UV-Vis absorption spectra and cyclic voltammetry (CV) were recorded by Shimadzu UV-1650PC and Princeton Applied Research Potentiostat/Galvanostat Model 273A. AFM imaging was performed using Multimode with a Nano Scope V Controller (Bruker) in tapping mode. The 2D-GIXD was measured by using the PLS-II 9A U-SAXS beamline in the Pohang Accelerator Laboratory, Korea. The incidence angle was adjusted to 0.12°

Device Fabrication and Evaluation

The patterned indium tin oxide (ITO) glass substrates were cleaned in an ultrasonic bath with acetone, and isopropanol, and then exposed to a UV/O_3 for 20min. PEDOT:PSS (Clavious P VP AI 4083) was spin-coated onto the ITO glass substrate at 5000 rpm for 30 s and the film was subsequently baked at 170 °C for 10min. A chlorobenzene (or CB:DIO = 99:1) solution (totally 17.5 mg mL^{-1}) of PBDS:$PC_{71}BM$ (1:1.5) blend was subsequently spin-coated (1500 rpm) on the PEDOT:PSS coated ITO glass to form active layer (ca. 80 nm) After drying the resulting films in a N_2 glovebox

at room temperature for 30min, thermall annealing treatment was conducted at 100 °C for 10 min. Then, Ca (5nm) was thermally deposited on PBDS:$PC_{71}BM$ film under a vacuum of 10^{-6} torr. Finally Al (80 nm) was thermally deposited under a vacuum of 10^{-6} torr.

For space-charge-limited currents (SCLC) measurement in this work, we have used Mott-Gurney law and fit the dark current under forward bias. The SCLC mobilities were calculated using the below equation:

$$J = \frac{9}{8}\varepsilon_0\varepsilon_r\mu\frac{V^2}{L^3}$$

In which ε_0 is the permittivity of free space, ε_r is the dielectric constant of the organic semiconductor material (herein ε_r was assumed to be 3 that typical value for organic semiconducting material), V is effective voltage with the equation of $V=V_{appl}-V_{bi}-V_r$ (V_{appl}: applied bias, V_{bi}: the built in potential due to the difference in electrical contact work function, V_r: the voltage drop due to contact resistance and series resistance across the electrodes) and L is the thickness of photoactive layer. The hole and electron only devices were fabricated respectively with the structure, ITO/PEDOT:PSS/BHJ layer/MO_3/Ag.

The current density-voltage (J-V) characteristics of the solar cells were measured suing a Keithley 4200 source measurement unit. The solar cell performances were characterized under AM 1.5G condition with an illumination intensity of 100 mW cm^{-2}, as generated using an Oriel Sol3A solar simulator (Oriel model 9023A). The

measurements were carried out through a shadow mask with well-defined aperture area of 0.04 cm^2 under an ambient atmosphere. The incident photon-to-current efficiency (IPCE) was measured using an Oriel QE/IPCE Measurement Kit composed of a 300 W xenon lamp, a monochromator (74125), an order sorting filter wheel, a Merlin lock-in amplifier (70104), a calibrated silicon photodiode (70356_70316NS) and an optical chopper.

2.4. Conclusion

In summary, we developed a new coplanar poly(arylene vinylene) with trans-stereoregular vinylene and a high molecular weight. We have found that introduction of 2D-BDT in the coplanar conjugated PPVTV backbone not only improves the charge transport properties but also stabilizes the HOMO level by aromatic stabilization. Consequently, solar cell devices prepared with $PC_{71}BM$ as the acceptor exhibited a maximum PCE of 5% with an enhanced V_{OC} of 0.81 V and J_{SC} of 10 mA cm^{-2} compared to the polymer without 2D-BDT (PPVTV). The results indicate that **PBDS** is a promising high-performance wide donor candidate polymer for tandem solar cells and ternary blend solar cells. In addition, there are many opportunities for improving the PCE of the PSC by structurally modifying **PBDS** because the vinylene group is good additional tuning site. For example, cyano groups or fluorine atoms could be

introduced to the vinylene structure, which might result in a lower bandgap, a deeper HOMO level, and stronger intermolecular interactions. Consequently, we are now working on modifying the structure to improve the performance of **PBDS**-based PSCs.

2.5. References

[1] L. Lu, T. Zheng, Q. Wu, A. M. Schneider, D. Zhao and L. Yu, Chemical reviews, 2015, 115, 12666-12731.

[2] M. C. Scharber, D. Mühlbacher, M. Koppe, P. Denk, C. Waldauf, A. J. Heeger and C. J. Brabec, Advanced materials, 2006, 18, 789-794.

[3] Y. Li, Acc. Chem. Res. 2012, 45, 723–733..

[4] H. Yao, L. Ye, H. Zhang, S. Li, S. Zhang and J. Hou, Chemical reviews, 2016, 116, 7397-7457.

[5] S. Zhang, L. Ye and J. Hou, Advanced Energy Materials, 2016, 6, 1502529.

[6] Y. Cai, L. Huo and Y. Sun, Advanced materials, 2017, 29.

[7] J. You, L. Dou, K. Yoshimura, T. Kato, K. Ohya, T. Moriarty, K. Emery, C. C. Chen, J. Gao, G. Li and Y. Yang, Nature communications, 2013, 4, 1446.

[8] T. Ameri, G. Dennler, C. Lungenschmied and C. J. Brabec, Energy & Environmental Science, 2009, 2, 347.

[9] H. Bin, L. Gao, Z. G. Zhang, Y. Yang, Y. Zhang, C. Zhang, S. Chen, L. Xue, C. Yang, M. Xiao and Y. Li, Nature communications, 2016, 7, 13651.

[10] Y. Olivier, D. Niedzialek, V. Lemaur, W. Pisula, K. Mullen, U. Koldemir, J. R. Reynolds, R. Lazzaroni, J. Cornil and D. Beljonne, Advanced materials, 2014, 26, 2119-2136.

[11] L. Huo, S. Zhang, X. Guo, F. Xu, Y. Li and J. Hou, Angewandte Chemie, 2011,

50, 9697-9702.

[12] Y. Liu, J. Zhao, Z. Li, C. Mu, W. Ma, H. Hu, K. Jiang, H. Lin, H. Ade and H. Yan, Nature communications, 2014, 5, 5293.

[13] J. Zhao, Y. Li, G. Yang, K. Jiang, H. Lin, H. Ade, W. Ma and H. Yan, Nature Energy, 2016, 1, 15027.

[14] J. W. Jo, J. W. Jung, H.-W. Wang, P. Kim, T. P. Russell and W. H. Jo, Chemistry of Materials, 2014, 26, 4214-4220.

[15] N. Leclerc, P. Chávez, O. Ibraikulov, T. Heiser and P. Lévêque, Polymers, 2016, 8, 11.

[16] M. Muratsubaki, Y. Furukawa, T. Noguchi, T. Ohnishi, E. Fujiwara and H. Tada, Chemistry Letters, 2004, 33, 1480-1481.

[17] N. C. Cates, R. Gysel, J. E. P. Dahl, A. Sellinger and M. D. McGehee, Chemistry of Materials, 2010, 22, 3543-3548.

[18] R. J. Kline, M. D. McGehee, E. N. Kadnikova, J. Liu, J. M. J. Fréchet, M. F. Toney, Macromolecules 2005, 38, 3312–3319.

[19] B. C. Thompson, B. J. Kim, D. F. Kavulak, K. Sivula, C. Mauldin, J. M. J. Fréchet, Macromolecules 2007, 40, 7425.

[20] T. Lei, J. H. Dou, X. Y. Cao, J. Y. Wang and J. Pei, Journal of the American Chemical Society, 2013, 135, 12168-12171.

[21] S. Pfeiffer, H. H. Horhold, Synth. Met. 1999, 101, 109.

[22] T.-L. Choi, K.-M. Han, J.-I. Park, D. H. Kim, J.-M. Park and S. Lee, Macromolecules, 2010, 43, 6045-6049.

[23] Suzuki, Y.; Hashimoto, K.; Tajima, K. Macromolecules 2007, 40, 6521– 6528

[24] K. Tajima, Y. Suzuki and K. J. Hashimoto, J. Phys. Chem. C, 2008, 112, 8507

[25] A. J. J. M. van Breemen, P. T. Herwig, C. H. T. Chlon, J. Sweelssen, H. F. M. Schoo, E. M. Benito, D. M. de Leeuw, C. Tanase, J. Wildeman and P. W. M. Blom, Advanced Functional Materials, 2005, 15, 872-876.

[26] K. G. Lim, J. M. Park, H. Mangold, F. Laquai, T. L. Choi and T. W. Lee, ChemSusChem, 2015, 8, 337-344.

[27] S. E. Shaheen, C. J. Brabec, N. S. Sariciftci, F. Padinger, T. Fromherz and J. C. Hummelen, Applied Physics Letters, 2001, 78, 841-843.

[28] Y. Li, H. Xu, L. Wu, F. He, F. Shen, L. Liu, B. Yang and Y. Ma, Journal of Polymer Science Part B: Polymer Physics, 2008, 46, 1105-1113.

[29] W. Lee, G.-H. Kim, S.-J. Ko, S. Yum, S. Hwang, S. Cho, Y.-H. Shin, J. Y. Kim and H. Y. Woo, Macromolecules, 2014, 47, 1604-1612.

[30] R. Rieger, D. Beckmann, A. Mavrinskiy, M. Kastler and K. Müllen, Chemistry of Materials, 2010, 22, 5314-5318.

[31] M. M. Wienk, J. M. Kroon, W. J. Verhees, J. Knol, J. C. Hummelen, P. A. van Hal and R. A. Janssen, Angewandte Chemie, 2003, 42, 3371-3375.

[32] O. V. Mikhnenko, H. Azimi, M. Scharber, M. Morana, P. W. M. Blom and M. A. Loi, Energy & Environmental Science, 2012, 5, 6960.

[33] D. M. Smilgies, Journal of applied crystallography, 2009, 42, 1030-1034.

[34] W. Chen, T. Xu, F. He, W. Wang, C. Wang, J. Strzalka, Y. Liu, J. Wen, D. J. Miller, J. Chen, K. Hong, L. Yu and S. B. Darling, Nano letters, 2011, 11, 3707-3713.

[35] Huo, L.; Zhang, S.; Guo, X.; Xu, F.; Li, Y.; Hou, J. Angew. Chem., Int. Ed. 2011, 50, 9697– 9702

[36] S. Boudiba, A. Růžička, C. Ulbricht, S. Enengl, C. Enengl, J. Gasiorowski, C. Yumusak, V. Pokorná, D. Výprachtický, K. Hingerl, D. R. T. Zahn, F. Tinti, N. Camaioni, S. Bouguessa, A. Gouasmia, V. Cimrová and D. Ayuk Mbi Egbe, Journal of Polymer Science Part A: Polymer Chemistry, 2017, 55, 129-143.

Chapter 3.

A Stereoregular β-Dicyanodistyrylbenzene (β-DCS)-based Conjugated Polymer for High-Performance Organic Solar Cells with Small Energy Loss and High Quantum Efficiency

3.1. Introduction

Bulk heterojunction (BHJ) organic solar cells (OSCs) have been extensively researched, because of their low-cost fabrication, light weight, and mechanical flexibility.[1] During the past two decades, there have been several attempts to increase their efficiencies, such as the development of low band gap donor polymers,[2–4] control of active layer morphology,[5–11] use of fluorinated donor polymers,[12–14] control of the aggregation properties of donor polymers,[15–17] and development of non-fullerene OSCs;[18–20] these efforts have resulted in power conversion efficiencies (PCEs) exceeding 10%. Despite this, to date, the most efficient OSCs have not achieved sufficiently high PCEs compared to inorganic and organic-inorganic hybrid solar cells.[21]

A key issue for the further improvement of OSCs is the minimization of the photon energy loss (E_{loss}), which is defined as the potential energy difference between the absorbed photon and the released electron ($E_g^{opt} - e \cdot V_{OC}$), [22] because OSCs typically have a relatively large E_{loss} values of 0.7–1.0 eV compared with those of

inorganic and perovskite solar cells (typically, E_{loss} = 0.4–0.55 eV).[23–26] The large E_{loss} of OSCs originates from the fact that ΔE_{HOMO} or ΔE_{LUMO} between donor (D) and acceptor (A) should be 0.3 eV or greater; otherwise the external quantum efficiency (EQE) drops considerably, resulting in very low PCEs.[23] Therefore, OSCs with small E_{loss} values exhibit low EQEs in general. However, recently, some OSCs have been developed that have high EQEs despite having small ΔE_{HOMO} or ΔE_{LUMO} (under 0.3 eV), resulting in very small E_{loss} values of up to 0.6 eV, which is the empirically obtained limit for OSCs.[24–28] These small E_{loss} values have been achieved using a D–A system where the open-circuit voltage (V_{OC}) is maximized: i) Eg (D) < Eg (A) and a small ΔE_{LUMO} or ii) Eg (D) > Eg (A) and a small ΔE_{HOMO}, which maximizes the energy difference between the HOMO of the donor and the LUMO of the acceptor. The smallest E_{loss} was achieved using a PffBT4T-2DT:FBR system that yields a very small E_{loss} of 0.5 eV and an EQEmax of 57%, arising from the small ΔE_{LUMO} of 0.05 eV.[24] In addition, PNOz4T:$PC_{71}BM$[25] and P3TEA:SF-PDI_2[26] systems also showed a high EQE_{max} values of 66% and E_{loss} values of 0.55 eV and 0.61 eV, respectively. Very recently, a very high EQEmax of 76.5% was achieved by a J71:3,9-bis(2-methylene-(3-(1,1-dicyanomethylene)-indanone))-5,5,11,11-tetrakis(4-hexylphenyl)-dithieno[2,3-d:2,3-d]-s-indaceno[1,2-b:5,6-b]dithiophene (ITIC) system despite the small E_{loss} of 0.65 eV, arising from the ΔE_{HOMO} of 0.11 eV.[27] Notwithstanding these examples, it is still very difficult to implement systems with small E_{loss} values and high EQEs, because of the scarcity of donor polymers with sufficiently deep FMOs to result in a

small energy

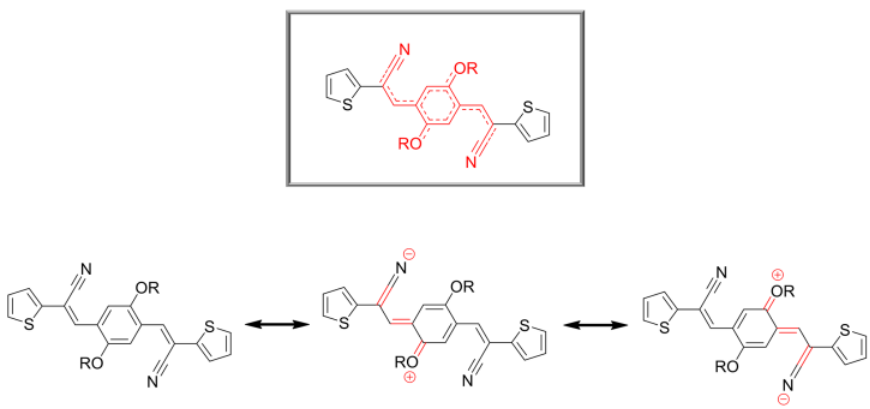

Figure 3-1. Resonance structures of **β-DCS**.

offset with the acceptor.

In recent years, substitutions of electron-withdrawing atoms such as fluorine[12–14] and sulfur atoms[29–31] have been widely used to further stabilize the FMOs of donor polymers; however, this stabilization is not sufficient to minimize the energy offset. The cyano group is one of the strongest electron-withdrawing groups but has been received little attention because it often induces non-coplanarity in the conjugated backbone.[32] In contrast, cyanostyrylbenzene (CS) molecules are highly attractive electron-accepting moieties owing to features such as strongly stabilized energy levels, strong intermolecular interactions arising from various secondary interactions, a coplanar structure in the solid state, high solubility caused by "twist elasticity" characteristics, and facile synthesis.[33,34] Among CS molecules, β-dicyanodistyrylbenzene (**β-DCS**) is a promising electron-accepting moiety. **β-DCS** is a strong electron-withdrawing group because of the presence of two cyano groups. In addition, **β-DCS** has a rigid structure, which arises from its unique resonance structure (Figure 3-1).[35,36] This structural rigidity allows for tight molecular stacking, facilitating efficient charge transport.[37] In addition, the rigid structure is expected to suppress *trans*-to-*cis* photoisomerization, a major problem of CS molecules for charge transport applications[38–40] because *cis* isomer is unfavorable for π-π stacking. Recently, because of our efforts in developing **β-DCS**-based n-type semiconductors, we

have achieved a high organic field-effect transistor electron mobility of 7.81 $cm^2V^{-1}s^{-1}$ [37,41] and a high non-fullerene OSC efficiency of 7.64%.[42–45] Moreover, we found that introduction of CS in conjugated polymers results in a narrow E_g, deep FMOs, and strong aggregation properties, which are characteristics of high-performance donor polymers for fullerene[2–4,15–17] and non-fullerene OSCs.[18,46] Despite such advantages, previously reported DCS-based polymers exhibited OSC efficiencies only up to 3.2%[47,48] because of the *trans*-to-*cis* photoisomerization, low polymer molecular weight, and inappropriate donating moieties that induce a large E_g and break the coplanarity of the conjugated backbone. For high-performance OSCs, it is far more important in polymers to prevent the photoisomerization than in small molecules because the separation of the *cis* forms in the polymer chain is not possible.

Based on the above considerations, we designed a new DCS-based polymer (**PBDCS**) consisting of *trans*-isomeric **β-DCS** and two-dimensional benzodithiophene (2D-BDT). 2D-BDT is expected to endow enhanced transport properties that arise from the π-extended molecular framework.[49–51] To minimize the generation of *cis*-DCS, we chose the rigid **β-DCS** structure and conducted polymerization in the dark. As a result, we obtained **PBDCS** that exhibits not only a *trans*-stereoregularity but also 100% endurance to photoisomerization under UV light, unlike other CS-based polymers. **PBDCS** has a deep HOMO (–5.59 eV) with a low bandgap (1.75 eV), which are beneficial properties for high

V_{OC} and high short-circuit current (J_{SC}) values. We fabricated OSC devices using $PC_{71}BM$ as an acceptor and a non-fullerene OSCs using the ITIC acceptor that has a HOMO similar to that of **PBDCS** and a low E_g, which is believed to be able to minimize the E_{loss} because of the small ΔE_{HOMO}. In addition, we discuss the origin of unique photoisomeric stability of **PBDCS**.

3.2. Results and discussion

Synthesis and characterization

Figure 3-2 shows the synthetic route of **PBDCS**. To obtain a high molecular weight and trans-stereoregularity, we used a C-C cross-coupling reaction, the Stille reaction, using a trans-isomeric **β-DCS** monomer rather than the Knoevenagel reaction, which usually results in an isomeric mixture.[40,52]

In addition, to prevent the trans-to-cis photoisomerization during the polymerization, we conducted the polymerization in the dark. Detailed descriptions of the synthetic steps for the monomers and polymer are provided in the Experimental part. The resulting polymer is readily soluble in chloroform, toluene, chlorobenzene, and dichlorobenzene at room temperature (10~30 °C). To determine the molecular weight, we used gel permeation chromatography (GPC) with 1,2-dichlorobenzene as the eluent. As shown in Figure 3-3, the GPC trace changed from bimodal to unimodal as the temperature increased, the high molecular weight peak in bimodal peak disappearing.

This change indicates that PBDCS forms aggregates in solution at room temperature

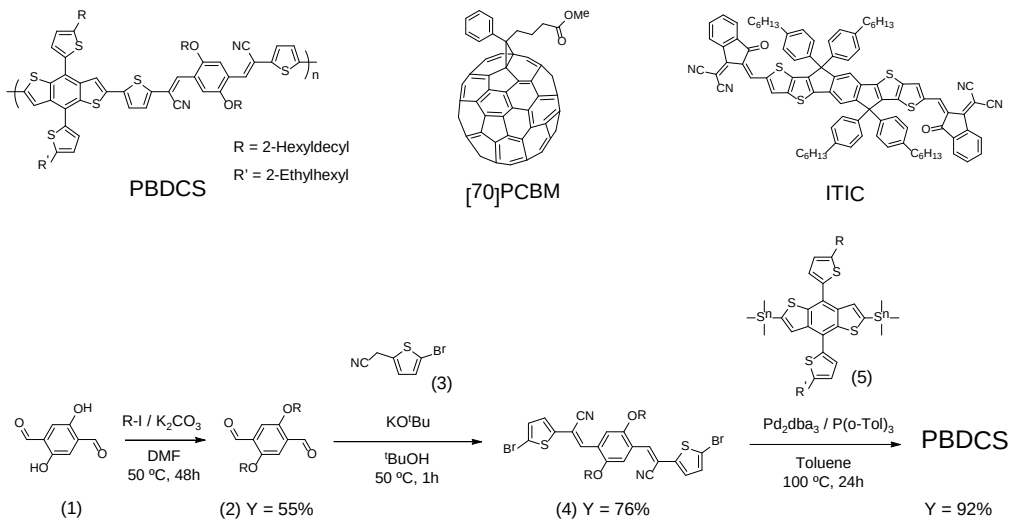

Figure 3-2. Chemical structures of compounds **PBDCS**, $PC_{71}BM$, and ITIC, and synthetic route to **PBDCS**.

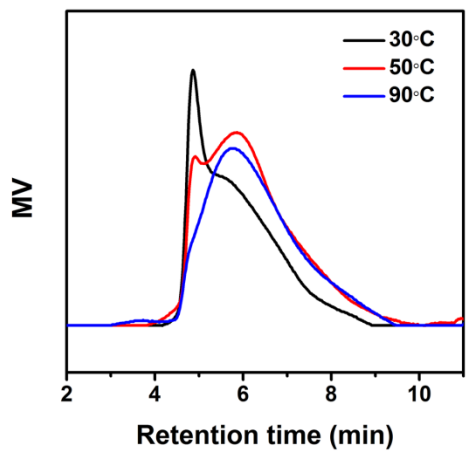

Figure 3-3. GPC traces of **PBDCS** under various temperature.

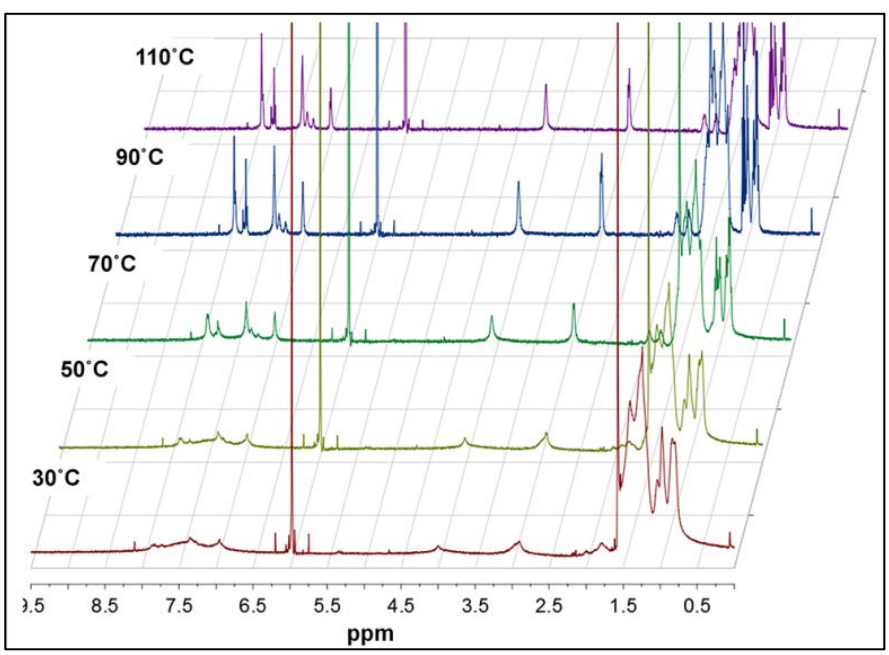

Figure 3-4. ^{1}H-NMR spectrum of **PBDCS** under various temperatures

This change indicates that PBDCS forms aggregates in solution at room temperature despite the dilute solution.[15] Thus, we determined the exact number-average molecular weight (Mn) and weight-averaged molecular weight (Mw) at a temperature greater than 90 °C: 90 kDa and 197 kDa, respectively. The aggregates of PBDCS in solution were also identified using the ^{1}H-NMR results. The chemical shift peaks changed from unclear, broad peaks to sharp peaks as the temperature increased (Figure 3-4). From this NMR result, we found that PBDCS was 100% trans-stereoregular, despite photoisomerization being generally inevitable in CS molecules.[38–40] This result implies that PBDCS may be intolerant toward photoisomerization. To verify this, we monitored the NMR chemical shift changes of the PBDCS solution under exposure of the polymer to 365-nm light (the wavelength for trans-to-cis photoisomerization). We found that photoisomerization did not occur (Figure 3-5). The photoisomeric stability of PBDCS most likely originates from the unique resonance structure of β-DCS, as mentioned in the Introduction part, which was identified by a comparative analysis of other CS molecules (for example, a comparison of bond lengths, molecular rotational energies, photoluminescence in solution, and 1H-NMR chemical shifts.) Detailed discussions are provided in the Supporting Information. In addition, the formation of aggregates in solution is considered a key factor preventing photoisomerization because the reaction is more difficult in the tightly packed solid state. Finally, both the

rigidity of β-DCS and the aggregation property of PBDCS result in its complete endurance to photoisomerization under UV light. This photoisomeric stability is very

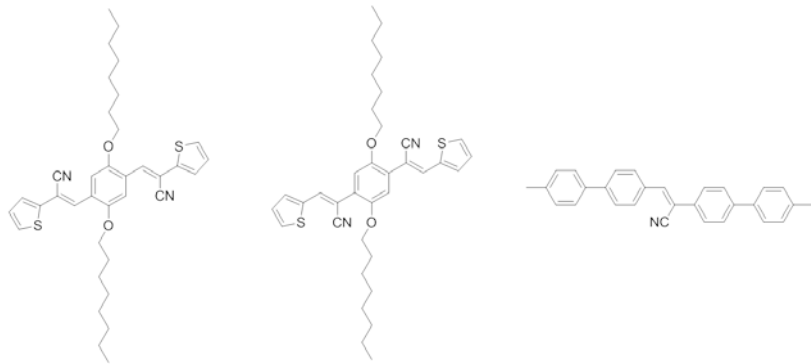

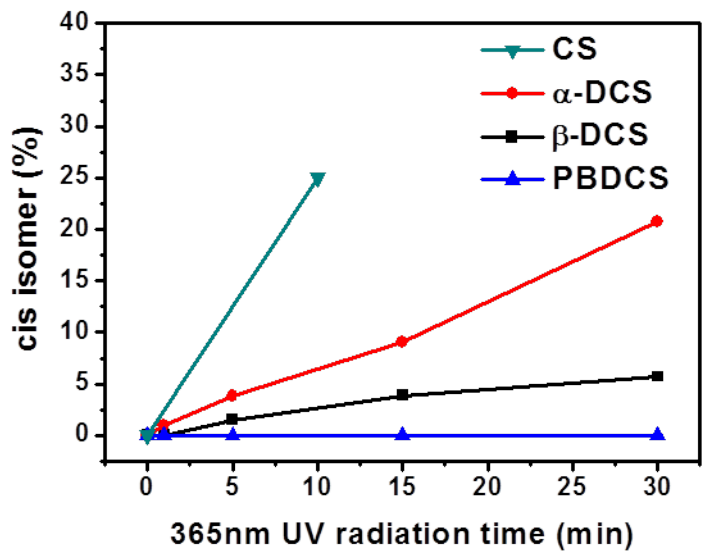

Figure 3-5. Photoisomerization test of α-DCS, β-DCS, PBDCS, and CS (CNMBE[S4]) under 365nm UV irradiation. (detected by ^{1}H-NMR spectrum)

important for the practical application of electronic devices, as well as efficient charge transport.

Thermogravimetric analysis (TGA) and differential scanning calorimetry (DSC) were performed to evaluate the thermal stability of the polymers. The polymer exhibited a high thermal decomposition temperature (5% weight loss) of 396.6 °C and no thermal transitions until 300 °C, indicating a sufficiently high thermal stability for their application in OSCs (Figure 3-6).

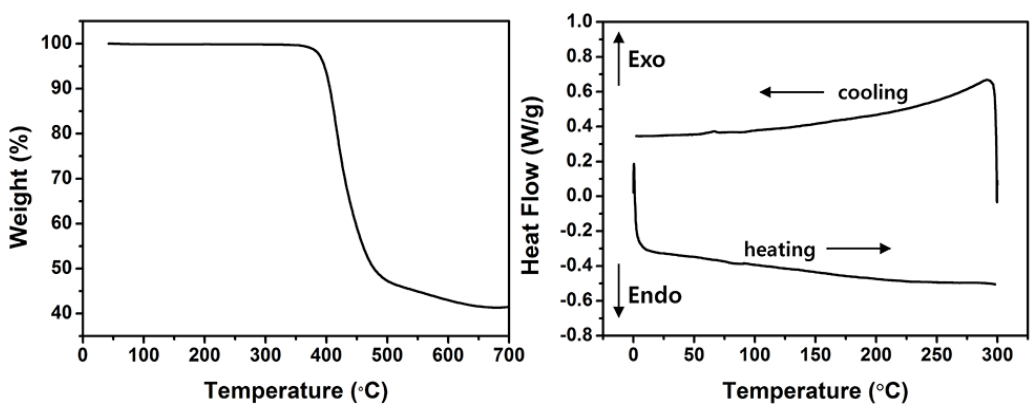

Figure 3-6. TGA curve (left) and DSC curve (right) of PBDCS. (5% weight loss: 396.7°C)

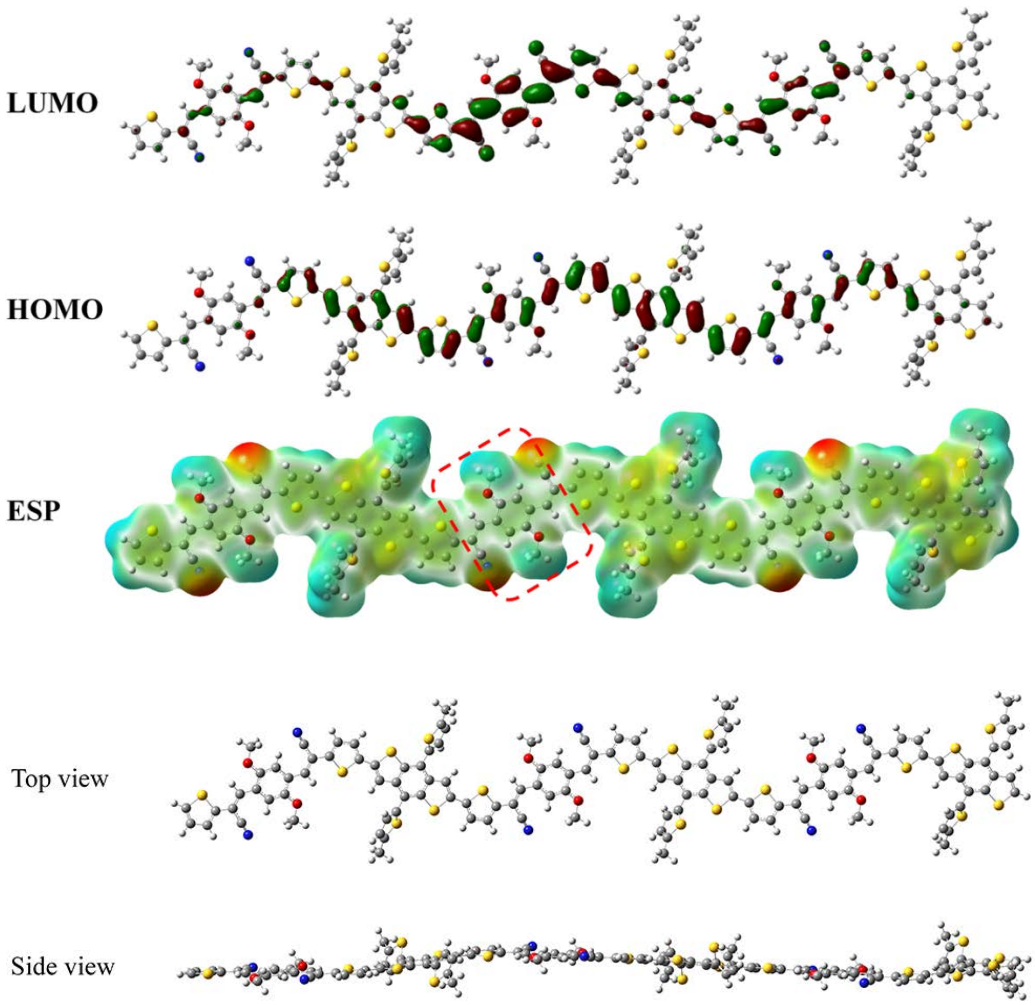

Figure 3-7. Geometries of HOMO, LUMO, and map of electrostatic potential (ESP) surfaces of optimized molecular structure for the trimer model compounds of the

polymers. Calculation were performed by the DFT method at B3LYP/6-31G(d,p) level. To simply the calculation, all alkyl chains were replaced with methyl group.

Optical and electrochemical properties

Density functional theory (DFT) calculations at the B3LYP/6–31G(d,p) level of theory were performed to analyze the optimized geometry, molecular orbital distributions, and electrostatic potential (ESP) surfaces. As shown in Figure 3-7, while the HOMO of PBDCS is delocalized over the entire polymer backbone, the LUMO of PBDCS is localized on the acceptor unit, implying that PBDCS is appropriate for hole transport. In addition, the backbone of PBDCS has good coplanarity and a curved conformation, which are beneficial for OSC applications, because this curved backbone geometry provides a small crystalline size and good miscibility with PCBM.[53,54] The ESP map shown in Figure 3-7 shows a similar potential along the backbone, except for a strongly negative nitrogen atom on the cyano group. A closer look reveals that **β-DCS** has the most positive potential (as shown by a dashed red rectangle in Figure 3-7), explaining that **β-DCS** is an accepting moiety. This interpretation is consistent with the explanation of the resonance structure of **β-DCS**.

Figure 3-8b shows the absorption spectra of **PBDCS** in solution. A large absorption band and two small absorption bands are observed at approximately 600 nm (2.0 eV), 425 nm (2.9 eV), and 350 nm (3.5 eV), which can be ascribed to the S1, S2, and S3 absorption bands, respectively.[55] At 10 °C, PBDCS exhibits clear absorbance of the 0–

0 peak at 624 nm and 0–1 peak at 588 nm on the S1 absorption band. However, as the temperature increased, the absorbance of the 0-0 peak decreased continuously, finally

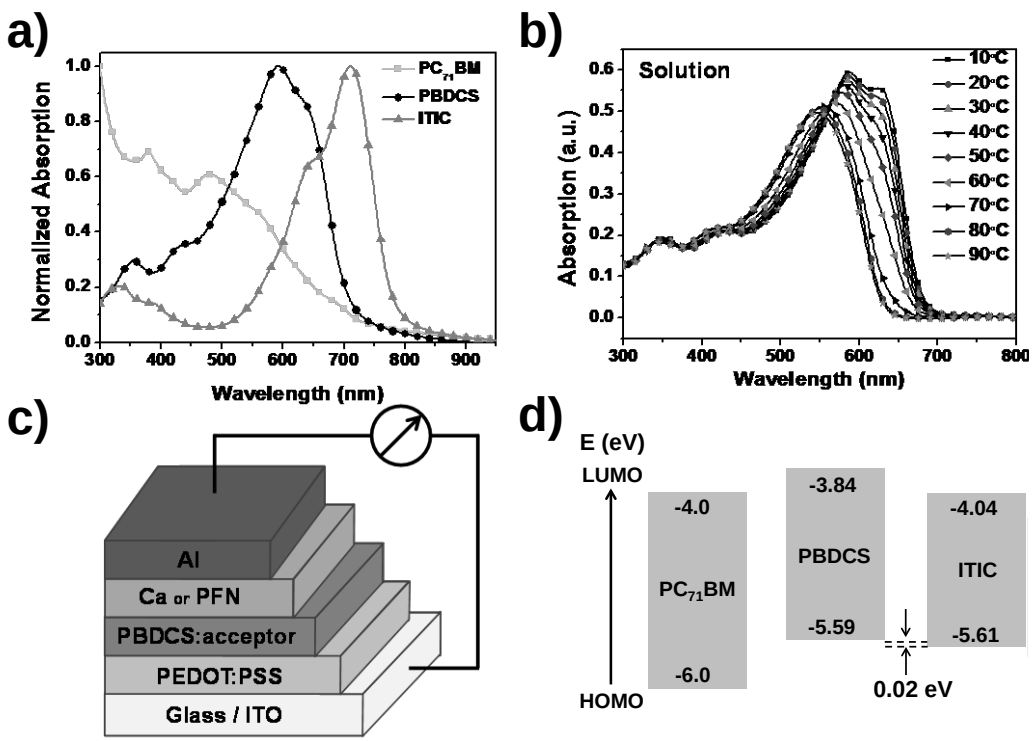

Figure 3-8. a) UV-vis absorption spectra of PBDCS, $PC_{71}BM$, and ITIC films, b) UV-vis absorption spectra of PBDCS in diluted chlorobenzene at various temperatures, c) Device structure of OSCs used in this study., d) schematic energy diagram of PBDCS, $PC_{71}BM$, and ITIC.

disappearing at 60 °C; afterwards the absorbance of the 0-1 peak became weak and blue-shifted gradually from 588 to 547 nm. However, the S2 and S3 absorption bands were invariant with temperature. From the results, we speculate that the S1 absorption band is related to the charge transfer state between the donor and acceptor units, which is affected by molecular rotations, and the S2 and S3 absorption bands are related to the locally excited states of the monomer units, which are not affected by molecular rotations. Therefore, the observed spectral changes of the S1 band indicate that PBDCS aggregates strongly at room temperature but that these aggregates are broken down into individual chains by thermally activated vibrational and the rotational motion of the conjugated backbone at high temperatures, which is in good agreement with the GPC and NMR results. The aggregation of PBDCS arises from the tight intermolecular stacking induced by β-DCS and the stereoregular structure, consistent with our previous report.[52] The formation of aggregates in solution results in a small domain size and high domain purity, which play a significant role in determining the performance of OSCs; in particular, these factors are essential for high-performance non-fullerene OSCs.[16,17,56]

We chose $PC_{71}BM$ and ITIC as acceptors. ITIC is known to be a non-fullerene acceptor with a low Eg and shallower LUMO than that of $PC_{71}BM$, resulting in higher J_{SC} and V_{OC} values.[18,57,58] Figure 3-8a shows the absorption spectrum of the PBDCS, $PC_{71}BM$, and ITIC films. PBDCS has the maximum absorption wavelength (λ_{max}) of

600 nm, which is complementary to those of $PC_{71}BM$ (λ_{max} = 300–400 nm) and ITIC (λ_{max} = 710 nm), indicating that PBDCS is a good donor pair for both $PC_{71}BM$ and ITIC in terms of solar energy absorption. PBDCS exhibited an optical band gap (Egopt) of 1.75 eV, which is smaller than that of $PC_{71}BM$ (Egopt = 2.0 eV)[59] and larger than that of ITIC (Egopt = 1.57 eV).[28] Therefore, to achieve the minimum E_{loss}, PBDCS should have a small ΔE_{LUMO} with $PC_{71}BM$ and a small ΔE_{HOMO} with ITIC, as mentioned in the Introduction.

The HOMO of **PBDCS** was evaluated by the onset oxidation potentials from the cyclic voltammetry result, and the LUMO was determined by E_g^{opt} – HOMO. The HOMO and LUMO of **PBDCS** were calculated to be –5.59 eV and –3.84 eV, respectively (Figure 3-8d). Such a deep HOMO value, which is the deepest value among those reported for BDT-containing donor polymers, is an encouraging characteristic for an OSC with a high V_{OC}. On the other hand, the shallow LUMO value of –3.2 eV is not suitable to achieve a low E_{loss} in fullerene-based OSCs because of the large ΔE_{LUMO} (Figure 3-8d). On the other hand, ITIC, a non- fullerene acceptor with a low E_g, is expected to show better performance in terms of the minimization of E_{loss} because the HOMO of ITIC is close to that of PBDCS.[28] To confirm this, we measured the FMOs of ITIC and PBDCS at the same time. The results showed that ΔE_{HOMO} between ITIC and PBDCS is 0.02 eV, a negligible value, and these energy levels satisfy the D-A

system (E_g (D) > E_g (A) and a small ΔE_{HOMO}) to achieve a minimal E_{loss}, as discussed in the Introduction part.

Photovoltaic properties

BHJ OSC devices with a conventional architecture were fabricated to assess the photovoltaic performance of PBDCS. A mixed solution of PBDCS and $PC_{71}BM$ or ITIC in chlorobenzene was spin cast on a PEDOT:PSS layer to form the active layer. Ca or poly [(9,9-bis(3'-(N,N-dimethylamino)propyl)-2,7-fluorene)-alt-2,7-(9,9–dioctylfluorene)] (PFN) were used as efficient cathode interfacial layers and deposited on the active layer (Figure 3-8c). The details of the device fabrication procedures are described in the Experimental part. Figure 3-9a shows the current density–voltage (J–V) curves, and detailed photovoltaic results are listed in Table 3-1. The PBDCS:$PC_{71}BM$ device showed a PCE of 8.75% with a high V_{OC} of 0.94 V, J_{SC} of 14.28 $mAcm^2$, and a fill factor (FF) of 65.1%. When PBDCS with a shorter side chain was used (see PBDCSa in Table 3-1, both V_{OC} and J_{SC} increased to 0.95 eV and 15.0 $mAcm^2$, respectively, and this J_{SC} value is one of the highest among those of fullerene-based OSCs with a high V_{OC} of over 0.95 eV. The PBDCS:ITIC device showed a PCE of 7.55% with an especially high V_{OC} of 1.08 V, J_{SC} of 13.6 $mAcm^2$, and an FF of 51.4%. The V_{OC} of 1.08 eV is the highest value among those of OSCs with ITIC as an acceptor, resulting from the negligibly small value of ΔE_{HOMO} between ITIC and PBDCS. After thermal annealing at 110 ℃ for 10 min, the PCE improved further to 7.81% owing to a

slight increase in J_{SC} and FF; however, the FF is still relatively low compared to the PBDCS:PC_{71}BM device due to imbalance of hole and electron mobility (Table 3-2). Like the PBDCS:PC_{71}BM device, when using PBDCS with a shorter side chain, the J_{SC} of the PBDCS:ITIC device improved to 15.8 $mAcm^2$, and the relationship between the side chain length and J_{SC} is consistent with that reported previously.[60,61] The OSC device results indicate that PBDCS is a promising moiety for the donor material to satisfy both a high J_{SC} and V_{OC} simultaneously, which is vital for further improvement in the PCE.[25]

The EQE spectra of the OSCs are shown in Figure 2-9 b and c. The PBDCS:PC_{71}BM device exhibits EQE values of about 80% (EQE_{max} = 82.7%) in a broad range from 400 to 700 nm. In the case of the PBDCS:ITIC device, the response range expanded to 800 nm because of the broad absorption of the ITIC acceptor, providing the possibility of a higher J_{SC} than that of PBDCS:PC_{71}BM. Note that an EQE_{max} of 74% was attained around 700 nm, where 700 nm is the maximum absorption range of ITIC and the absorption edge of PBDCS, illustrating the efficient hole transfer from ITIC to PBDCS despite the negligible ΔE_{HOMO} value (~0.02 eV). Moreover, an unexpectedly high EQE value (~65%) was attained around 400 nm, although the absorbance of the PBDCS:ITIC blend film is very low near 400 nm. We believe that such a high EQE value with low absorbance can be explained by the unique hot exciton dynamics of PBDCS,[55,62,63] which is a beneficial characteristic for a high-performance donor material. The calculated J_{SC} values from the EQE spectra were 14 and 13.9 mA cm^2 for

the PBDCS:$PC_{71}BM$ and PBDCS:ITIC devices, respectively, which match well with the values obtained from the $J-V$ curves.

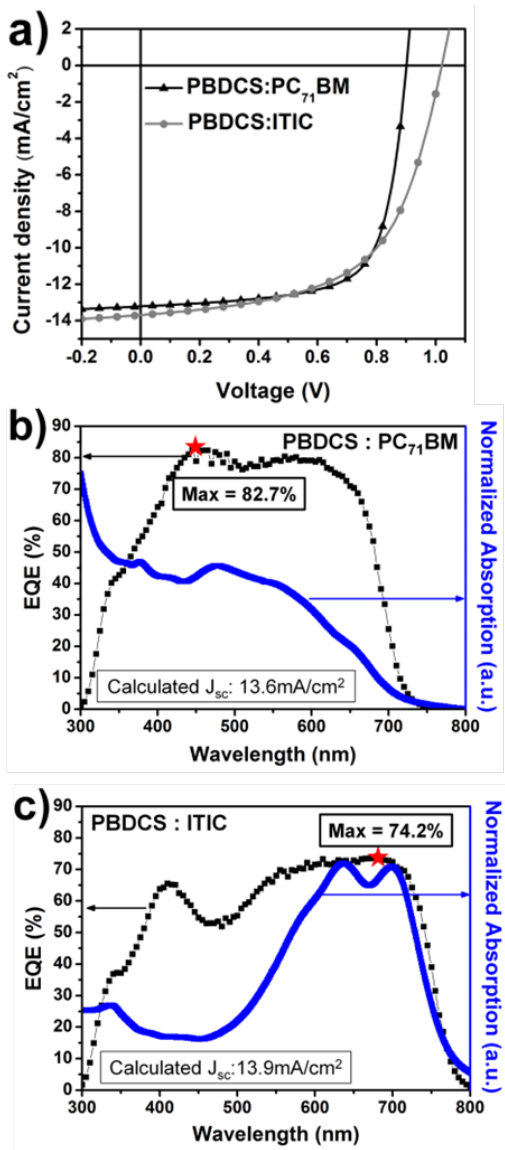

Figure 3-9. a) J–V curves, EQE plots and UV-vis absorption spectra of b) PBDCS:$PC_{71}BM$ and c) PBDCS:ITIC solar cells.

Table 3-1. Photovoltaic parameters of PBDCS:$PC_{71}BM$ and PBDCS:ITIC BHJ devices.

Polymer : Acceptor	V_{OC} [V]	J_{SC} [mAcm^{-2}]	FF	PCE [%]	E_{loss} [eV]
PBDCS : $PC_{71}BM$	0.94	14.3	0.65	8.75(8.64)[c]	0.81
PBDCS[a] : $PC_{71}BM$	0.95	15.0	0.60	8.55(8.34)	0.80
PBDCS : ITIC	1.08	13.6	0.51	7.55(7.32)	0.49
PBDCS : ITIC[b]	1.06	14.0	0.53	7.81(7.51)	0.51
PBDCS[a] : ITIC	1.03	15.8	0.45	7.28(7.09)	0.54

a PBDCS with smaller side chain (R = 2-butyloctyl). b Thermal annealing at 110˚C for 10 min. c The values in parentheses are average efficiencies from 9 devices.

Table 3-2. SCLC hole mobilities of PBDCS:$PC_{71}BM$ and PBDCS:ITIC blend.

Donor	**Acceptor**	**Hole mobility ($cm^2 \cdot V^{-1}sec^{-1}$)**	**Electron mobility ($cm^2 \cdot V^{-1}sec^{-1}$)**	**Mobility balance (electron/hole)**
PBDCS	**PC71BM**	$6.48X10^{-4}$	$9.658X10^{-4}$	1.49
PBDCS	**ITIC**	$1.72X10^{-4}$	$5.137X10^{-5}$	0.3

As mentioned in the Introduction, the minimization of E_{loss} is key issue to further improving the PCE.[23–26] An E_{loss} value of 0.6 eV has been referenced as the empirical obtained limit value for OSCs.[22] The V_{OC} values of the OSCs with $PC_{71}BM$ as the acceptor are 0.94−0.95 V, which are relatively large values for fullerene-based OSCs, corresponding to relatively small E_{loss} values of 0.80–0.81 eV. The V_{OC} values of the OSCs with ITIC as the acceptor are 1.06−1.08 V, which are the largest among those of ITIC-based OSCs reported so far; hence, the E_{loss} is 0.49−0.51 eV, which is much smaller than the empirically low threshold of 0.6 eV and is the smallest in an OSC with a high EQE (>70%). Such surprisingly low Eloss values are attributed to the negligible ΔE_{HOMO} (0.02 eV) between PBDCS and ITIC.

Morphology investigation

The active layer morphology has been studied using atomic force microscopy (AFM) and transmission electron microscopy (TEM). As shown in Figure 3-10, the PBDCS:$PC_{71}BM$ and PBDCS:ITIC films have smooth surfaces with small root-mean-square roughness values of 0.7 and 1.2 nm, respectively, and small domain sizes (10–

30 nm). This small domain size is close to the exciton diffusion length of conventional conjugated polymers, which contributes to the attainment of high J_{SC} values.[64] The TEM images show good mixing between the donor and acceptor in both films with

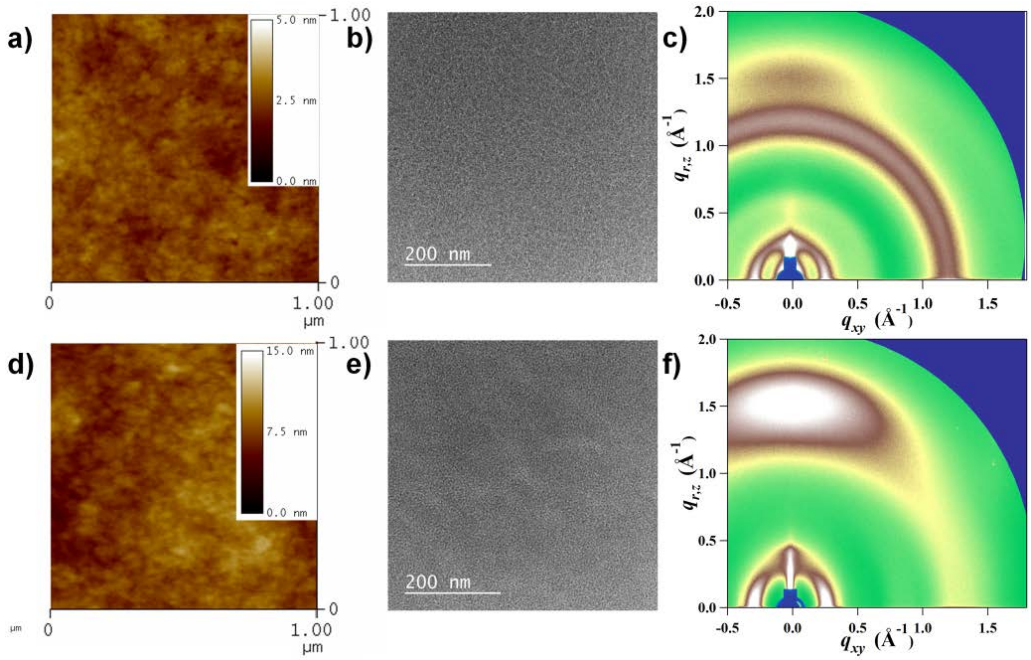

Figure 3-10. AFM topography images (a,d) TEM images (b,e), and 2D-GIXD images (d,f) of **PBDCS**:$PC_{71}BM$ (upper side) and **PBDCS**:ITIC (bottom side) blend films.

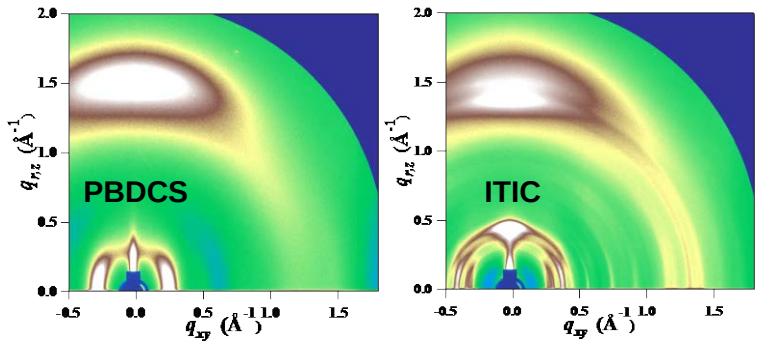

Figure 3-11. 2D-GIXD images of **PBDCS** and ITIC films

very small fibrillar nanostructures, consistent with the AFM results (Figure 3-10). Grazing incidence wide angle X-ray scattering (GIWAXS) experiments were performed to study the molecular packing and orientation of the polymer and blend films. As shown in Figure 3-11, only a strong π–π stacking (010) peak for the PBDCS film was observed in the out-of-plane direction, indicating weak lamellar stacking and predominant face-on π-π stacking orientation. The (010) diffraction peak for the PBDCS film was observed at $q_Z \approx 1.584$ Å^{-1}, corresponding to a π-π stacking distance of ~3.97 Å. The coherence length of the π–π stacked structures was calculated using the Scherer equation and the full width at half-maximum (FWHM) of the diffraction peak.[65] The FWHM of the (010) peak of the PBDCS film was 0.28 Å^{-1} with a corresponding coherence length of 2.2 nm (Figure 3-12). In the case of the PBDCS:$PC_{71}BM$ blend film, the intensity of the π–π stacking peak was reduced and the FWHM of the (010) peak was increased to 0.33 Å^{-1}, yielding a coherence length of 1.9 nm, which is similar to that of the PTB7:$PC_{71}BM$[66] blend film (Figure 3-12). We

believe that such small coherence length and the excellent mixing with acceptor arise from the curved conformation of the conjugated backbone of PBDCS.[53,54] Meanwhile, the ITIC film exhibits only a strong π–π stacking peak at $q_Z \approx 1.421$ Å^{-1}, which is similar to that of a PBDCS film (Figure 3-12). The (010) diffraction peak of the PBDCS:ITIC blend film seems to be located at one spot at $q_Z \approx 1.582$ Å^{-1}, implying that PBDCS:ITIC blend is a very well-mixed system (Figure 3-12). Thus, the coherence lengths could not be evaluated because it is difficult to determine the peak indicative of PBDCS or ITIC. From the morphological analyses, we postulate that the small domain size and the nanocrystalline structure of PBDCS contribute to the high J_{SC} despite the active layer being thin (~90 nm).

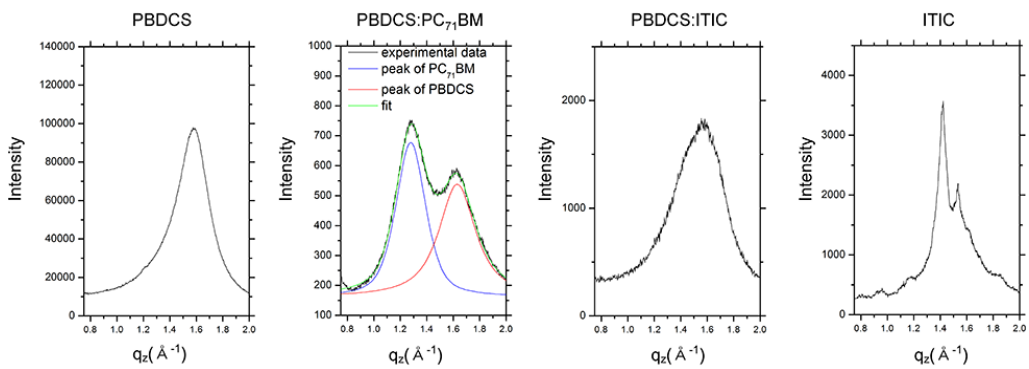

Figure 3-12. Diffraction profiles cut along the ~q_z axis of the 2D GIXD images. Fit (green line) fitted to pseudo-Voigt functions.

Rigidity of β-DCS molecules

Figure 3-13 shows the bond length of α-DCS and β-DCS in crystal. (a) bond is longer than (c) bond, and (d) bond is shorter than (d') bond, which is good agreement with the resonance structure of β-DCS in scheme 1. Figure 3-14 shows the ^{1}H-NMR chemical shift differences between α-DCS and β-DCS in solution. The protons of phenyl ring and alkoxy in β-DCS are located in the downfield compared with those of α-DCS, which means they are more electron deficient protons. This electron density difference also supports the resonance structure of β-DCS. According to the resonance structure of β-DCS, the electron distribution of the structure between both cyano groups in β-DCS is well delocalized, which implies structural rigidity of that structure. To verify this, we calculated the rotational energies of α-DCS and β-DCS by DFT method at the B3LYP/6–31G(d,p) level of theory (Figure 3-15). The rotational energy of β-DCS was twice as large as that of α-DCS, which supports the resonance structure and rigidity of β-DCS.

In general, CS molecules have large torsional or conformational changes in solution, leading to very low photoluminescence quantum yield (PLQY) as shown in figure 3-16. On the other hands, the β-DCS with an alkoxy side chain shows relatively high PLQY (25~30%) in solution, which means that it is hard for β-DCS to rotate or change the conformation in solution. Whereas, β-DCS with an alkyl side chain or without side chain show low PLQY (0.2~1.6%), which means that dialkoxy plays an important role in formation the resonance structures of β-DCS (Fig S13).

In conclusion, dialkoxy-β-dicyanodistyrylbenzene (β-DCS) has the unique resonance structures between alkoxy group and cyano group (Scheme 1). The alkoxy group and the cyano group are strong electron donating (push) and electron withdrawing (pull) arising from resonance effect, respectively. As a result, such strong push-pull structure strengthens the resonance structure, thereby rendering more rigid structure than other cyanostyrylbenzene (CS) molecules.

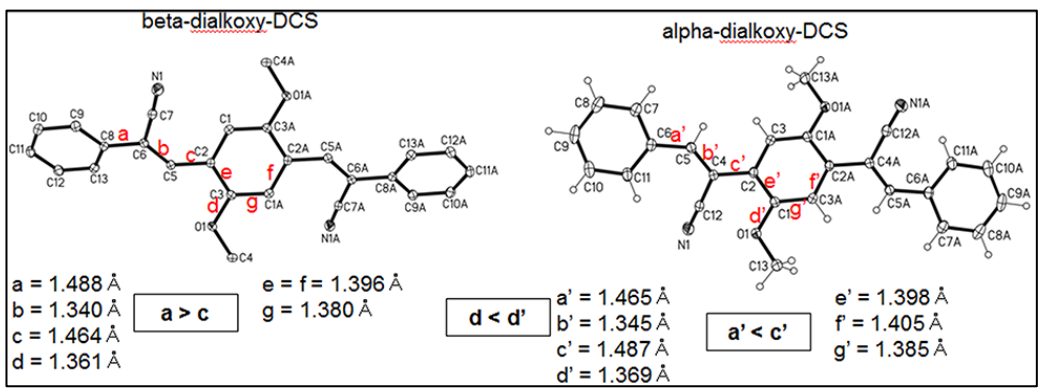

Figure 3-13. Crystallographic information[35] of β-DCS (left) and α-DCS (right)

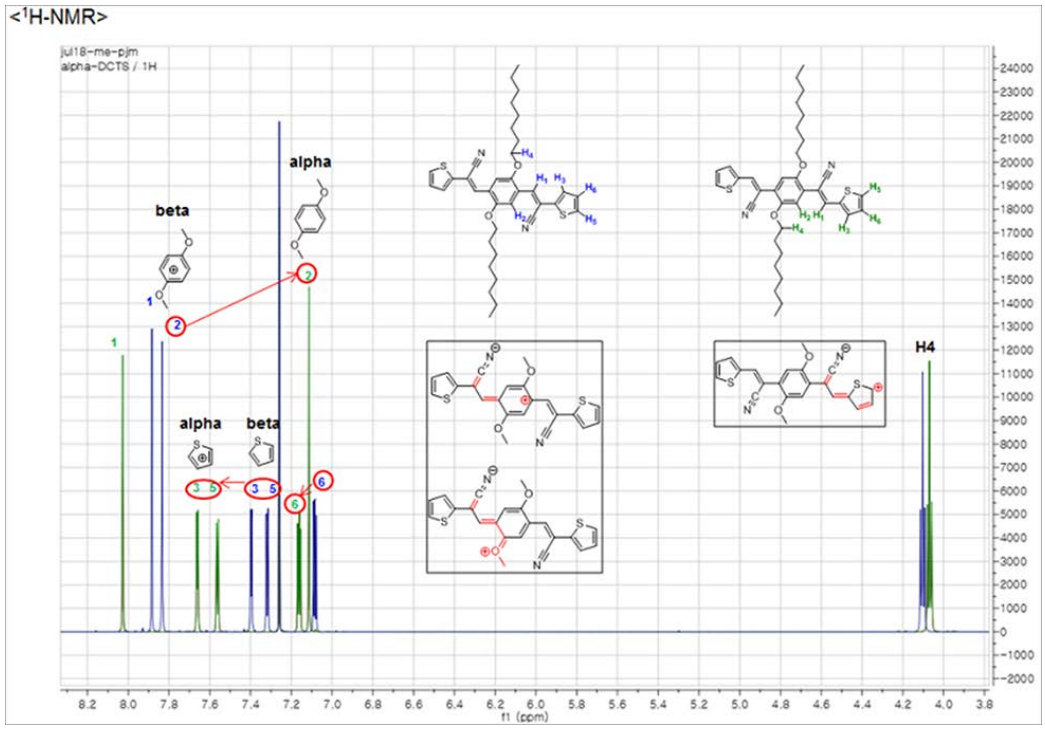

Figure 3-14. ^{1}H-NMR spectrum of α-DCS and β-DCS

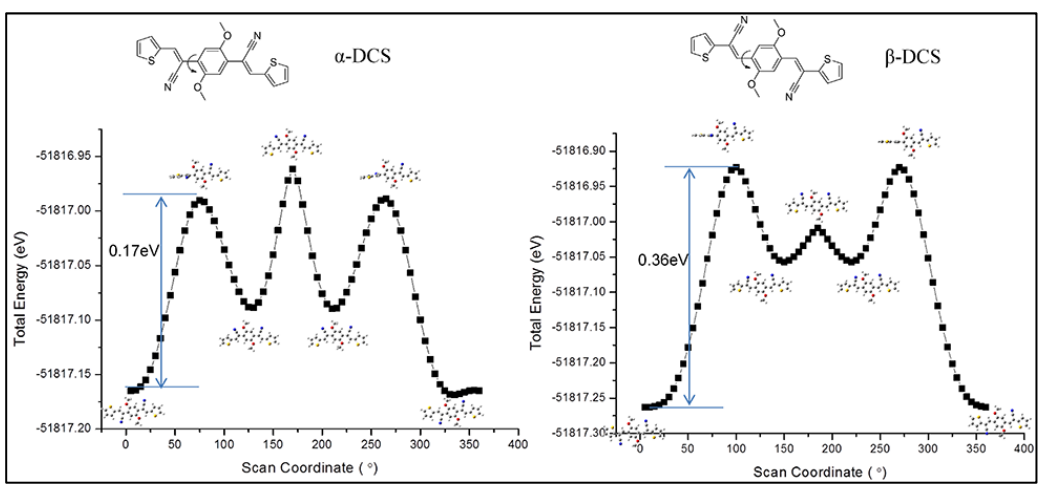

Figure 3-15. Torsion potential energies calculated using DFT with a basis set of B3LYP/6-31G(d,p).

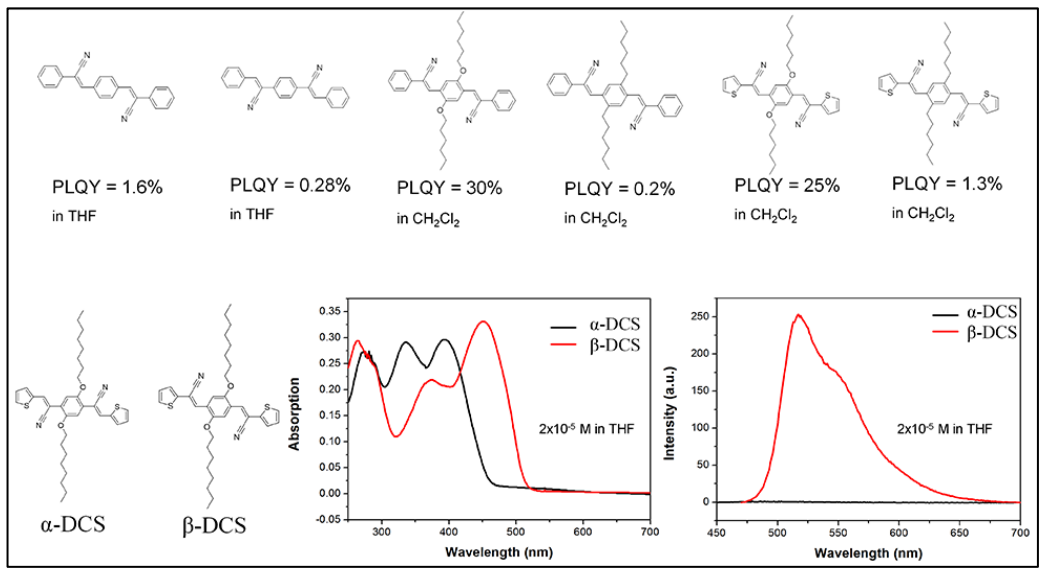

Figure 3-16. Molecular structures of various CS molecules and their PLQYs in solution.[67,68]

3.3. Experimental

General

All reagents were purchased from commercial sources and used as received. Anhydrous toluene was prepared by distillation with sodium and benzophenone. Compound 1^{S1}, 3^{S2}, and 5^{S3} were prepared following previously reported procedures. ^{1}H-, ^{13}C-NMR, MALDI-TOF and elemental analysis were measured by using a Bruker Avance-500, SCIEX TOF/TOF 5800 and CE instruments EA1110,

respectively. Gel permeation chromatography (GPC) was performed by using a Waters system and Waters styragel HT4 column eluted with 1,2-dichlororbenzene. UV-Vis absorption spectra and cyclic voltammetry (CV) were recorded by Shimadzu UV-1650PC and Princeton Applied Research Potentiostat/Galvanostat Model 273A. Thermogravimetric analysis (TGA) and differential scanning calorimetry (DSC) were measured by using TA instruments Q50 and DSC-Q1000, respectively, under a nitrogen atmosphere with heating rate of 10°C/min. AFM imaging was performed using Multimode with a Nano Scope V Controller (Bruker) in tapping mode. The 2D-GIXD was measured by using the PLS-II 9A U-SAXS beamline in the Pohang Accelerator Laboratory, Korea. The incidence angle was adjusted to 0.12°

Device Fabrication and Evaluation:

The patterned indium tin oxide (ITO) glass substrates were cleaned in an ultrasonic bath with acetone, and isopropanol, and then exposed to a UV/O_3 for 20min. PEDOT:PSS (Clavious P VP AI 4083) was spin-coated onto the ITO glass substrate at 5000 rpm for 30 s and the film was subsequently baked at 170 °C for 10min. A chlorobenzene:diphenylether (CB:DPE = 98:2) solution (totally 17.5 mg mL^{-1}) of PBDCS:$PC_{71}BM$ blend or a chlorobenzene solution (totally 14mg mL^{-1}) was subsequently spin-coated (1400 rpm for PBDCS:$PC_{71}BM$, 1600 rpm for PBDCS:ITIC) on the PEDOT:PSS coated ITO glass to form active layer (ca. 100 nm for PBDCS:$PC_{71}BM$, ca. 85 nm for PBDCS:ITIC). After drying the resulting films in a N_2 glovebox at room temperature for 30min, PFN (5nm) was spin-coated on the

PBDCS:$PC_{71}BM$ film, or Ca (5nm) was thermally deposited on PBDCS:ITIC film under a vacuum of 10^{-6} torr. Finally Al (80 nm) was thermally deposited under a vacuum of 10^{-6} torr.

For space-charge-limited currents (SCLC) measurement in this work, we have used Mott-Gurney law and fit the dark current under forward bias. The SCLC mobilities were calculated using the below equation:

$$J = \frac{9}{8}\varepsilon_0\varepsilon_r\mu\frac{V^2}{L^3}$$

(1)

In which ε_0 is the permittivity of free space, ε_r is the dielectric constant of the organic semiconductor material (herein ε_r was assumed to be 3 that typical value for organic semiconducting material), V is effective voltage with the equation of $V=V_{appl}-V_{bi}-V_r$ (V_{appl}: applied bias, V_{bi}: the built in potential due to the difference in electrical contact work function, V_r: the voltage drop due to contact resistance and series resistance across the electrodes) and L is the thickness of photoactive layer. The hole and electron only devices were fabricated respectively with the structure, ITO/PEDOT:PSS/BHJ layer/V_2O_5/Ag and ITO/ZnO/BHJ layer/Ca/Al.

The current density-voltage (J-V) characteristics of the solar cells were measured suing a Keithley 4200 source measurement unit. The solar cell performances were characterized under AM 1.5G condition with an illumination intensity of 100 mW cm^{-2}, as generated using an Oriel Sol3A solar simulator (Oriel model 9023A). The

measurements were carried out through a shadow mask with well-defined aperture area of 0.04 cm^2 under an ambient atmosphere. The incident photon-to-current efficiency (IPCE) was measured using an Oriel QE/IPCE Measurement Kit composed of a 300 W xenon lamp, a monochromator (74125), an order sorting filter wheel, a Merlin lock-in amplifier (70104), a calibrated silicon photodiode (70356_70316NS) and an optical chopper.

Synthesis

Compound 2

(R=2-hexyldecyl) According to previous report [1,2], 2-hexyldecy iodide (1.9 g, 5.4 mmol) and K_2CO_3 (746 mg, 5.4 mmol) were added to solution of the compound 1 (299 mg, 1.8 mmol) in DMF (5 ml). The reaction was stirred at 50°C for 1 day. The resulting mixture was cooled to room temperature. After aqueous work-up, the mixture was dried over anhydrous $MgSO_4$, and then the solvent was removed in vacuo. Finally, the crude product was purified by column chromatography (methylene chloride/n-hexane) to afford yellow liquid (808 mg, 73 %). ^{1}H NMR (400 MHz, $CDCl_3$, δ): 10.51 (s, 2H, -CHO), 7.43 (s, 2H, Ar-H), 3.97 (d, 4H, -CH2-), 1.82 (m, 2H, -CH-), 1.42-1.25 (m, 48H, -CH2-), 0.86(m, 12H, -CH3); ^{13}C NMR(400 MHz, $CDCl_3$, δ): 189.18, 155.33, 129.24, 111.40, 71.82, 37.82, 31.82, 31.75, 31.36, 29.90, 29.58, 29.49, 29.25, 26.77, 22.60, 14.02; MS (MALDI-TOF, m/z) Calcd for $C_{40}H_{70}O_4$: 614.53, found, 614.5.

(R=2-butyloctyl)

The same reaction conditions were used as above. Yield: 70% (351 mg). ^{1}H NMR (400 MHz, $CDCl_3$, δ): 10.51 (s, 2H, -CHO), 7.43 (s, 2H, Ar-H), 3.97 (d, 4H, -CH2-), 1.82 (m, 2H, -CH-), 1.42-1.26 (m, 32H, -CH2-), 0.88(m, 12H, -CH3); ^{13}C NMR(400 MHz, $CDCl_3$, δ): 189.25, 155.34, 129.25, 111.41, 71.84, 37.87, 31.74, 31.37, 31.06, 29.57, 28.98, 26.76, 22.94, 22.59, 14.02; MS (MALDI-TOF, m/z) Calcd for $C_{32}H_{54}O_4$: 502.40, found, 502.6.

Compound 4

(R=2-hexyldecyl) According to previous report [1,2], the mixture of compound 2 (614 mg, 1 mmol) and compound 3 (424 mg, 2.1 mmol) were dissolved in tert-butyl alcohol (10 mL) at 50 °C. Potassium tert-butoxide (224 mg, 2 mmol) was added quickly into the mixture. The reaction was stirred at 50°C for 30min. The reaction mixture was diluted in methanol, and then resulting precipitate was filtered. Finally, the crude product was purified by column chromatography (methylene chloride) and recrystallization (ethylacetate/methanol) to afford red solid (637 mg, 65%). ^{1}H NMR (500 MHz, $CDCl_3$, δ): 7.82 (s, 2H, vinyl−H), 7.74 (s, 2H, Ar-H), 7.14 (d, 2H, Ar-H), 7.04 (d, 2H, Ar-H), 3.98 (d, 4H, -OCH_2-), 1.85 (m, 2H, -CH-), 1.52-1.26(m, 48H, -CH2-), 0.90(m, 12H –CH3); ^{13}C NMR(400 MHz, $CDCl_3$, δ): 151.70, 141.07, 133.20, 131.05, 127.34, 125.40, 116.53, 113.64, 110.63, 105.40, 72.14, 38.07, 31.83, 31.35, 31.32, 29.89, 29.70, 29.17, 26.93, 23.05, 22.68, 14.08; MS (MALDI-TOF, m/z) Calcd for $C_{52}H_{74}Br_2N_2O_2S_2$: 980.36, found, 981.0.

(R=2-butyloctyl) The same reaction conditions were used as above. Yield: 70% (607 mg). ^{1}H NMR (400 MHz, $CDCl_3$, δ): 7.82 (s, 2H, vinyl−H), 7.75 (s, 2H, Ar-H), 7.14 (d, 2H, Ar-H), 7.05 (d, 2H, Ar-H), 3.98 (d, 4H, -OCH_2-), 1.85 (m, 2H, -CH-), 1.51-1.26(m, 32H, -CH2-), 0.90(m, 12H –CH3); ^{13}C NMR(400 MHz, $CDCl_3$, δ): 151.68, 141.06, 133.20, 131.04, 127.34, 125.40, 116.53, 113.64, 110.63, 105.39, 72.15, 38.07, 31.84, 31.72, 31.36, 29.75, 29.19, 26.95, 23.10, 22.70, 14.10; MS (MALDI-TOF, m/z) Calcd for $C_{44}H_{58}Br_2N_2O_2S_2$: 868.23, found, 868.3.

PBDCS

(R=2-hexyldecyl) A 20ml schlenk tube was charged with compound 4 (90.4mg, 0.1mmol), compound 5 (98.3mg, 0.1mmol), $Pd_2(dba)_3$ (2mg, 0.0022mmol), $P(o\text{-}tol)_3$ (2.7mg, 0.0088mmol) and anhydrous toluene (4ml), The schlenk tube was degassed with argon for 15min. The reaction was heated to 100°C for 24 hours. The polymer was precipitated into excess methanol, followed by soxhlet extraction with methanol, acetone, n-hexane and chloroform. The chloroform solution was precipitated into methanol. The polymer was filtered, then dried in vacuo to give product PBDCS as a black solid (130mg, 92%). GPC (1,2-DCB, 90°C): Mn = 90 kDa, PDI = 2.19. ^{1}H-NMR (400 MHz, 1,1,2,2-tetrachloroethane-d_2, 120 °C, δ): 7.95 (m, 4H, Ar−H, vinyl−H), 7.76-7.81 (m, 2H, Ar−H), 7.39 (m, 4H, Ar−H), 7.24-7.32 (m, 2H, Ar−H), 7.01 (m, 2H, Ar−H), 4.10 (s, 4H, −O−CH_2−), 2.98 (m, 4H, −Ar−CH_2−), 1.96 (m, 2H, −CH−), 1.80 (m, 2H, −CH−), 1.34−1.60 (m, 64H, −CH_2−), 0.88−1.08 (m, 24H, −CH_3). Anal.

Calcd for $C_{86}H_{116}N_2O_2S_6$: C, 73.66; H, 8.34; N, 2.00; O, 2.28; S, 13.72. Found: C, 73.93; H, 8.27; N, 2.04; O, 2.22; S, 13.66.

(R=2-butyloctyl) The same reaction conditions were used as above. Yield = 90% (116 mg). GPC (chloroform, 90°C): Mn = 60 kDa, PDI = 2.55. ^{1}H-NMR (400 MHz, 1,1,2,2-tetrachloroethane-d_2, 110 °C, δ): 7.95 (m, 4H, Ar−H, vinyl-H), 7.75-7.81 (m, 2H, Ar−H), 7.39 (m, 4H, Ar−H), 7.24-7.32 (m, 2H, Ar−H), 7.01 (m, 2H, Ar−H) 4.11 (s, 4H, −O−CH_2−), 2.98 (m, 4H, −Ar−CH_2−), 1.96 (m, 2H, −CH−), 1.82 (m, 2H, −CH−), 1.31−1.62 (m, 48 −CH_2−), 0.88−1.08 (m, 24H, −CH_3). Anal. Calcd for $C_{78}H_{100}N_2O_2S_6$: C, 72.62; H, 7.81; N, 2.17; O, 2.48; S, 14.91. Found: C, 72.70; H, 7.82; N, 2.24; O, 2.49; S, 14.79.

3.4. Conclusion

In summary, we developed a new β-DCS-based polymer (PBDCS) that contains no cis isomers and is completely tolerant to the photoisomerization reaction, unlike other CS-based polymers. We have shown that the photoisomeric stability originates from the unique resonance structure of β-DCS and the aggregation properties of the polymer. PBDCS showed a deep HOMO (–5.59 eV) and a low band gap (1.75 eV), and it has a small domain size and a small nanocrystalline structure in the film. As a result, an OSC based on a PBDCS:$PC_{71}BM$ attained a high V_{OC} of 0.95 V and high J_{SC} of 15 $mAcm^{-2}$

simultaneously, leading to a high PCE of 8.75%. Moreover, the OSC based on a PBDCS:ITIC exhibited a high PCE of 7.81% with a remarkably high V_{OC} of 1.08 V despite the small bandgap of 1.57 eV of the acceptor, resulting in an extremely small E_{loss} (0.49 eV), which is the smallest value in an efficient OSC and similar to those of inorganic solar cells and perovskite solar cells (E_{loss} = 0.4–0.55 eV). Importantly, a very high EQE (EQE_{max} = 74%) was attained despite the low E_{loss}, indicating that the charge generation and extraction process of the OSC work efficiently even with a small driving force. These results demonstrate the possibility of further improving the PCE of OSCs by achieving an E_{loss} of less than 0.5 eV with an EQE of over 70%. In addition, they suggest that β-DCS is promising accepting moiety of the donor polymer to realize a small E_{loss}.

3.5. Reference

[1]. L. Lu, T. Zheng, Q. Wu, A. M. Schneider, D. Zhao and L. Yu, Chemical reviews, 2015, 115, 12666-12731.

[2]. R. Kroon, M. Lenes, J. C. Hummelen, P. W. M. Blom and B. de Boer, Polymer Reviews, 2008, 48, 531-582.

[3]. D. Mühlbacher, M. Scharber, M. Morana, Z. Zhu, D. Waller, R. Gaudiana and C. Brabec, Advanced materials, 2006, 18, 2884-2889.

[4]. B. C. Thompson, Y.-G. Kim, T. D. McCarley and J. R. Reynolds, Journal of the American Chemical Society, 2006, 128, 12714-12725.

[5]. L. Ye, Y. Jing, X. Guo, H. Sun, S. Zhang, M. Zhang, L. Huo and J. Hou, The Journal of Physical Chemistry C, 2013, 117, 14920-14928.

[6]. F. Padinger, R. S. Rittberger and N. S. Sariciftci, Advanced Functional Materials, 2003, 13, 85-88.

[7]. G. Li, V. Shrotriya, J. Huang, Y. Yao, T. Moriarty, K. Emery and Y. Yang, Nature materials, 2005, 4, 864-868.

[8]. G. Li, Y. Yao, H. Yang, V. Shrotriya, G. Yang and Y. Yang, Advanced Functional Materials, 2007, 17, 1636-1644.

[9]. J. K. Lee, W. L. Ma, C. J. Brabec, J. Yuen, J. S. Moon, J. Y. Kim, K. Lee, G. C. Bazan and A. J. Heeger, Journal of the American Chemical Society, 2008, 130, 3619-3623.

[10]. J. Peet, J. Y. Kim, N. E. Coates, W. L. Ma, D. Moses, A. J. Heeger and G. C. Bazan, Nature materials, 2007, 6, 497-500.

[11]. K. Schmidt, C. J. Tassone, J. R. Niskala, A. T. Yiu, O. P. Lee, T. M. Weiss, C. Wang, J. M. Frechet, P. M. Beaujuge and M. F. Toney, Advanced materials, 2014, 26, 300-305.

[12]. N. Leclerc, P. Chávez, O. Ibraikulov, T. Heiser and P. Lévêque, Polymers, 2016, 8, 11.

[13]. H.-Y. Chen, J. Hou, S. Zhang, Y. Liang, G. Yang, Y. Yang, L. Yu, Y. Wu and G. Li, Nature Photonics, 2009, 3, 649-653.

[14]. S. C. Price, A. C. Stuart, L. Yang, H. Zhou and W. You, Journal of the American Chemical Society, 2011, 133, 4625-4631.

[15]. Z. Chen, P. Cai, J. Chen, X. Liu, L. Zhang, L. Lan, J. Peng, Y. Ma and Y. Cao, Advanced materials, 2014, 26, 2586-2591.

[16]. Y. Liu, J. Zhao, Z. Li, C. Mu, W. Ma, H. Hu, K. Jiang, H. Lin, H. Ade and H. Yan, Nature communications, 2014, 5, 5293.

[17]. J. A. Bartelt, J. D. Douglas, W. R. Mateker, A. E. Labban, C. J. Tassone, M. F. Toney, J. M. J. Fréchet, P. M. Beaujuge and M. D. McGehee, Advanced Energy Materials, 2014, 4, 1301733.

[18]. W. Zhao, D. Qian, S. Zhang, S. Li, O. Inganas, F. Gao and J. Hou, Advanced materials, 2016, 28, 4734-4739.

[19]. S. Li, L. Ye, W. Zhao, S. Zhang, S. Mukherjee, H. Ade and J. Hou, Advanced materials, 2016, 28, 9423-9429.

[20]. D. Baran, R. S. Ashraf, D. A. Hanifi, M. Abdelsamie, N. Gasparini, J. A. Rohr, S. Holliday, A. Wadsworth, S. Lockett, M. Neophytou, C. J. Emmott, J. Nelson, C. J. Brabec, A. Amassian, A. Salleo, T. Kirchartz, J. R. Durrant and I. McCulloch, Nature materials, 2017, 16, 363-369.

[21]. https://www.nrel.gov/pv/assets/images/efficiency-chart.png.

[22]. D. Veldman, S. C. J. Meskers and R. A. J. Janssen, Advanced Functional Materials, 2009, 19, 1939-1948.

[23]. W. Li, K. H. Hendriks, A. Furlan, M. M. Wienk and R. A. Janssen, Journal of the American Chemical Society, 2015, 137, 2231-2234.

[24]. D. Baran, T. Kirchartz, S. Wheeler, S. Dimitrov, M. Abdelsamie, J. Gorman, R. S. Ashraf, S. Holliday, A. Wadsworth, N. Gasparini, P. Kaienburg, H. Yan, A. Amassian, C. J. Brabec, J. R. Durrant and I. McCulloch, Energy Environ Sci, 2016, 9, 3783-3793.

[25]. K. Kawashima, Y. Tamai, H. Ohkita, I. Osaka and K. Takimiya, Nature communications, 2015, 6, 10085.

[26]. J. Liu, S. Chen, D. Qian, B. Gautam, G. Yang, J. Zhao, J. Bergqvist, F. Zhang, W. Ma, H. Ade, O. Inganäs, K. Gundogdu, F. Gao and H. Yan, Nature Energy, 2016, 1, 16089.

[27]. H. Bin, L. Gao, Z. G. Zhang, Y. Yang, Y. Zhang, C. Zhang, S. Chen, L. Xue, C. Yang, M. Xiao and Y. Li, Nature communications, 2016, 7, 13651.

[28]. H. Bin, Z. G. Zhang, L. Gao, S. Chen, L. Zhong, L. Xue, C. Yang and Y. Li, Journal of the American Chemical Society, 2016, 138, 4657-4664.

[29]. C. Cui, W.-Y. Wong and Y. Li, Energy Environ. Sci., 2014, 7, 2276-2284.

[30]. C. Cui, Z. He, Y. Wu, X. Cheng, H. Wu, Y. Li, Y. Cao and W.-Y. Wong, Energy Environ. Sci., 2016, 9, 885-891.

[31]. L. Ye, S. Zhang, W. Zhao, H. Yao and J. Hou, Chemistry of Materials, 2014, 26, 3603-3605.

[32]. A. Casey, Y. Han, Z. Fei, A. J. P. White, T. D. Anthopoulos and M. Heeney, J. Mater. Chem. C, 2015, 3, 265-275.

[33]. B.-K. An, J. Gierschner and S. Y. Park, Accounts of chemical research, 2012, 45, 544-554.

[34] J. Gierschner and S. Y. Park, Journal of Materials Chemistry C, 2013, 1, 5818.

[35] S.-J. Yoon, S. Varghese, S. K. Park, R. Wannemacher, J. Gierschner and S. Y. Park, Advanced Optical Materials, 2013, 1, 232-237.

[36] see rigidity of β-DCS molecules part in supporting information.

[37] S. W. Yun, J. H. Kim, S. Shin, H. Yang, B.-K. An, L. Yang and S. Y. Park, Advanced materials, 2012, 24, 911-915.

[38] J. W. Park, S. Nagano, S.-J. Yoon, T. Dohi, J. Seo, T. Seki and S. Y. Park, Advanced materials, 2014, 26, 1354-1359.

[39] J. W. Chung, S.-J. Yoon, B.-K. An and S. Y. Park, The Journal of Physical Chemistry C, 2013, 117, 11285-11291.

[40] Y. Li, H. Xu, L. Wu, F. He, F. Shen, L. Liu, B. Yang and Y. Ma, Journal of Polymer Science Part B: Polymer Physics, 2008, 46, 1105-1113.

[41] J. H. Kim, S. K. Park, J. H. Kim, D. R. Whang, W. S. Yoon and S. Y. Park, Advanced materials, 2016, 28, 6011-6015.

[42] O. K. Kwon, J.-H. Park, S. K. Park and S. Y. Park, Advanced Energy Materials, 2015, 5, n/a-n/a.

[43] O. K. Kwon, J. H. Park, D. W. Kim, S. K. Park and S. Y. Park, Advanced materials, 2015, 27, 1951-1956.

[44] O. K. Kwon, M. A. Uddin, J. H. Park, S. K. Park, T. L. Nguyen, H. Y. Woo and S. Y. Park, Advanced materials, 2016, 28, 910-916.

[45] J. Min, O. K. Kwon, C. Cui, J.-H. Park, Y. Wu, S. Y. Park, Y. Li and C. J. Brabec, J. Mater. Chem. A, 2016, 4, 14234-14240.

[46] S. Zhang, Y. Qin, M. A. Uddin, B. Jang, W. Zhao, D. Liu, H. Y. Woo and J. Hou, Macromolecules, 2016, 49, 2993-3000.

[47] M. M. Koetse, J. r. Sweelssen, K. T. Hoekerd, H. F. M. Schoo, S. C. Veenstra, J. M. Kroon, X. Yang and J. Loos, Applied Physics Letters, 2006, 88, 083504.

[48] J.-H. Kim, H. U. Kim, W. S. Shin, S.-J. Moon, S. C. Yoon and D.-H. Hwang, Solar Energy Materials and Solar Cells, 2012, 101, 131-139.

[49] L. Ye, S. Zhang, L. Huo, M. Zhang and J. Hou, Accounts of chemical research, 2014, 47, 1595-1603.

[50] L. Huo, S. Zhang, X. Guo, F. Xu, Y. Li and J. Hou, Angewandte Chemie, 2011, 50, 9697-9702.

[51] S. Zhang, L. Ye and J. Hou, Advanced Energy Materials, 2016, 6, 1502529.

[52] J.-M. Park, S. K. Park, W. S. Yoon, J. H. Kim, D. W. Kim, T.-L. Choi and S. Y. Park, Macromolecules, 2016, 49, 2985-2992.

[53] W. Lee, G.-H. Kim, S.-J. Ko, S. Yum, S. Hwang, S. Cho, Y.-H. Shin, J. Y. Kim and H. Y. Woo, Macromolecules, 2014, 47, 1604-1612.

[54] R. Rieger, D. Beckmann, A. Mavrinskiy, M. Kastler and K. Müllen, Chemistry of Materials, 2010, 22, 5314-5318.

[55] Y. Kasai, Y. Tamai, H. Ohkita, H. Benten and S. Ito, Journal of the American Chemical Society, 2015, 137, 15980-15983.

[56] W. Ma, G. Yang, K. Jiang, J. H. Carpenter, Y. Wu, X. Meng, T. McAfee, J. Zhao, C. Zhu, C. Wang, H. Ade and H. Yan, Advanced Energy Materials, 2015, 5, 1501400.

[57] Y. Lin, J. Wang, Z. G. Zhang, H. Bai, Y. Li, D. Zhu and X. Zhan, Advanced materials, 2015, 27, 1170-1174.

[58] K. Zhao, Q. Wang, B. Xu, W. Zhao, X. Liu, B. Yang, M. Sun and J. Hou, J. Mater. Chem. A, 2016, 4, 9511-9518.

[59] Y. Yang, W. Chen, L. Dou, W.-H. Chang, H.-S. Duan, B. Bob, G. Li and Y. Yang, Nature Photonics, 2015, 9, 190-198.

[60] W. Li, K. H. Hendriks, A. Furlan, W. S. Roelofs, S. C. Meskers, M. M. Wienk and R. A. Janssen, Advanced materials, 2014, 26, 1565-1570.

[61] H. Bronstein, D. S. Leem, R. Hamilton, P. Woebkenberg, S. King, W. Zhang, R. S. Ashraf, M. Heeney, T. D. Anthopoulos, J. d. Mello and I. McCulloch, Macromolecules, 2011, 44, 6649-6652.

[62] G. Grancini, M. Maiuri, D. Fazzi, A. Petrozza, H. J. Egelhaaf, D. Brida, G. Cerullo and G. Lanzani, Nature materials, 2013, 12, 29-33.

[63] T. Hahn, J. Geiger, X. Blase, I. Duchemin, D. Niedzialek, S. Tscheuschner, D. Beljonne, H. Bässler and A. Köhler, Advanced Functional Materials, 2015, 25, 1287-1295.

[64] O. V. Mikhnenko, H. Azimi, M. Scharber, M. Morana, P. W. M. Blom and M. A. Loi, Energy & Environmental Science, 2012, 5, 6960.

[65] D. M. Smilgies, Journal of applied crystallography, 2009, 42, 1030-1034.

[66] W. Chen, T. Xu, F. He, W. Wang, C. Wang, J. Strzalka, Y. Liu, J. Wen, D. J. Miller, J. Chen, K. Hong, L. Yu and S. B. Darling, Nano letters, 2011, 11, 3707-3713. 57-66

[67] S.-J. Yoon and S. Park, Journal of Materials Chemistry, 2011, 21, 8338.

[68] S. E. Döttinger, M. Hanack, J. L. Segura, E. Steinhuber, M. Hohloch, A. Tompert and D. Oelkrug, Advanced materials, 1997, 9, 233-236.

Chapter 4.

Designing Thermally Stable Conjugated Polymers with Balanced Ambipolar Field-Effect Mobilities by Incorporating Cyanovinylene Linker Unit

4.1. Introduction

Polymer-based organic field-effect transistors (OFETs) have been extensively researched over the past two decades as an attractive candidate for implementation in flexible displays, sensors, radio-frequency identification (RFID) tags, and low-cost electronics on account of their mechanical flexibility, ductility, and favorable solution processability (e.g., printing technique).[1-7] Furthermore, ambipolar materials that exhibit balanced hole and electron mobility have attracted considerable attention on account of the demonstration of complementary inverters with a single organic semiconductor, which is the most ideal strategy for simplicity of device fabrication.[2,8-11] Despite these merits, commercialization of OFETs has been impeded by insufficient charge transport mobility and instability of the organic semiconductor used in OFETs. Nevertheless, charge mobility and environmental stability (e.g., oxygen and humidity) of the organic semiconductor have been sufficiently improved for commercialization, resulting in development of numerous materials and device fabrication methods.[3,12-15]

In contrast, operational device stabilities have been not received much attention.[16] Among them, thermal stability—i.e., thermally robust charge mobility—is an important factor for practical application because additional thermal processes are needed for device fabrication and utilizing the final applications.[17] Moreover, Joule heating is always generated during operation of the electronic device.[18,19] In particular, thermal stability of the device is much more important in ambipolar OFETs for steady

performance. To meet this demand for thermal stability, thermally stable semiconducting polymers are required. However, conventional semiconducting polymers show that hole or electron mobility is changed by thermal annealing, which is accompanied by the changes in nanostructure.[20-22] Therefore, design of ambipolar semiconducting materials that have thermal stability, along with balanced hole and electron mobility, is critical for developing thermally stable ambipolar OFETs.

The donor–acceptor (D–A) alternating copolymer is the most widely used design of low bandgap polymer for OFETs and OPV applications because the frontier molecular orbitals are essentially ascribed to the electron donating and accepting strength of D and A moieties.[23] As a rule, the D–A alternating copolymer is a suitable design for realizing ambipolar materials. However, until now ambipolar and/or n-type semiconducting polymers have rarely been achieved compared to the p-type semiconducting polymers on account of the scarcity of strong accepting units for a low-lying LUMO level and delocalized LUMO over the whole polymer backbone, which facilitates electron transport.[24-27] Therefore, utilization of the strong electron withdrawing group as a substituent or linker in D–A copolymers is a good strategy for development of n-type and ambipolar polymers.

Cyano (CN) group is a strong electron withdrawing group that provides stabilization of the frontier molecular orbitals for semiconducting materials. Moreover, it offers a strong intermolecular interaction.[28-31] Indeed, since CN substituted poly(phenylene vinylene) (CN-PPV) was firstly developed for OLED applications,[32]

CN substituted materials have been researched for various electronic applications using the electronic effects of the CN group.[28, 29, 33-36] Recently, Heeney et al. reported an n-type D–A copolymer via CN substitution on a benzothiadiazole (BT) accepting unit, which promotes the electron accepting strength.[37] Kwon and co-workers also reported CN substituted polymers of which the field-effect electron mobility exhibited up to 7 $cm^2\ V^{-1}s^{-1}$.[13,38] Meanwhile, we have intensively investigated the cyanovinylene (CNV) containing small molecules, focusing on structural effects of the CNV group; facilitating self-assembled nanostructures formation and aggregation-induced enhanced emission (AIEE).[39,40] Recently, we additionally developed an n-type material with high n-type field-effect mobility (2.14 $cm^2\ V^{-1}\ s^{-1}$) and a high-performance non-fullerene acceptor for organic photovoltaics (OPVs) via tight stacking between CNV containing small molecules.[41,42]

In this study, we focus on a design of thermally stable and highly balanced ambipolar polymer by insertion of CNV as a linker into the p-type D–A copolymer—comprised of BDT and DPP units—which has a high decomposition temperature.[43] Consequently, CNV containing polymer (PBCDC) exhibited highly balanced ambipolar mobility ($\mu_{h,max}$ ~ 0.2 $cm^2\ V^{-1}s^{-1}$, $\mu_{e,max}$ ~ 0.2 $cm^2\ V^{-1}s^{-1}$). Furthermore, the ambipolar mobilities were surprisingly invariant, regardless of annealing temperatures. To provide evidence of the significant role of CNV, we additionally prepared copolymer without CNV (PBD) and performed a comparative analysis with PBCDC by thermal analysis, UV-Vis absorption spectroscopy, ultraviolet photoelectron

spectroscopy (UPS), two-dimensional grazing incidence X-ray diffraction (2D-GIXD), and atomic force microscopy (AFM). As a result, we found that CNV facilitates the high thermal stability and enhanced ambipolar mobility of PBCDC.

4.2. Results and Discussion

Synthesis

Figure 4-1 shows the synthetic procedure of PBDCD, where CNV was incorporated as a linker between the BDT and DPP units. In addition, polymer without CNV (PBD), which has the same alkyl side chain as PBCDC, was synthesized for precise comparative analysis with PBCDC in respect of thermal and electronic properties. The PBD was prepared with a high molecular weight (Mn = 148 kDa, Mw = 444 kDa) via conventional Stille coupling reaction between M1 and M4. The PBCDC was synthesized via Suzuki coupling reactions between M2 and M3 instead of the Knoevenagel reaction, which is a general method for preparing CNV containing polymers.[32,35,44,45] This is because the latter has the disadvantage of obtaining high molecular weight polymer on account of using alcohol as a solvent; i.e., alcohol is a poor solvent for polymers with an alkyl side chain. Consequently, we obtained PBDCD with a high molecular weight (Mn = 198 kDa, Mw = 846 kDa), which was sufficiently high to compare with PBD, excluding the molecular weight effect on the OFET

performance.[46-48] The detailed synthetic procedures of the monomers and polymers are described in the Experimental section.

Optical and Electrical Properties

UV-Vis absorption spectra of the polymers were measured in chloroform solution and film (Figure 4-2). In the case of PBD, the film displays a red shifted absorption spectrum compared with the solution, as well as an increased shoulder peak at 739 nm, which is attributed to the intermolecular π–π stacking of conjugated backbone.[21,37,49] In the case of PBCDC, absorption spectrum of the film is also red shifted, similar to PBD. On the other hand, the shape of the absorption spectra are essentially unchanged from solution to film, which implies that the polymer has a similar conformational structure in both solution and film states. Therefore, it could be postulated that PBCDC forms aggregates even in a solution state by a strong intermolecular interaction induced from the CNV group.[30]

Another important feature is energy-level tuning by introduction of CNV. The

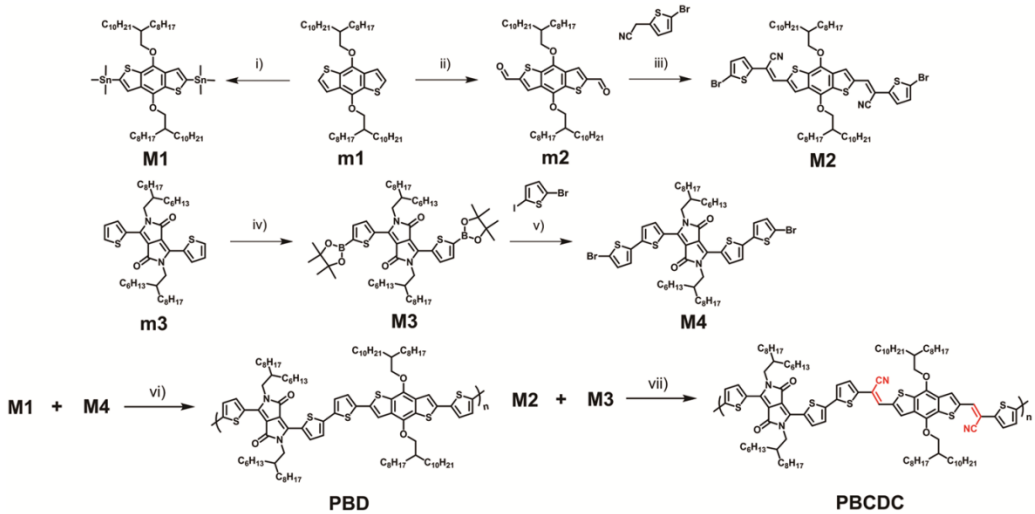

Figure 4-1. Synthesis of PBD, PBCDC, and their monomers. Reaction conditions: i) n-BuLi, Me3SnCl, dry THF, -78° C~r.t; ii) n-BuLi, dry DMF, dry THF, -78° C~r.t; iii) KOtBu, tBuOH, 50° C; iv) LDA, 2-Isopropoxy-4,4,5,5-tetramethyl-1,3,2-dioxaborolane, -78° C~r.t; v) Pd(PPh3)4, Na2CO3(aq)(2M), THF, 70° C; vi) Pd2(dba)3, P(o-tol)3, dry Toluene, 100° C ; vii) Pd2(dba)3, P(o-tol)3, Na2CO3(aq)(2M), Toluene, 100° C.

difference in the absorption onsets (ca. 40 nm, Figure 4-2b) between the polymer films reveals that PBCDC shows slightly lower energy gap (1.44 eV) compared to the PBD case (1.51 eV). For analysis of the electronic energy level change, HOMO and LUMO levels of the polymers were determined from results of the UPS measurement and optical bandgap (Figure 4-2c). The results indicate that CNV efficiently stabilizes the

frontier molecular orbitals of the polymers. In this regard, it should be noted that the LUMO level difference (0.32 eV) is larger than that of the HOMO level (0.25eV), which implies that CNV further stabilizes the LUMO than the HOMO level, which leads to the bandgap difference.

Density functional theory (DFT) calculations based on B3LYP/6-31G∗ were performed to further analyze the energy levels and molecular orbital distributions (Figure 4-3). The results of the calculations show that the theoretical HOMO and LUMO values are all higher in energy than the experimental values. Nevertheless, the calculation results qualitatively well reflect the trend of experimentally defined energy levels, i.e., the LUMO level is more stabilized than the HOMO level by introduction of CNV. In addition, molecular orbital distribution from optimized geometries of PBD and PBCDC repeat units is depicted in Figure 4-3. According to calculations, PBD shows delocalized character of HOMO over the entire polymer backbone; however, the LUMO is localized on the acceptor unit; showing typical molecular orbital distribution of p-type conjugated polymers. In contrast, LUMO of PBCDC is fully delocalized over

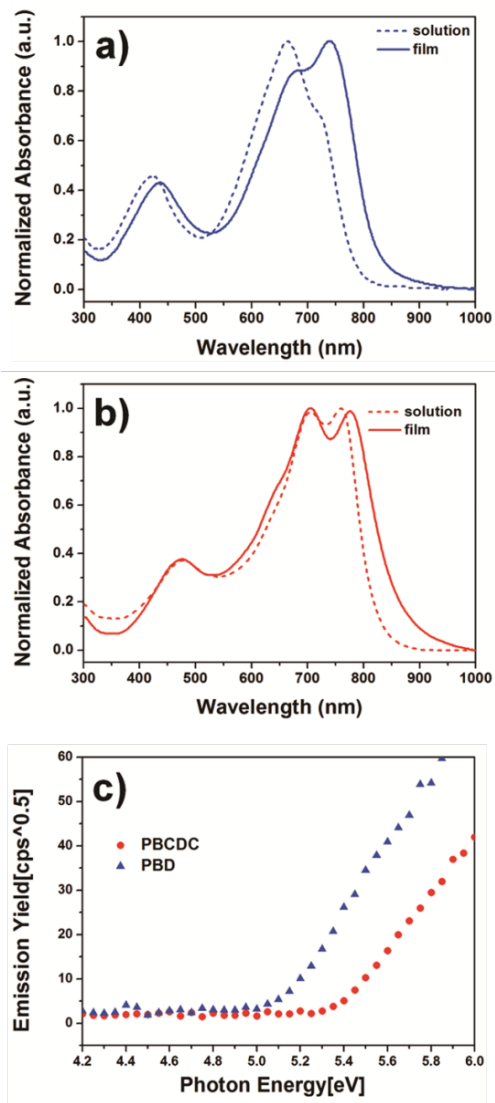

Figure 4-2. Normalized UV-Vis absorption spectra of (a) PBD and (b) PBCDC. (c) UPS spectra of PBD and PBCDC.

the backbone structure, which can benefit inter- and intra-chain electron transfer. Thus, these results imply that electron transport is facilitated by introduction of CNV into p-type polymer on account of the change of molecular orbital distribution as well as energy level.

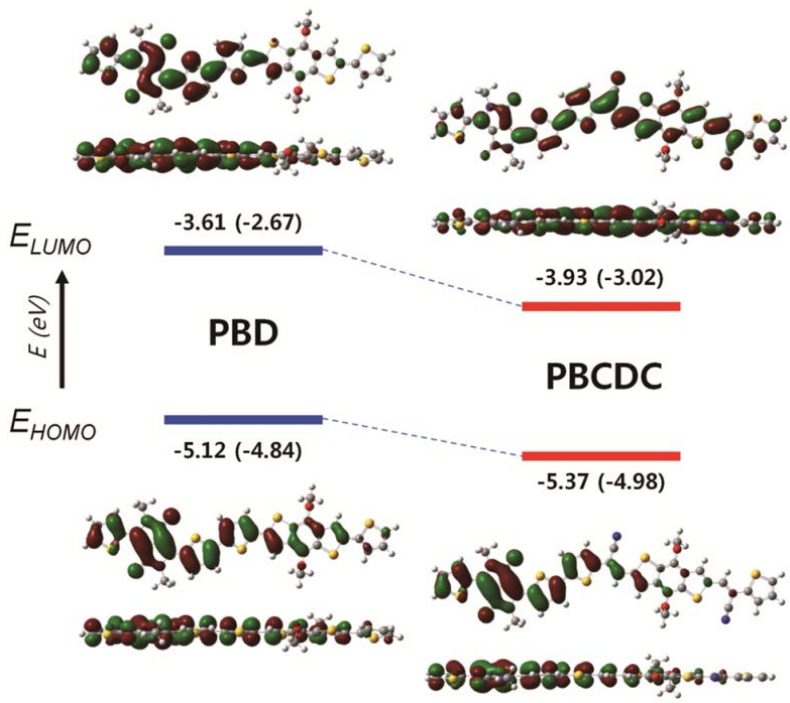

Figure 4-3. Experimental and theoretical (values in parentheses) HOMO and LUMO energy levels of PBD and PBCDC. Also shown are optimized geometries by DFT calculation with charge density iso-surfaces for LUMO and HOMO of the PBD and PBCDC repeat units (branched alkyl chains on BDT and DPP units were omitted for simplicity).

OFET performance and thermal properties

Bottom-gate/top-contact (BGTC) configuration OFET devices were fabricated using the polymers. After the active layer was spin-coated on substrate, a baking process was performed at 80°C for 2 h to evaporate the residual solvent with high boiling point (1,2-dichlorobenzene, 180.5°C). Additional thermal annealing was carried out at 150°C, 200°C, and 250°C for 20 min in nitrogen condition. Figure 4 displays transistor mobilities as a function of annealing temperature and transfer curves of the OFET devices. PBD exhibits typical p-type charge carrier transporting behavior with a maximum hole mobility of ~ 0.1 $cm^2\ V^{-1}s^{-1}$. The hole mobilities were preserved until a 150°C annealing temperature; however, they show abrupt decrease when the devices were annealed at over 200°C.

The PBD devices exhibit varying hole mobilities depending on the annealing temperature, which has also been shown in previously reported results; however with different optimized annealing temperature by varied alkyl side chain.[43] On the other hand, PBCDC exhibits an ambipolarity with improved field-effect mobilities ($\mu_{h,max}$ ~0.2 $cm^2\ V^{-1}s^{-1}$, $\mu_{e,max}$ ~0.2 $cm^2\ V^{-1}s^{-1}$), and the characteristic curves show excellent symmetry, reflecting highly balanced properties. Furthermore, PBCDC devices show that the field-effect mobilities are invariant from 80°C to 250°C, which is an exceptional character compared with typical conjugated polymers.

To understand the mobility change dependency on annealing temperature, we

analyzed the thermal properties by TGA and DSC measurements (Figure 4-4, 4-5). The TGA data show that the thermal decomposition temperature (T_d, 5% weight loss) of PBCDC is 11°C higher than that of PBD; Td (PBD) = 363.2°C, T_d (PBCDC) = 374.2°C. In addition, DSC data also show that the endothermic onset point of the PBCDC is 34.1°C higher than that of the PBD; $T_{endo,onset}$ (PBD) = 283.5°C, $T_{endo,onset}$ (PBCDC) = 317.6°C. It is postulated that these thermal stabilities of the polymers affects the mobility difference between PBD and PBCDC at a high annealing temperature. These results indicate that the introduction of CNV affects the thermal properties as well as the electronic properties.

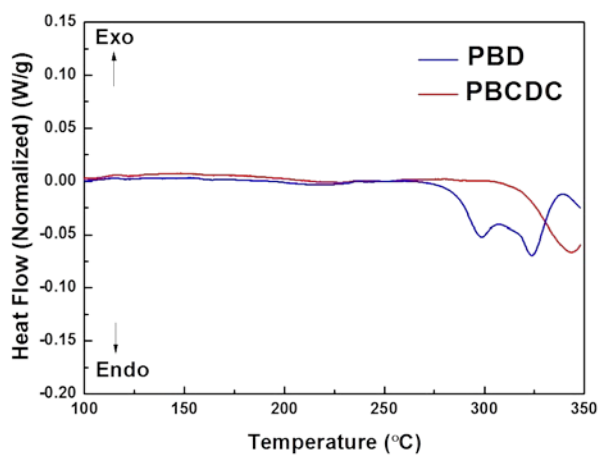

Figure 4-4. DSC of the polymers (PBD (endothermic onset, 283.5°C), PBCDC (endothermic onset, 317.6°C)).

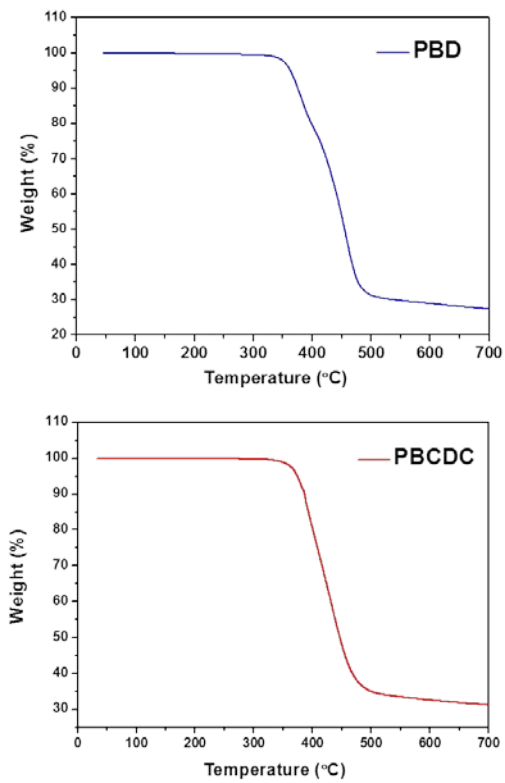

Figure 4-5. TGA of the polymers: (a) PBD (5% loss, 363.2°C), (b) (5% loss, 374.2°C).

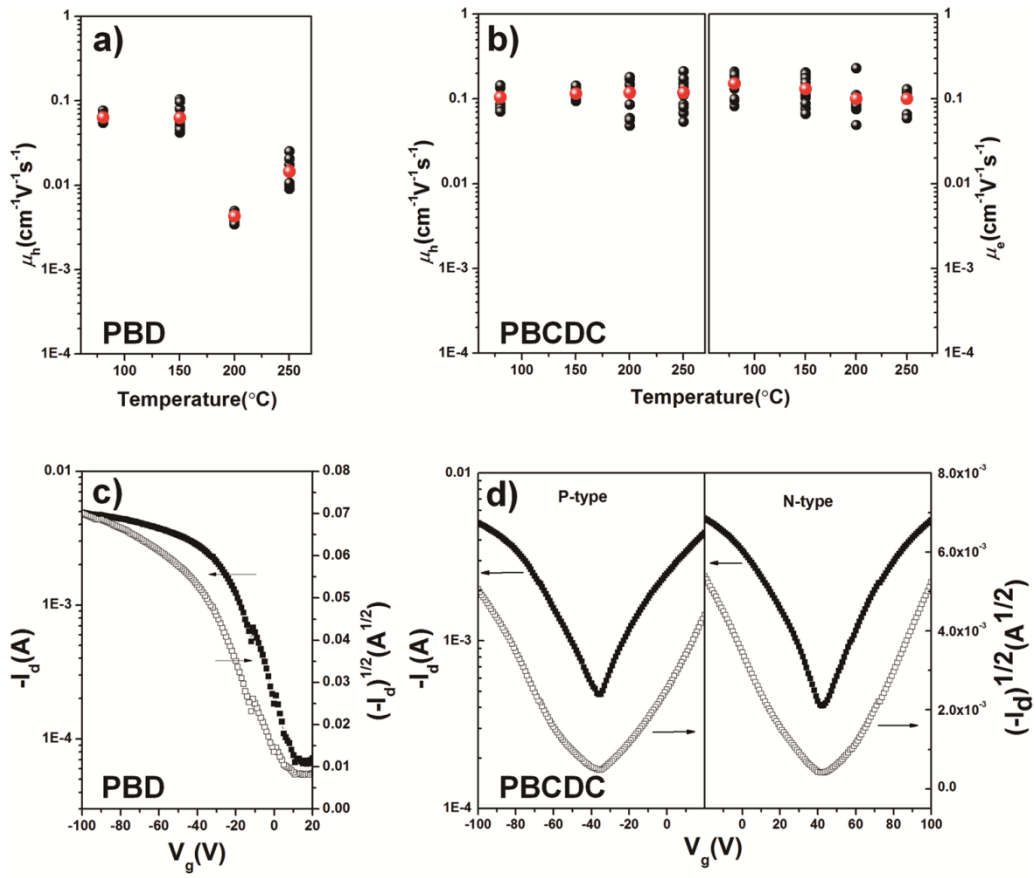

Figure 4-6. Transistor mobilities as a function of annealing temperature for (a) PBD and (b) PBCDC (right); ten devices were tested for each material. Transfer characteristics of (c) PBD and (d) PBCDC.

Structural Analysis

To understand the enhanced field-effect mobilities that are independent of the annealing temperature of PBCDC, two-dimensional grazing incidence X-ray diffraction (2D-GIXD) measurement was performed on the polymer films (Figure 4-7). 2D-GIXD images of the PBD and PBCDC films annealed at all temperatures show broad π–π stacking diffractions (q ~1.5 $Å^{-1}$) as an arc in the q_z axis and weak lamellar diffractions (q = 0.25, 0.5, 0.75 $Å^{-1}$), indicating predominant face-on orientations and mixed face-on and edge-on orientated nanostructures, respectively. These results imply that both the PBD and the PBCDC films are face-on-orientated semi-crystalline polymer with small crystal domains that have face-on and edge-on mixed orientations.

In the case of the PBD film, the annealing at higher temperatures gradually increased the lamellar diffraction—(100), (200), and (300) in the q_z axis—indicating the increased population of edge-on crystallites and larger crystal sizes, which are typical features of conjugated polymers.[21,22] On the other hand, changes in diffractions of the PBCDC films are minimized with an increasing annealing temperature. For an in-depth exploration of the diffraction pattern changes by annealing temperatures, pole figure analyses were performed in the same manner as the previously reported method.[50] The pole figures were extracted by circular cut from the lamellar diffraction, (100), of 2D-GIXD images of the PBD and the PBCDC films. We integrated pole figures by polar angle χ ranges: 0–45° and 55–125° correspond to face-on; and 135–

180°C correspond to edge-on orientation fractions (Figure 4-8b). It should be noted that, while the ratio of edge-on to face-on orientations for the PBD film was rapidly changed at high annealing temperature, those of the PBCDC films were almost the same. This finding is consistent with the uniform mobility of the PBCDC devices for all annealing temperatures (Figure 4-8c). The relationship between annealing temperature and nanostructure of the polymer films was further verified by AFM measurements (Figure 4-9). The surface root-mean-square (RMS) roughness values were determined from AFM images. RMS of the PBD film rapidly increased at a high annealing temperature compared to the PBCDC film (Figure 4-10). This finding is also consistent with the trend observed in the pole figures analyses of 2D-GIXD. The data from both 2D-GIXD and AFM indicate that the thermally stable charge carrier mobility of PBCDC originated from unvarying nanostructure in film regardless of annealing temperature on account of the introduction of CNV, providing a strong intermolecular interaction that restricts the molecular motion.

Strong intermolecular interaction by CNV also affects the interlayer distance (d-spacing). The lamellar and π–π stacking distances of the polymer films were determined from 2D-GIXD data (Figure 4-8a). The lamellar stacking distances of the PBCDC film (21.9Å) were closer than that of the PBD (22.4Å), even though they have same alkyl side chains, probably due to the increment of dihedral angles induced from the CN group.13 In particular, the π–π stacking distance of PBCDC (3.96Å) was shorter than that of PBD (4.10Å) by the strong intermolecular interaction induced from

CNV. From these results, we surmise that the tight stacking structure induced from CNV provides higher charge-carrier mobilities and thermal stability of PBCDC.

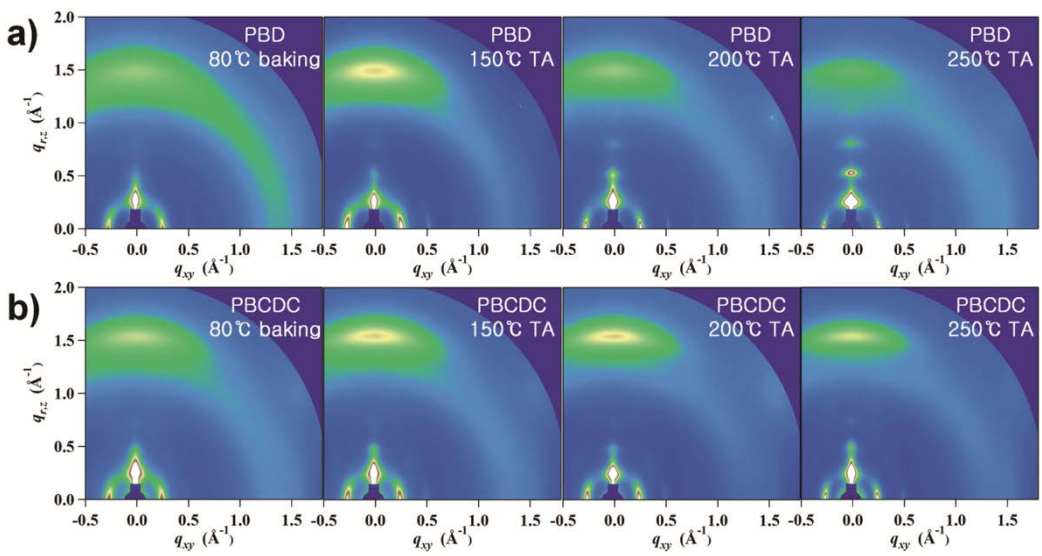

Figure 4-7. 2D-GIXD images of PBD (a) PBCDC (b) thin films just baked and additionally annealed at 150°C, 200°C, and 250°C, respectively.

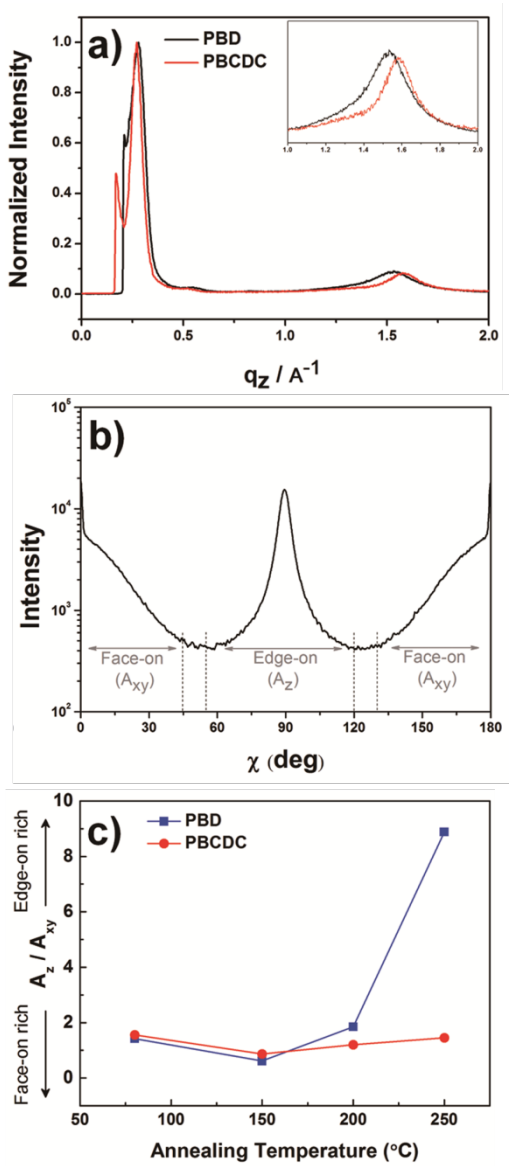

Figure 4-8. (a) Out-of-plane (qxy = 0) X-ray diffraction patterns of the polymer, (b) pole figures extracted from the lamellar diffraction, (100), and (c) dependence of Az/Axy on annealing temperatures, where Az/Axy is the ratio of the edge-on to face-on orientation.

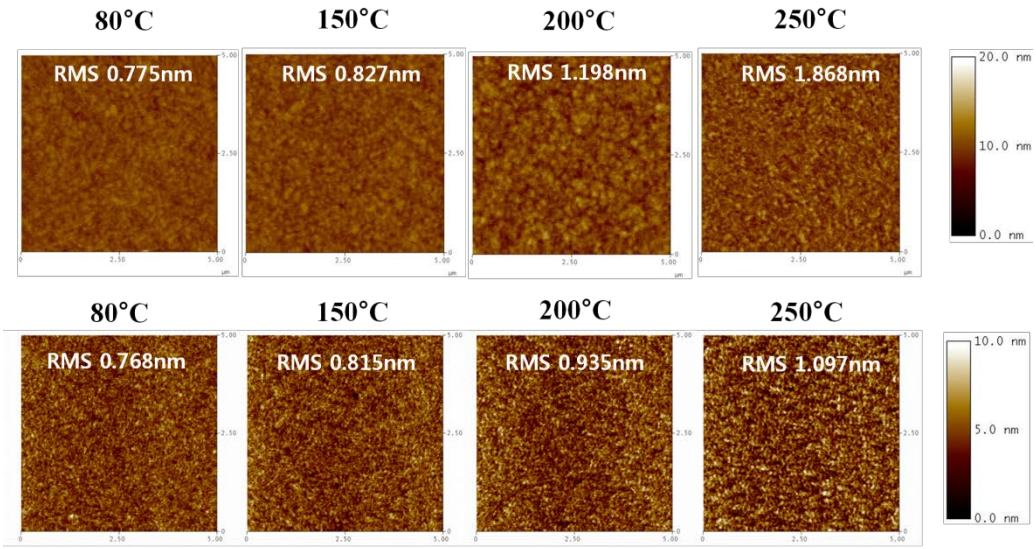

Figure 4-9. AFM height images (5μm x 5μm) of PBC (upper) and PBCDC (bottom) at different annealing temperatures

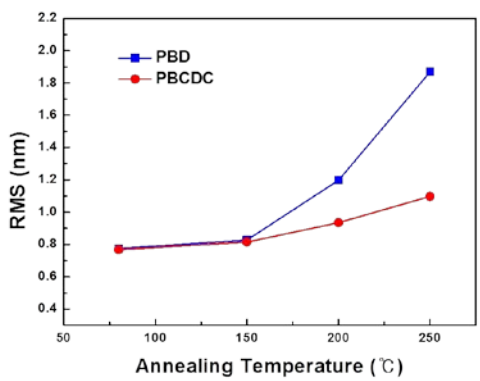

Figure 4-10. RMS plotted as a function of annealing temperature

4.3. Experimental

Materials and Characterization

All reagents were purchased from commercial sources and used as received. Anhydrous toluene and anhydrous THF were prepared by distillation with sodium and benzophenone. The m1,m2, m3, M1 and M3 were prepared by known method51-53. 1H-, 13C-NMR, MALDI-TOF and elemental analysis were measured by using a Bruker Avance-500, SCIEX TOF/TOF 5800 and CE instruments EA1110, respectively. Gel permeation chromatography (GPC) was performed by using a Waters system and Waters styragel HR4 column eluted with chloroform at 90°C. UV-Vis absorption spectra and UPS were recorded by Shimadzu UV-1650PC and Hitachi High Tech AC-2, respectively. Thermogravimetric analysis (TGA) and differential scanning calorimetry (DSC) were measured by using TA instruments Q50 and DSC-Q1000, respectively, under a nitrogen atmosphere with heating rate of 10°C/min. AFM imaging was performed using Multimode with a Nano Scope V Controller (Bruker) in tapping mode. The 2D-GIXD was measured by using the PLS-II 9A U-SAXS beamline in the Pohang Accelerator Laboratory, Korea. The incidence angle was adjusted to 0.12°

Device Fabrication and Evaluation

For organic field-effect transistor fabrication, p-doped SiO2/Si (thermally grown, 300 nm thick SiO2 layer) substrates were used after cleaning procedures (10 min sonication

using acetone and isopropylalcohol, respectively). The octadecyltrichlorosilane (OTS) self-assembled monolayer was introduced by vacuum phase treatment (80 °C, 150 min), after applying UV-O3 for 20 minutes. The polymer solution were prepared using a mixture solvent (chloroform : 1,2-dichlorobenzene, 4 : 1, v : v) with concentration of 5 mg / 1ml. The solution was spin-coated (1500 rpm, 60 s) onto the OTS treated SiO2/Si substrates after 2 min of retention time in a nitrogen-filled glovebox. To remove residual solvent, all the as-prepared films were baked in 80 °C using a hot-plate for 120 min; thermal annealing procedures were carried out with temperature conditions of 150 °C, 200 °C, and 250 °C for 20 min. Top-contact Au source-drain electrodes (50 nm) were thermally deposited through shadow masks with a deposition rate of 0.2 Å/s with high vacuum condition (ca. 1 -6 torr). The device evaluation was performed using a Keithley 4200 SCS instrument in the nitrogen-filled glovebox.

Synthesis and Characterization.

(Synthesis of M2) The mixture of m2 (840mg, 1mmol) and 2-(5-bromothiophen-2-yl)acetonitrile54 (444.5mg, 2.2mmol) were dissolved in tert-butyl alcohol (50 mL) at 50 °C. Potassium tert-butoxide (224.4g, 2mmol) was added quickly into the mixture. The reaction was stirred at 50° C for 30min. The reaction mixture was diluted in methanol (100 ml), and then resulting precipitate was filtered. Finally, the crude product was purified by column chromatography (methylene chloride) and

recrystallization (ethylacetate/methanol) to afford red solid (664mg, 55%). 1H NMR (500 MHz, CDCl3, δ): 7.79 (s, 2H, Ar-H), 7.32 (s, 2H, vinyl), 7.14 (d, 2H, Ar-H), 7.04 (d, 2H, Ar-H), 4.2 (d, 4H, -OCH2-), 1.90 (m, 2H, -CH-), 1.66(m, 4H, -CH2-), 1.54(m, 4H, -CH2-), 1.45-1.25(m, 60H, -CH2-), 0.88(m, 12H –CH3); 13C NMR(126 MHz, CDCl3, δ): 145.30, 140.21, 137.87, 132.63, 132.02, 131.47, 130.37, 128.11. 127.25, 115.94, 114.21, 105.34, 77.49, 77.23, 77.13, 76.98, 39.43, 32.18, 31.47, 30.31, 29.99, 29.95, 29.64, 27.22, 22.94, 14.35; MS (MALDI-TOF, m/z) Calcd for C64H90Br2N2O2S4: 1204.43, found, 1206.1; Anal. Calcd for C64H90Br2N2O2S4: C, 63.66; H, 7.51; Br, 13.23; N, 2.32; O, 2.65; S, 10.62, Found: C, 63.61; H, 7.53; N, 2.33; O, 2.66; S, 10.63.

(Synthesis of M4) M3 (1g, 1mmol) and 2-bromo-5-iodothiophene (635mg, 2.2mmol) were dissolved in degassed THF, followed by Na_2CO_3 aqueous solution (2M, 4.4ml) and $Pd(PPh_3)_4$ were added. The reaction was heated to reflux 12 h under argon atmosphere. The resulting mixture was cooled to room temperature. After aqueous work-up, the mixture was dried over anhydrous $MgSO_4$, and then the solvent was removed in vacuo. Finally, the crude product was purified by column chromatography (methylene chloride/n-hexane(1:1)) to afford black solid (450mg, 42%). 1H NMR (500 MHz, CDCl3, δ): 8.86 (d, 2H, Ar-H), 7.22 (d, 2H, Ar-H), 7.05 (d, 2H, Ar-H), 7.02 (d, 2H, Ar-H), 4.01 (d, 4H, -CH2-), 1.94 (m, 2H, -CH-), 1.32-1.21(m, 24H, -CH2-),

0.86(m, 12H, -CH3); 13C NMR(126 MHz, CDCl3, δ): 161.82, 141.61, 139.65, 137.90, 136.69, 131.31, 128.71, 125.36, 125.11, 113.39, 108.82, 77.49, 77.23, 76.98, 46.55, 38.18, 32.12, 32.04, 31.57, 30.27, 29.93, 29.78, 29.54, 26.57, 26.55, 22.89, 22.85, 14.31; MS (MALDI-TOF, m/z) Calcd for C54H74Br2N2O2S4: 1068.30, found, 1071.0.

(Synthesis of PBD) A 20ml schlenk tube was charged with M1 (221.8mg, 0.2mmol), M4 (214.2mg, 0.2mmol), Pd2(dba)3 (4mg, 0.0044mmol), P(o-tol)3 (5.3mg, 0.0176mmol) and anhydrous toluene (5ml), The schlenk tube was degassed with argon for 15min. The reaction was heated to 100°C for 24 hours. The polymer was precipitated into excess methanol, followed by soxhlet extraction with methanol, acetone, n-hexane and chloroform. The chloroform solution was precipitated into methanol. The polymer was filtered, then dried in vacuo to give product PBD as a black solid (292mg, 86.2%). GPC (CHCl3, 90°C): Mn = 148 kDa, PDI = 3.0; Anal. Calcd for C104H158N2O4S6: C, 73.79; H, 9.41; N, 1.65; O, 3.78; S, 11.36. Found: C, 73.70; H, 9.60; N, 1.65; O, 3.71; S, 11.31.

(Synthesis of PBD) A 20ml schlenk tube was charged with M2 (241.5mg, 0.2mmol), M3 (200.2mg, 0.2mmol), Pd2(dba)3 (4mg, 0.0044mmol), P(o-tol)3 (5.3mg, 0.0176mmol), aliquat 336 (2 drops) and toluene (5ml). The schlenk tube was degassed with argon for 15min, followed by the addition of degassed Na2CO3 aqueous solution

(1M, 1ml). The reaction was heated to 100°C for 24 hours. The polymer was precipitated into excess methanol, followed by soxhlet extraction with methanol, acetone, n-hexane and chloroform. The chloroform solution was precipitated into methanol. The polymer was filtered, then dried in vacuo to give product PBCDC as a black solid (250mg, 69.6%). GPC (CHCl3, 90°C): Mn = 198 kDa, PDI = 4.3; Anal. Calcd for C110H160N4O4S6: C, 73.61; H, 8.99; N, 3.12; O, 3.57; S, 10.72. Found: C, 73.49; H, 9.01; N, 3.11; O, 3.61; S, 10.72.

4.4. Conclusion

We synthesized a novel conjugated polymer, PBCDC, consisting of DPP and BDT building blocks connected by CNV linkage for OFET application. The PBCDC exhibited highly balanced ambipolar properties with a hole and electron mobility of up to 0.2 cm2 V-1s-1, which was consistent up to 250°C of the annealing temperature. We additionally investigated the effects of CNV via a comparative analysis with polymer without CNV (PBD). We found that CNV is attributed to lowering the LUMO level and delocalizing the LUMO over the structure of the polymer, furthermore shortening the lamellar and π–π stacking distances. It thereby provides enhanced charge mobility and thermal stability of chemical and physical structures. As a result, by the electronic

and structural effects of CNV, PBCDC was found to display excellent potential ambipolar material that can withstand harsh conditions in the manufacturing of the final electronics.

4.5. References

[1] Sekitani, T.; Zschieschang, U.; Klauk, H.; Someya, T. Nat. Mater 2010, 9, 1015-1022.

[2] Baeg, K. J.; Caironi, M.; Noh, Y.-Y. Adv. Mater 2013, 25, 4210-4244.

[3] Nielsen, C. B.; Turbiez, M.; McCulloch, I. Adv. Mater 2013, 25, 1859-1880.

[4] Zhang, L.; Di, C.-a.; Yu, G.; Liu, Y. J. Mater. Chem 2010, 20, 7059-7073.

[5] Yan, H.; Chen, Z.; Zheng, Y.; Newman, C.; Quinn, J. R.; Dotz, F.; Kastler, M.; Facchetti, A. Nature 2009, 457, 679-686.

[6] Minemawari, H.; Yamada, T.; Matsui, H.; Tsutsumi, J.; Haas, S.; Chiba, R.; Kumai, R.; Hasegawa, T. Nature 2011, 475, 364-367.

[7] de Gans, B. J.; Duineveld, P. C.; Schubert, U. S. Adv. Mater 2004, 16, 203-213.

[8] Cho, S.; Lee, J.; Tong, M.; Seo, J. H.; Yang, C. Adv. Funct. Mater 2011, 21, 1910-1916.

[9]Yuen, J. D.; Fan, J.; Seifter, J.; Lim, B.; Hufschmid, R.; Heeger, A. J.; Wudl, F. J. Am. Chem. Soc 2011, 133, 20799-20807.

[10] Zhao, Y.; Guo, Y.; Liu, Y. Adv. Mater 2013, 25, 5372-5391.

[11] Lee, J.; Han, A.-R.; Yu, H.; Shin, T. J.; Yang, C.; Oh, J. H. J. Am. Chem. Soc 2013, 135, 9540-9547.

[12] Yuan, Y.; Giri, G.; Ayzner, A. L.; Zoombelt, A. P.; Mannsfeld, S. C.; Chen, J.;

Nordlund, D.; Toney, M. F.; Huang, J.; Bao, Z. Nat. Commun 2014, 5, 3005.

[13] Yun, H.-J.; Kang, S.-J.; Xu, Y.; Kim, S. O.; Kim, Y.-H.; Noh, Y.-Y.; Kwon, S.-K. Adv. Mater 2014, 26, 7300-7307.

[14] Tseng, H. R.; Phan, H.; Luo, C.; Wang, M.; Perez, L. A.; Patel, S. N.; Ying, L.; Kramer, E. J.; Nguyen, T. Q.; Bazan, G. C.; Heeger, A. J. Adv. Mater 2014, 26, 2993-2998.

[15] Wang, C.; Dong, H.; Hu, W.; Liu, Y.; Zhu, D. Chem. Rev 2012, 112, 2208-2267.

[16] Bobbert, P. A.; Sharma, A.; Mathijssen, S. G.; Kemerink, M.; de Leeuw, D. M. Adv. Mater 2012, 24, 1146-1158.

[17] Kuribara, K.; Wang, H.; Uchiyama, N.; Fukuda, K.; Yokota, T.; Zschieschang, U.; Jaye, C.; Fischer, D.; Klauk, H.; Yamamoto, T.; Takimiya, K.; Ikeda, M.; Kuwabara, H.; Sekitani, T.; Loo, Y.-L.; Someya, T. Nat. Commun 2012, 3, 723.

[18] Sporea, R. A.; Burridge, T.; Silva, S. R. Sci. Rep 2015, 5, 14058.

[19] Boroumand, F. A.; Hammiche, A.; Hill, G.; Lidzey, D. G. Adv. Mater 2004, 16, 252-256.

[20] Cho, S.; Seo, J. H.; Park, S. H.; Beaupre, S.; Leclerc, M.; Heeger, A. J. Adv. Mater 2010, 22, 1253-1257.

[21] Zhang, W.; Han, Y.; Zhu, X.; Fei, Z.; Feng, Y.; Treat, N. D.; Faber, H.; Stingelin, N.; McCulloch, I.; Anthopoulos, T. D.; Heeney, M. Adv. Mater 2015, 28, 3922-3927.

[22] Chen, C.-M.; Sharma, S.; Li, Y.-L.; Lee, J.-J.; Chen, S.-A. J. Mater. Chem. C 2015, 3, 33-36.

[23] Mullen, K.; Pisula, W. J. Am. Chem. Soc 2015, 137, 9503-9505.

[24] Meager, I.; Nikolka, M.; Schroeder, B. C.; Nielsen, C. B.; Planells, M.; Bronstein, H.; Rumer, J. W.; James, D. I.; Ashraf, R. S.; Sadhanala, A.; Hayoz, P.; Flores, J.-C.; Sirringhaus, H.; McCulloch, I. Adv. Funct. Mater 2014, 24, 7109-7115.

[25] Anthony, J. E.; Facchetti, A.; Heeney, M.; Marder, S. R.; Zhan, X. Adv. Mater 2010, 22, 3876-3892.

[26] Kronemeijer, A. J.; Gili, E.; Shahid, M.; Rivnay, J.; Salleo, A.; Heeney, M.; Sirringhaus, H. Adv. Mater 2012, 24, 1558-1565.

[27] Holliday, S.; Donaghey, J. E.; McCulloch, I. Chem. Mater 2014, 26, 647-663.

[28] Peng, Z.; Galvin, M. E. Chem. Mater 1998, 10, 1785-1788.

[29] Zhao, X.; Zhan, X. Chem. Soc. Rev 2011, 40, 3728-3743.

[30] Yoon, S.-J.; Kim, J. H.; Chung, J. W.; Park, S. Y. J. Mater. Chem 2011, 21, 18971-18973.

[31] Yoon, S.-J.; Chung, J. W.; Gierschner, J.; Kim, K. S.; Choi, M.-G.; Kim, D.; Park, S. Y. J. Am. Chem. Soc 2010, 132, 13675-13683.

[32] Greenham, N. C.; Moratti, S. C.; Bradley, D. D. C.; Friend, R. H.; Holmes, A. B. Nature 1993, 365, 628-630.

[33] Zhan, X.; Liu, Y.; Wu, X.; Wang, S.; Zhu, D. Macromolecules 2002, 35, 2529-2537.

[34] Chua, L.-L.; Zaumseil, J.; Chang, J.-F.; Ou, E. C. W.; Ho, P. K. H.; Sirringhaus, H.; Friend, R. H. Nature 2005, 434, 194-199.

[35] Thompson, B. C.; Kim, Y.-G.; McCarley, T. D.; Reynolds, J. R. J. Am. Chem. Soc 2006, 128, 12714-12725.

[36] Holcombe, T. W.; Woo, C. H.; Kavulak, D. F. J.; Thompson, B. C.; Fréchet, J. M. J. J. Am. Chem. Soc 2009, 131, 14160-14161.

[37] Casey, A.; Han, Y.; Fei, Z.; White, A. J. P.; Anthopoulos, T. D.; Heeney, M. J. Mater. Chem C 2015, 3, 265-275.

[38] Yun, H.-J.; Choi, H. H.; Kwon, S.-K.; Kim, Y.-H.; Cho, K. ACS Appl. Mater. Interfaces 2015, 7, 5898-5906.

[39] Gierschner, J.; Park, S. Y. J. Mater. Chem. C 2013, 1, 5818-5832.

[40] An, B.-K.; Gierschner, J.; Park, S. Y. Acc. Chem. Res 2012, 45, 544-554.

[41] Yun, S. W.; Kim, J. H.; Shin, S.; Yang, H.; An, B.-K.; Yang, L.; Park, S. Y. Adv. Mater 2012, 24, 911-915.

[42] Kwon, O. K.; Park, J.-H.; Kim, D. W.; Park, S. K.; Park, S. Y. Adv. Mater 2015, 27, 1951-1956.

[43] Ma, L.; Yi, Z.; Wang, S.; Liu, Y.; Zhan, X. J. Mater. Chem. C 2015, 3, 1942-1948.

[44] Chen, S.-A.; Chang, E.-C. Macromolecules 1998, 31, 4899-4907.

[45] Sato, S.; Tajima, K.; Hashimoto, K. Macromolecules 2009, 42, 1785-1788.

[46] Kline, R. J.; McGehee, M. D.; Kadnikova, E. N.; Liu, J.; Fréchet, J. M. J. Adv. Mater 2003, 15, 1519-1522.

[47] Kline, R. J.; McGehee, M. D.; Kadnikova, E. N.; Liu, J.; Fréchet, J. M. J.; Toney, M. F. Macromolecules 2005, 38, 3312-3319.

[48] Tsao, H. N.; Cho, D. M.; Park, I.; Hansen, M. R.; Mavrinskiy, A.; Yoon do, Y.; Graf, R.; Pisula, W.; Spiess, H. W.; Mullen, K. J. Am. Chem. Soc 2011, 133, 2605-2612.

[49] Nguyen, T. L.; Choi, H.; Ko, S.-J.; Uddin, M. A.; Walker, B.; Yum, S.; Jeong, J.-E.; Yun, M. H.; Shin, T. J.; Hwang, S.; Kim, J. Y.; Woo, H. Y. Energy Environ. Sci 2014, 7, 3040-3051.

[50] Vohra, V.; Kawashima, K.; Kakara, T.; Koganezawa, T.; Osaka, I.; Takimiya, K.; Murata, H. Nat. Photonics 2015, 9, 403-408.

[51] Yamamoto, T.; Ikai, T.; Kuzuba, M.; Kuwabara, T.; Maeda, K.; Takahashi, K.; Kanoh, S. Macromolecules 2011, 44, 6659-6662.

[52] Cortizo-Lacalle, D.; Arumugam, S.; Elmasly, S. E. T.; Kanibolotsky, A. L.; Findlay, N. J.; Inigo, A. R.; Skabara, P. J. J. Mater. Chem 2012, 22, 11310-11315.

[53] Si, P.; Liu, J.; Deng, G.; Huang, H.; Xu, H.; Bo, S.; Qiu, L.; Zhen, Z.; Liu, X. RSC Adv 2014, 4, 25532-25539.

[54] Chung, J. W.; Yang, H.; Singh, B.; Moon, H.; An, B.-k.; Lee, S. Y.; Park, S. Y. J. Mater. Chem 2009, 19, 5920-5925.

[55] Hwang, D. K.; Fuentes-Hernandez, C.; Kim, J.; Potscavage, W. J.; Kim, S.-J.; Kippelen, B. Adv. Mater 2011, 23, 1293-1298.

[56] Dong, H.; Fu, X.; Liu, J.; Wang, Z.; Hu, W. Adv. Mater. 2013, 25, 6158-6183.

Abstract in Korean

공액 고분자는 1977 년 발견 된 이래로 전도성 및 반도체 특성으로 인해 광범위하게 연구되어왔다. 이러한 전하 수송 특성으로 인해 유기 태양 전지 및 유기 전계 효과 트랜지스터와 같은 다양한 전자소자 응용 분야에서 응용되어왔다. 이러한 전자소자에 응용을 위해서는 기본적으로 반도체는 적절한 에너지 레벨과 높은 전하 이동성을 가지고 있어야 한다. 공액 고분자에서 이러한 특성을 실현하기 위한 핵심 설계는 공액 주쇄의 효과적인 π-π 스태킹을 유도하게 하는것과 필요한 에너지 알맞은 전자주개 단량체 및 전자받개 단량체를 선택하는 것이다. 이 연구에서는 비닐렌 함유 공액 고분자 및 그의 유도체인 시아노 비닐렌 함유 공액 고분자 구조에 집중하였다. 이 고분자 구조들은 동일 평면의 백본을 만들 수 있는 능력과 에너지 레벨 튜닝이 쉬운 장점들이 있지만, 낮은 전하 수송 특성으로 인해 OSC 및 OFET 용 반도체로서 주목을 받지 못하였다. 이러한 낮은 전하 수송 특성은 π-π 스태킹을 불리하게 만드는 비닐렌 그룹의 구조적 불규칙성에 기인한다. 이 연구에서는 이러한 구조적 불규칙성을 제어하여서 유기 태양 전지 및 유기 전계 효과 트랜지스터 용 고성능 비닐렌 및 그 유도체 (시아 노 비닐 렌) 함유 공액 고분자를 설계하였다.

첫째, 폴리(페닐렌비닐렌) (PPV)는 대표적인 비닐렌 고분자이다. 그러나,

PPV는 매우 낮은 전하 수송 특성을 갖는다. 최근에, 티오펜이 도입 된 PPV 형 고분자 (PPVTV)인 경우 비교적 높은 정공 이동도를 나타내었고 유기 태양 전지적용 시 비교적 높은 효율 (3.5 %)을 달성 하였다. 그러나, PPVTV는 단순한 페닐기와 티오펜기만으로 되어있으므로, 다른 잘 알려진 좋은 분자를 사용함으로써 성능을 더 향상시킬 가능성이 있다고 생각하였고, 이러한 생각을 바탕으로 새로운 비닐렌 폴리머 (PBDS)를 설계하였다. 이 고분자는 우수한 전하 수송 분자로 알려져 있는 2 차원 벤조 [1,2-b : 4,5-b] 디티 오펜 (2D-BDT)을 매우 높은 평면도 및 트랜스 - 입체 규칙 형 고분자인 PPVTV에 도입한 구조이다. 흥미롭게도, 2D-BDT는 정공 이동도를 개선할 뿐만 아니라 HOMO 에너지도 낮추는 역할도 한다는 것을 발견했다. 결과적으로 PBDS : PC71BM 기반 태양 전지는 2D-BDT가 없는 경우에 비해 0.81V의 향상된 개방 회로 전압 (V_{OC})과 10mA cm-2의 향상된 단락 회로 전류 (JSC)를 나타내어 전력 변환 효율 (PCE)은 5%를 달성하였다. 이것은 폴리머가 2.0eV의 넓은 밴드 갭을 가진다는 것을 고려하였을 때, 높은 효율이며, 따라서 넓은 밴드갭이 필요한 탠덤 태양 전지 및 삼원 조화 태양 전지 응용에 적합한 고효율 공액고분자임을 확인하였다. (제 2 장)

다음으로, 추가적으로 효율을 개선하기 위해 PBDS에 시아노 그룹을 도입하였다. 시아노 비닐렌 함유 중합체는 좋은 광학 특성을 나타내지 만,

트랜스에서 시스 형태로의 광 이성화 반응이 있어서 유기트랜지스터나 태양전지에는서는 높은 성능을 나타내지 않았다. 이 연구에서 평면구조이면사 분자간 상호작용을 유도하는 베타 시아노비닐렌 중합체(PBDCS)를 디자인하였고, 흥미롭게도, PBDCS는 다른 시아노스티릴벤젠과 달리 자외선에 노출에도 광 이성질체화가 되지않고 100 % 트랜스 입체 규칙성구조를 유지하였다. 게다가 PBDCS는 PBDS에 비해 훨씬 더 깊은 FMO와 낮은 밴드 갭을 가지며 솔루션에서 응집현상을 보여주었다. 그 결과, PBDCS : PC71BM을 기반으로 하는 태양전지에서 15 mAcm-2의 높은JSC와 0.95 V의 높은 V_{OC}을 가지며, 높은 82.7 %의 높은 EQE를 가지며, 결과 PCE 8.75 %를 달성하였다. 또한, PBDCS : ITIC에 태양전지 경우는 1.08V의 매우 높은 V_{OC} 및 15.9mAcm-2의 높은 JSC를 얻어 7.81 %의 높은 PCE를 달성하였다. 또한 이 태양전지경우 0.49eV의 매우 작은 에너지 손실에도 불구하고 74.2 %의 높은 EQE를 보였다. 이러한 결과로부터 cyanovinylene 그룹은 강한 분자간 상호 작용과 강력하게 안정화된 FMO를 제공한다는 것을 발견했다 (3 장).

마지막으로, 우리는 양극성 반도체 성 폴리머를 디자인하기 위해 cyanovinylene 그룹을 사용했다. 일반적으로, 양극성 전하 수송특성을 갖기위해서는 HOMO 및 LUMO 에너지 레벨이 모두 전극에 비슷한 위치에

있어야하므로 구조가 제한적이다. 가장 많이 사용되고 있는 전자주개-받개 교대공중합체 경우 일반적으로 p-type 이 n-type에 비하여 월등히 많다. 이는 충분히 강한 전자받개분자가 적기 때문이다. 이 연구에서는 일반적으로 p-type인 전자주개-받개 교대공중합체에 에너지레벨을 낮추기 위해 트렌스 구조의 시아노비닐기를 도입하였다. 그결과 HOMO 및 LUMO가 많이 낮아져서 전자,정공 이동의 균형이 매우좋은 양극성 전하 수송특성을 갖게되었다. 또한 강한 인접분자간 인력으로인해 열에 의한 모폴로지 변화가 매우 줄어들게 되어, 80 ° C ~ 250 ° C 범위에서 전자,정공이동도의 변화가 거의 없었다. (4 장)

주요어: 비닐렌 고분자, 폴리아릴렌비닐렌, 시아노비닐렌고분자, 유기전계효과트렌지스터, 유기태양전지, 양극성트랜지스터

학생 번호: 2010-30092

List of Publications

Original Papers

1. Tae-Lim Choi, Kuk-Min Han, Jeong-Il Park, Do Hwan Kim, **Jun-Mo Park**, Sangyoon Lee "*High performance organic thin-film transistor based on amorphous A, B-alternating poly (arylenevinylene) copolymers*" *Macromolecules*. **2010**, *43*, 6045-6049.

2. Tae Jin Kang Yong-Seung Chi, **Jun-Mo Park** "*Preparation and Characterization of Iptycene Polymer/SWCNT Nanocomposites*" *Fibers and Polymers*. **2012**, *13*, 1023-1030.

3. Kyung Ho Kim, Ajeong Choi, **Jun-Mo Park**, Sung Ju Hong, Min Park, In-Hwan Lee, Eun Sang Choi, Alan B Kaiser, Tae-Lim Choi, Yung Woo Park "*Magnetoresistance of a copolymer: FeCl 3-doped poly (2, 5-dioctyloxy-p-phenylene vinylene-alt-3, 4-ethylenedioxythiophene vinylene)*" *Synthetic Metals*. **2014**, *188*, 30-34.

4. Kyung-Geun Lim, **Jun-Mo Park**, Hannah Mangold, Frédéric Laquai, Tae-Lim Choi, Tae-Woo Lee "*Bimolecular Crystals with an Intercalated Structure Improve Poly (p-phenylenevinylene)-Based Organic Photovoltaic Cells*" *ChemSusChem*. **2015**, *8*, 337-344.

5. **Jun-Mo Park**, Sang Kyu Park, Won Sik Yoon, Jin Hong Kim, Dong Won Kim, Tae-Lim Choi*, and Soo Young Park* "*Designing Thermally Stable Conjugated Polymers with Balanced Ambipolar Field-Effect Mobilities by Incorporating Cyanovinylene Linker Unit*" *J. Phys. Chem. Lett*. **2016,** *49*,2985-2992.

6. Won Sik Yoon, Dong Won Kim, **Jun-Mo Park**, Illhun Cho, Oh Kyu Kwon, Dong Ryeol Whang, Jin Hong Kim, Jung-Hwa Park, Soo Young Park* "*A Novel Bis-Lactam Acceptor with Outstanding Molar Extinction Coefficient and Structural Planarity for Donor–Acceptor Type Conjugated Polymer*" *Macromolecules*. **2016**, *49*, 8489-8497.

7. **Jun-Mo Park,** Dong Won Kim, Hae Yeon Chung, Ji Eon Kwon, Seung Hwa Hong, Tae-Lim Choi,* and Soo Young Park* "*A Stereoregular β-Dicyanodistyrylbenzene (β-DCS)-based Conjugated Polymer for High-Performance Organic Solar Cells with Small Energy Loss and High Quantum Efficiency*" *J. Mater. Chem. A*, 2017, **Accepted,** DOI: 10.1039/C7TA04127F

List of Presentations

International

1. **(Poster) Jun-Mo Park**, Sang Kyu Park, Won Sik Yoon, Jin Hong Kim, Dong Won Kim and Soo Young **Park*** "*High performance ambipolar field-effect transistor based on diketopyrrolopyrrole and benzodithiophene copolymer with cyanovinylene linkage*" 2015 International Chemical Congress of Pacific Basin Societies, Hawaii, 2015-12-16.

2. **(Poster) Jun-Mo Park**, Dong Won Kim, and Tae-Lim Choi,* and Soo Young Park* *"Efficient dicyanodistyrylbenzene-based low bandgap polymer for fullerene and non-fullerene polymer solar cells with small photon energy loss*" 13th International Symposium on Functional π-Electron Systems, Hongkong, 2017-06-05.

List of Patents

Domestic

1. 박수영, 윤원식, 김동원, **박준모** “유기태양전지 광 활성층용 고분자 및 이를 포함하는 유기태양전지” 대한민국, 출원번호 10-2017-0033529